明治大学大学院理工学研究科

２０１１年度

博士学位請求論文

Gas Transport and Optical Properties of High Free Volume Silicon- or Fluorine-containing Polymer Membranes

高い自由体積を有するケイ素・フッ素含有高分子膜の気体透過性と光学的性質

学位請求者　応用化学専攻

佐　藤　修　一

ABSTRACT

The high free volume polymer membrane has the potential to be an important membrane gas separation material due to the fact that it has the highest gas permeability among all polymeric membranes. Additionally, the optic device application has been expected because these polymers show high transparency. In the past study, the studies to produce high gas permeable and separation polymer membrane and to produce high transparency polymer material were independent, respectively. Therefore, I systematically investigated the gas transport and separation properties and optical properties (e.g., refractive index and photo alignment characteristic) of these high free volume polymer membranes for the application to gas separation and optic device. At fast, the study of separation membrane which was possible to capture volatile organic compound (VOC) component (e.g. benzene) from air (e.g., water and nitrogen) was the permeability, diffusivity, and solubility of benzene vapor and water vapor in high free volume silicon- or fluorine-containing polymer membranes. Secondly, the study of optic device which was possible to design next generation anti refraction film was the relationship between gas transport properties and refractive index in high free volume fluorine-containing polyimide membranes. I proposed the new free volume model based on refractive index. Finally, these polymer films with high heat resistance and high transparency showed new function. The polymers showed photo alignment of liquid crystal molecule. I could discover polymer materials of photo alignment characteristic with high heat resistance and the photo alignment mechanism was systematically investigated.

ACKNOWLEDGMENTS

The author wishes to express his sincere appreciation for the guidance and advice in this research by Professor Kazukiyo Nagai (Department of Applied Chemistry, Meiji University). Without his suggestions and simulating interest in this subject matter, this thesis would not have been completed.

The author also wishes to express his appreciation to the thesis committee members, Professor Takeo Kurata and Professor Tetsuo Miyakoshi (Department of Applied Chemistry, Meiji University) for their cooperation.

The author would like to acknowledge the invaluable assistance of Mr. Shinji Kanehashi (Department of Applied Chemistry, Meiji University), Dr. Sou Miyata and Mr. Yoichi Takahashi (Lintec Co.), Mr. Masashi Ono (JSP Co.), Mr. Johta Yamauchi (Toyota Motor Co.), Mr. Takamasa Ose, Mr. Kaoru Nakamura, Mr. Takayuki Wada, Mr. Daiki Gondo, and Mr. Yusuke Ishiba (Department of Applied Chemistry, Meiji University). The author also wishes to thank the members of Professor Kazukiyo Nagai's Laboratory at Meiji University.

Additionally, the author would like to express his acknowledgments to the names that have been supportive all the time.

They are: Prof. Setsuko Matsumoto, Meiji University

Prof. Hironaga Matsumoto, Meiji University

Dr. Yuki Iwai, Futaba Co.

Dr. Tatsuro Mizunuma, Kyushu University

Mr. Hiroto Ito, Optical Coatings Japan Co.

Mr. Taihei Yabumoto, Stanley Electric Co.

Mr. Kozo Nishimura, Meiji University

Finally, the author wishes to express his sincere gratitude to his parents. This thesis would not have been achieved without their encouragement and support for his study and life.

Octorber, 2011

Shuichi Sato

TABLE OF CONTENTS

LIST OF TABLES

Chapter 3 RELATIONSHIP BETWEEN GAS TRANSPORT PROPERTIES AND REFRACTIVE INDEX IN HIGH FREE VOLUME FLUORINE-CONTAINING POLYIMIDE MEMBRANES

Chapter 4 SUBSTITUTE EFFECT OF FLUORINE-CONTAINING POLYIMIDES WITH HEXAFLUOROISOPROPYLIDENE GROUP ON PHOTO ALIGNMENT OF LIQUID CRYSTAL MOLECULE

No Table

LIST OF FIGURES

Chapter 1

GENERAL INTRODUCTION

1.1. POLYMERS WITH HIGH FREE VOLUME

Recently, the research and development of various polymer materials are carried out activity in each industrial field. Particularly, the polymer materials with high fractional free volume which is measurement of the space between polymer segments were expected to show high permeability. Therefore, the application as the gas separation membrane was considered [1]. Additionally, these polymers were expected to the optic device application (e.g. liquid crystal display and organic electroluminescence) with high transparency [2, 3]. In such application, the polymer designing method of increasing fractional free volume for introducing bulky substitute and integrity polymer chain is mainly used. The method of introducing integrity polymer chain is the use of phenyl group polymer such as polyimide. The method of introducing bulky substitute is the use of the atoms with high occupied volume such as silicon or fluorine. Therefore, the silicon- or fluorine-containing polymers with high free volume showed solvent solubility. The fractional free volume in polymer material is an important parameter for polymer segment cohesiveness and depends on the various properties.

1.2. FRACTIONAL FREE VOLUME

The polymer chain moves by micro-Brownian motion at the high temperature.

As the temperature decreases, the mobility weakens. And the group of polymer chain coheres by each polymer chain, respectively. The state of this amorphous polymer is glassy state. In the case of crystalline polymers, crystallite is formed and is cooled, and then the part of amorphous structure becomes glassy state. Generally, the polymer density is approximately 1.0–1.3 g/cm^3 in this state. On the contrary, as the temperature increase from glassy state, micro-Brown motion is occurred when the freeze of molecular chain is removed. When the mobility of polymer chain is not active, the polymer does not have the free space that can move. However, as the temperature increase, this free space increases. Figure 1.1 presents the conventional relationship between polymer specific volume and temperature. V_0 is occupied volume and V_g is the polymer specific volume in glassy state. V_f (i.e., V_g–V_0) is fractional free volume. V_f shows the free space of possible to move polymer chain. The temperature when the motion of polymer chain is removed from a freeze state is observed in the V–T curve bend, and this temperature is called glass transition temperature (T_g). The phenomenon is glass transition. When the temperature increased more than T_g, the polymer structure changes the flow state without the connection such as the cross linking between polymer chains. However, because the length of polymer chain is so long that the polymer chain climb all over it, the polymer maintains solid state, even the temperature that is higher than T_g. the polymer shows rubbery state. Of course when the polymer structure is cross link state, the polymer segment mobility is prevented, and this state becomes at stable state in wide temperature range. In this state (i.e., rubbery state), the elasticity is low. Therefore, the polymer greatly transforms by slight force and shows an elastic property to come back to the form with the removal of the external force. In contrast, glassy polymers

showed elasticity, but these polymers is fragile, in other words, show brittleness. The T_g values depend on the chemical structure, because they are dependent on the cohesiveness polymer chain and substitute.

This fractional free volume can be measured by such as Dilatometric method in wide temperature range. The problem is how to measure the occupied volume. Most simplest and easiest method is group contribution method based on the occupied volume assumed by van der Walls volume [4]. There is a lot of study through free volume calculated by such a method in thermodynamics and mass transport field. Additionally, recently, there are many reports which directly clarified free volume including size distribution and the ratio of space between high polymer chains by the positron extinction method [5-8]. And then, the polymer cohesiveness is lively performed.

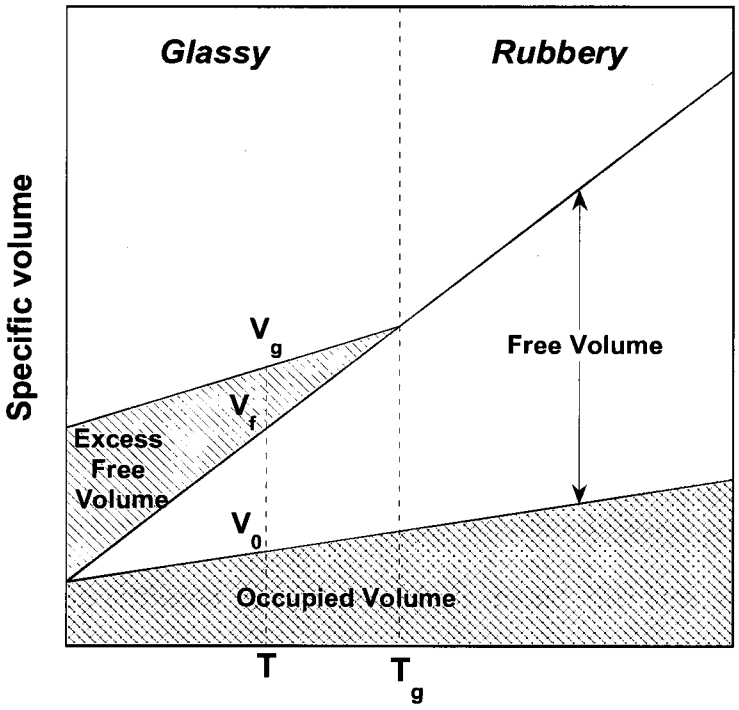

Figure 1. 1 Schematic representation of a typical specific volume vs. temperature relationship in amorphous polymer.

1.3. GAS AND VAPOR SEPARATION POLYMER MEMBRANES

Many investigate apply to a gas permeation membrane increasing the size of the space to occur between polymer segments by using the concept of this FFV. The first successful gas separation membrane process is hydrogen separation using polymer membranes. In the early 1970s, Permasep® which is hollow fiber type gas separation membrane made from polyester was proposed by Du'Pont [9]. However, the hollow fiber of those days was a symmetric membrane, and since hydrogen permeability was low and was not economically enough, it did not succeed gas separation membrane process. In the 1980s, U.S. Monsanto (Air Product) introduced polymeric hollow fiber gas separation membranes and succeed gas separation membrane process. The commercial application was focused on purge gases from ammonia plants [10]. Then, carbon dioxide separation membrane for removing global warming gases and oxygen permeable membrane for industrial fuel and medical treatment were developed for global environment problems. Additionally, water vapor separation membrane has been required in air conditioning application.

The concept of gas separation membranes is summarized in Figure 1.2. In porous membrane, there is the mechanism by Knudsen diffusion (Case I) [11], surface diffusion (Case II) [12], capillary condensation flow (Case III) [13], and molecular sieving flow (Case IV) [14]. On the other hand, permeation of a gas molecule in a dense polymer membrane is usually governed by solution-diffusion mechanism (Case V) [15]. In solution-diffusion mechanism, it is based the idea that at first gas molecules are dissolved in membrane surface, and the penetrants are dissolved to the polymer chain gap. By controlling the polymer chain gap, gas permeability is changed broadly. Therefore, it is possible to discover hydrogen permeability which is different

about 10,000 times by the difference in chemical structure of polymer.

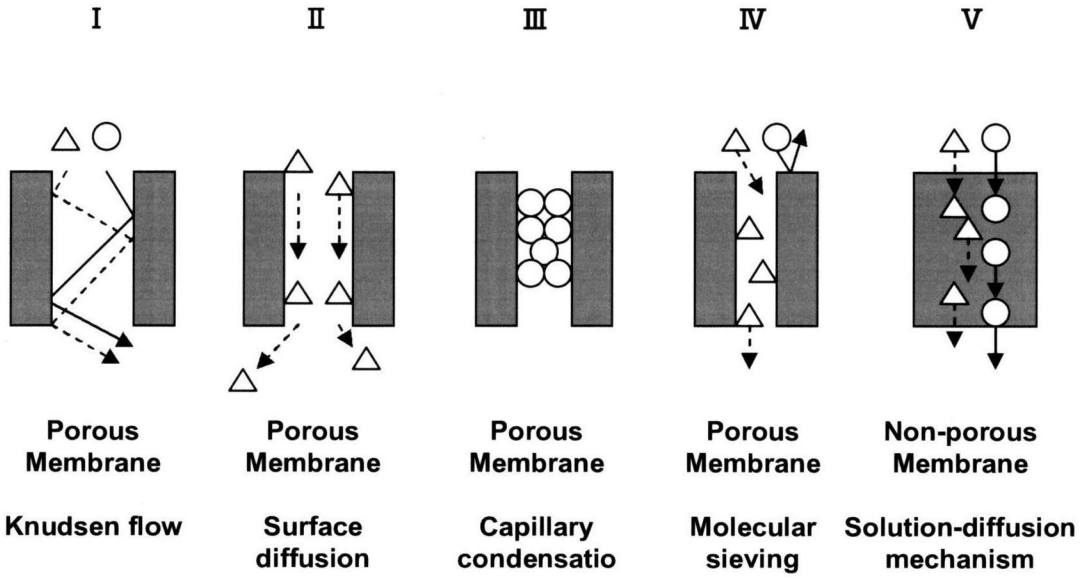

Figure 1. 2 Gas separation mechanisms through separation membranes.

The permeability, P, is the product of diffusivity, D, and solubility, S, was determined from equation (1. 1)

$$P = D \times S \tag{1. 1}$$

when the permeance of gas through a membrane is determined from equation (1. 2)

$$Q = \frac{DSAt}{L}(p_1 - p_2) = \frac{PAt}{L}(p_1 - p_2) \tag{1. 2}$$

where p_1 is the upstream pressure, p_2 is the down stream pressure, L is the effective membrane thickness, A is the membrane area, t is the time. For a binary gas mixture permeating through a polymer membrane, the separation factor for component A relative to component B, $\alpha(A/B)$, is determined from equation (1. 3)

$$\alpha(A/B) = \frac{Y_A / Y_B}{X_A / X_B} = \frac{Y_A X_B}{X_A Y_B} \tag{1. 3}$$

where Y_i and X_i are the concentration of component i in the gas phase at the down

stream and upstream faces of the membrane, respectively. When the downstream pressure is negligible relative to the upstream pressure, the separation factor can be written as the ratio of permeability. The $\alpha(A/B)$ provides a measure for assessing the relative ability of various polymers to separate gas mixtures. It is called $\alpha(A/B)$ the ideal selectivity. Factoring the permeability into diffusivity and solubility terms, the ideal selectivity may be expressed as equation (1. 4).

$$\alpha(A/B) = \frac{P_A}{P_B} = \left(\frac{S_A}{S_B}\right) \times \left(\frac{D_A}{D_B}\right) \qquad (1.4)$$

where (D_A/D_B) is the ratio of the concentration averaged diffusivity of components A and B is referred to as the diffusivity selectivity. (S_A/S_B) is the ratio of solubility of components A and B is called the solubility selectivity. In order to make the permeability selectivity of the component A to B increase, it is necessary to make solubility selectivity or diffusivity selectivity increase. From equation (1. 2), it is necessary for making the gas permeance increasing to enlarge membrane area, to use high permeability material, and to make membrane thickness as thin as possible. As high permeability membrane, development of polymer with integrity polymer chain and a high fractional free volume has been performed. The dense layer of commercial polymer membranes makes as thin as possible to increase gas permeability. Furthermore, a hollow fiber membrane is developed to increase membrane area per unit volume as much as possible. Therefore, this polymer membrane with high free volume and integrity polymer segment has been developed for the application of gas and vapor separation.

1.4. POLYMERS FOR OPTICAL DEVICE

The high free volume polymer membranes are expected to show high gas permeable. Therefore, these polymers are used as the material in gas separation application. On the other hand, these polymers are used in the materials in optic device. These are expected to show high transparency with a lot of cavities less than visible light. The polymers with high free volume are designed by introducing bulky substitute and integrity polymer chain. For that reason, these polymers showed high T_g, have high heat resistance property. The high transparent non-porous amorphous polymers have been extensively required in optic device such as liquid crystal display. Figure 1.3 showed cross section of liquid crystal display. Inorganic materials such as a color filter or the glass substrate are mainly used in a liquid crystal display. On the other hand, polymer materials are used in anti refraction film located in the surface of liquid crystal display which transmit backlight and prevent refraction from the surroundings. Additionally, polymer materials are used in the liquid crystal photo alignment film which is located in the outside the liquid crystal layer and is possible to orient liquid crystal molecules. For such application, heat resistance and long durability is required in these high transparency polymer materials. Therefore, the high free volume polymers are important materials in optic device application.

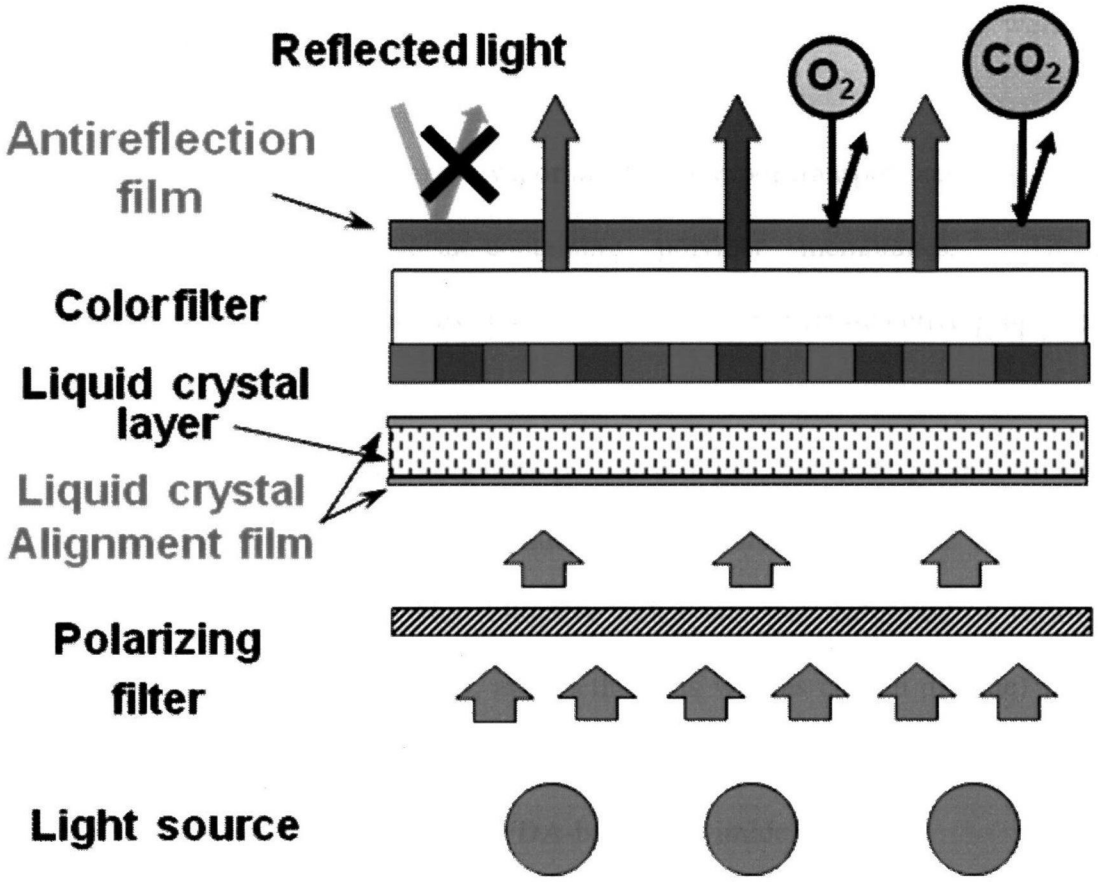

Figure 1. 3 Cross section of LCD display.

1.5. GOAL AND ORGANIZATION OF THIS DISSERTATION

This dissertation focuses mainly on the high free volume silicon- or fluorine-containing polymer membranes. The use of high free volume silicon- or fluorine-containing polymers for gas and vapor separation and optical properties is investigated to prepared novel functions. A fundamental investigation of high free volume polymer membranes is carried out for development of novel polymer membranes with high separation, low refractive index, and high photo alignment characteristic including high durability and heat resistance.

This dissertation is organized into five chapters as explained below.

Chapter 1 provides the general introduction of this dissertation, including a

brief history of polymer membranes with high fractional free volume as well as background of this study.

Chapter 2 provides the benzene vapor and water vapor transport and separation properties of silicon- or fluorine-containing polymer membranes. These silicon-containing polymer membranes showed large molecule permselective properties as a novel function.

Chapter 3 discusses the relationship between gas transport properties and refractive index in a family of 4,4-(hexafluoro-isopropylidene) diphthalic anhydride (6FDA)-based polyimide films. The refractive index and permeabilities of various gases (i.e., hydrogen, oxygen, nitrogen, and methane as well as carbon dioxide) were investigated in terms of their polymer fractional free volumes to obtain a fundamental understanding on the optical property of 6FDA-based polyimide materials.

Chapter 4 focuses on the substituent effect of fluorine-containing polyimides with 6FDA group on the photo alignment of the liquid crystal (LC) molecule. 6FDA-2,3,5,6-tetramethyl-1,4-phenylene diamine (TeMPD) showed the photo alignment characteristic of the LC molecule with high heat resistance. The use of 6FDA-TeMPD structures with higher glass transition as photo alignment was investigated. Additionally, the chemical structure change was systematically investigated.

Chapter 5 summarizes this research and presents the conclusions.

1.6. REFERENCES

[1] R. W. Baker, J. G. Wijmans, *Polymeric Gas Separation Membranes, Chapter 8*, D. R. Paul, Y. P. Yampolskii eds., CRC Press, Boca Raton, FL (1994).

[2] D. J. Liaw, W.H. Chen, C. K. Hu, K. R. Lee, J. Y. Lai, High optical transparency, low dielectric constant and light color of novel organosoluble polyamides with bulky alicyclic pendent group, *Polymer.* **48** (2007) 6571-6580.

[3] C. Wang, X. Zhao, G. Li, J. Jiang, High solubility and optical transparency of novel polyimides containing 3,3',5,5'-tetramethyl pendant groups and 4-tert-butyltoluene moiety, *Polym. Degrad. Stab.* **94** (2009) 1526-1532.

[4] D. W. van Krevelen, *Properties of Polymers. Fourth ed.*, Elsevier B. V., Oxford. (2009)

[5] Y. C. Jean, Positron annihilation spectroscopy for chemical analysis: a novel probe for microstructural analysis of polymers, *Microchem. J.* **42** (1990) 72-102.

[6] Y. Jiang, F.T. Willmore, D. Sanders, Z. P. Smith, C. P. Ribeiro, C.M. Doherty, A. Thornton, A.J. Hill, B.D. Freeman, I.C. Sanchez, Cavity size, sorption and transport characteristics of thermally rearranged (TR) polymers, *Polymer* **52** (2011) 2244-2254.

[7] S. J. Pas, M. D. Ingram, K. Funke, A. J. Hill, Free volume and conductivity in polymer electrolytes, *Electrochim. Acta* **50** (2005) 3955-3962.

[8] X. Y. Wang, A. J. Hill, B. D. Freeman, I. C. Sanchez, Structural, sorption and transport characteristics of an ultrapermeable polymer, *J. Membr. Sci.* **314** (2008) 15-23.

[9] R. J. Gardner, R. A. Crane, J. F. Hannan, *C. E. P.*, Octorber (1977) 76-78.

[10] Monsanto Co. USP. 4,230,463(1980).

[11] M. Knudsen, *The Kinetic Theory of gases-some modern aspects, Methuens Monografhs on Physical Subjects*, London, (1952).

[12] S. T. Hwang, K. Kammermeyer, Surface diffusion in microporous media, *Canad. J. Chem. Eng.*, **44** (1966) 82-89.

[13] K. H. Lee, S. T. Hwang, The transport of condensible vapors through a microporous Vycor glass membrane, *J. Colloid Interface Sci.*, **110** (1986) 544-555.

[14] J. S. Masaryk, R. M. Fulrath, Diffusivity of helium in fused silica, *J. Chem. Phys.* **59** (1973) 1198-1202.

[15] R. W. Baker, *Membrane Technology and Applications*, McGraw-Hill, New York (2000).

Chapter 2

PERMEABILITY, DIFFUSIVITY, AND SOLUBILITY OF BENZENE VAPOR AND WATER VAPOR IN HIGH FREE VOLUME SILICON- OR FLUORINE-CONTAINIG POLYMER MEMBRANES

2.1. ABSTRACT

The diffusivity, solubility, and permeability of benzene and water vapors, as well as nitrogen (i.e., major component of air) were systematically investigated for high free volume silicon-containing polymers, including, poly(dimethylsiloxane) (PDMS), poly(trimethylsilylmethylmethacrylate) (PTMSMMA), poly(1-trimethylsilyl-1-propyne) (PTMSP), fluorine-containing 4,4-(hexafluoro-isopropylidene) diphthalic anhydride (6FDA)-based polyimide. The infinite-dilution permeability coefficient, P_0, of benzene vapor and water vapor was diffusion controlled and did not depend on either the mobility of the polymer segments, the space between polymer segments, or cohesive energy density of the polymer but was dependent on the balance among them. In ideal permselectivity, which was determined from pure gas experiments, all silicon-containing polymers used in this study showed benzene vapor-permselective behavior while all fluorine-containing polymers had the opposite property (i.e., nitrogen-permselective). All polymers used in this study showed water vapor-permselective behavior. The benzene vapor/nitrogen permselectivity depended on diffusivity selectivity for fluorine-containing polymers and solubility selectivity for silicon-containing polymers. Additionally, the water vapor/nitrogen permselectivity

depended on solubility selectivity for PTMSP and some 6FDA-based polyimides with methyl substituent, and both selectivity balance for PDMS, PTMSMMA, and some a 6FDA-based polyimide without methyl substituent.

Keywords: benzene vapor; water vapor; permeability; selectivity; polymer membrane

2.2. INTRODUCTION

Chemicals are extensively used in the industrial field, and they play an important role in improving our standard of living. However, the issue of discharging hazardous chemical substances such as volatile organic compound (VOC), halogen substance, and heavy metals remains a problem. Several countries have laws and regulations in place to address this issue. For example, in Japan, this issue has been clarified by the Pollutant Release and Transfer Register (PRTR) law since 2001. The PRTR law is a system of managing the amount of discharge and transfers of chemicals. Toluene, xylene, and benzene (BTX component) occupy the first to third positions in the PRTR ranking, respectively, which scores the most hazardous chemicals in terms of amount of discharge, exposure, and carcinogenic effect.

Benzene is among the most dangerous chemicals. It is a natural resource, and it is contained in petroleum at 1–4 %. Benzene resources are automobile exhaust gas, volatile oil, and discharge gas from industries. The last abandonment of benzene is discharged in the atmosphere at the rate of 99 % [1]. Usually, benzene in the atmosphere is a very small component and can be expressed in ppm unit.

To solve the environmental problem that benzene causes, the development of a production and manufacturing process that does not employ chemicals and/or of a

technology of separation and recovery of benzene is essential. In this study, we considered contributing to saving energy by risk reduction through the use of separation membrane technology. Benzene resources are the impurities from petroleum refining and coke oven gas. Coke oven gas includes benzene as vapor and air (nitrogen, oxygen, water vapor, etc.). The removal of water vapor from air is also desirable in this industrial field.

Taking the critical volume, which is a measure of molecular size, the values are 256 cm^3/mol for benzene vapor, 55.9 cm^3/mol for water vapor, and 90.1 cm^3/mol for nitrogen [2]. It is good separation efficiency to use small-component-permselective membrane from air [3]. That is, the development of permselective membranes for benzene vapor and water vapor from air is required for the separation process. Silicon-containing polymers such as poly(dimethylsiloxane) (PDMS) and poly(1-trimethylsilyl-1-propyne) (PTMSP) show ethylbenzene-permselective behavior from nitrogen, which is expected to provide benzene-permselective behavior [4]. In our preliminary experiments for this study, we found that 4,4-(hexafluoro isopropylidene) diphthalic anhydride (6FDA)-based polyimide showed water vapor permselective behavior. As will be discussed later in Table 2. 1, these polymers have higher free volume among existing polymers.

In this study, the diffusivity, solubility, and permeability of benzene and water vapors, as well as nitrogen (i.e., major component of air) were systematically investigated for silicon-containing polymers, including PDMS, poly(trimethylsilylmethylmethacrylate) (PTMSMMA), PTMSP, and fluorine-containing polyimide, and for four 6FDA-based polyimides. This is the first article on permeation properties of benzene and water vapors in these highly-permeable silicon-containing

and fluorine-containing polymers.

Table 2. 1 Physical properties of silicon- or fluorine-containing polymer membranes

Type	Polymer	T_g (°C)	ρ (g/cm^3)	*FFV*	*CED* (MPa)	δ (MPa$^{1/2}$)
Si-containing polymer	PDMS	−123	0.97±0.02	0.19	228	15.1
	PTMSMMA	79.0	1.00±0.01	0.17	313	17.7
	PTMSP	>250	0.75±0.02	0.29	251	15.8
F-containig polymer	6FDA-mPD	297	1.46±0.01	0.17	765	27.7
	6FDA-MPD	322	1.40±0.01	0.17	740	27.2
	6FDA-TMPD	386	1.34±0.01	0.19	697	26.4
	6FDA-TeMPD	422	1.32±0.01	0.19	679	26.1

2.3. EXPERIMENTAL

2.3.1. Preparation of membranes

Pure PDMS membrane (product name KE103) was specially prepared without any additives. It was kindly supplied by the Shin-Etsu Chemical Industry Co., Ltd., Tokyo, Japan. The PTMSMMA, PTMSP, and the four 6FDA-based polyimides used in this study were synthesized according to the literature [5-7]. A ^{1}H-NMR (JNM-ECA500, JEOL Ltd., Tokyo, Japan) and FT-IR (FT-IR 460+. JASCO Co., Tokyo, Japan) analyses confirmed the chemical structures of these polymers, as shown in Figure 2. 1.

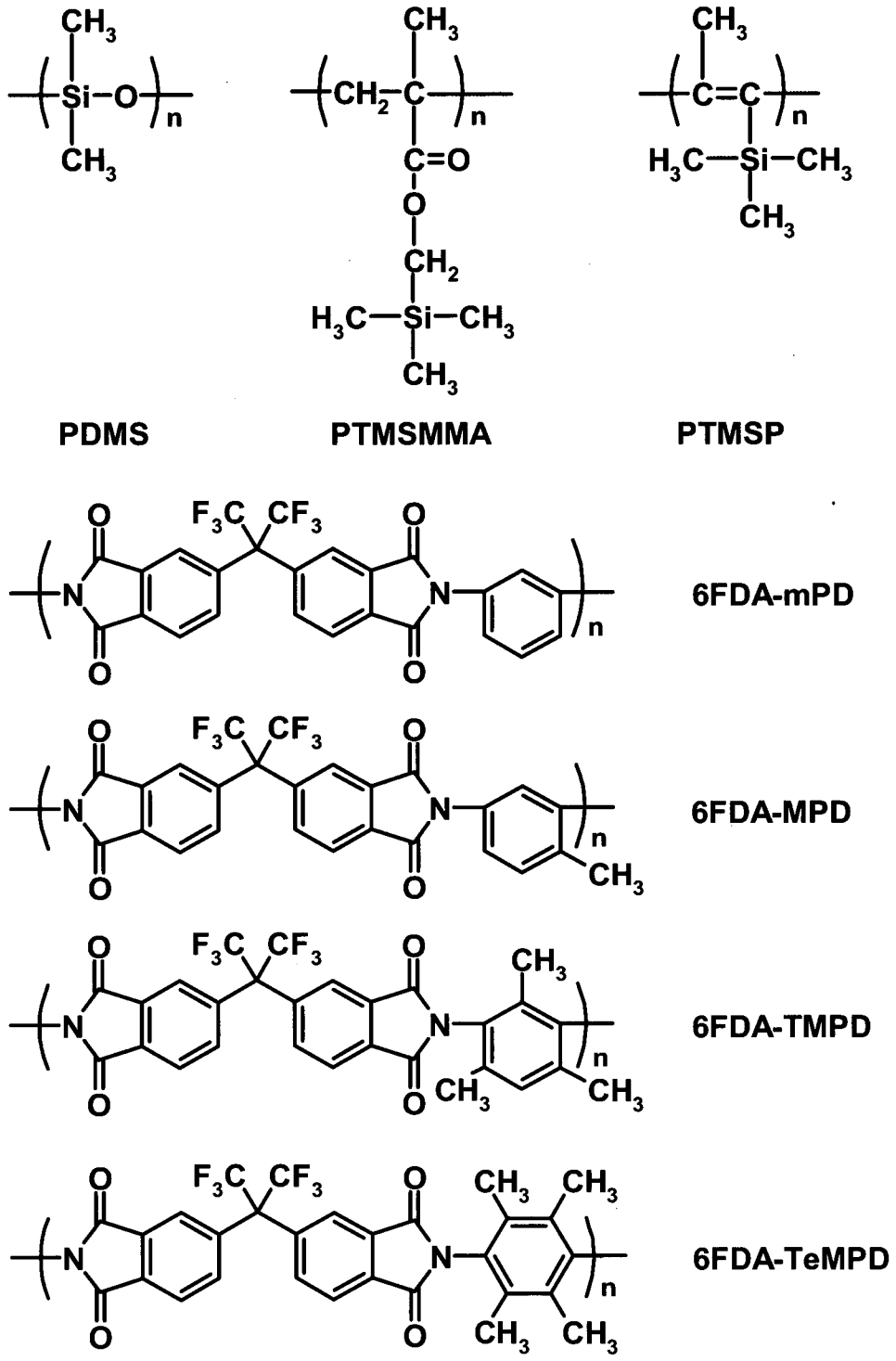

Figure 2. 1 Chemical structures of silicon- or fluorine-containing polymers: poly(dimethylsiloxane) (PDMS), poly(trimethylsilylmethylmethacrylate) (PTMSMMA), poly(1-trimethylsilyl-1-propyne) (PTMSP), 6FDA-based polyimides: 4,4-(hexafluoro-isopropylidene) diphthalic anhydride (6FDA), 1,3-phenylene diamine (mPD), 4-methyl-1,3-phenylene diamine (MPD), 2,4,6-trimethyl-1,3-phenylene diamine (TMPD), and 2,3,5,6-tetramethyl-1,4-phenylene diamine (TeMPD).

The thickness of the PDMS membrane was 800 μm. The PTMSMMA and PTMSP membranes were prepared by casting 3 wt% toluene solutions of each onto a flat-bottomed Petri dish in a glass bell-type vessel at room temperature. The 6FDA-based polyimide membranes were prepared by casting 3.5 wt% dichloromethane solutions of each onto a flat-bottomed Petri dish in a glass bell-type vessel at room temperature. Each solvent was allowed to evaporate slowly over a period of about 7 to 10 days in the vessel. The thickness of the dry membranes used for the experiments was that between 150 and 200 μm for PTMSMMA and PTMSP membranes and between 40 and 60 μm for 6FDA-based polyimides membranes.

2.3.2. Characterization analysis

Differential scanning calorimeter (DSC) analysis was performed to determine the glass transition temperature, T_g, with a Diamond DSC (Perkin–Elmer Inc., Shelton, USA) at a heating rate of 10°C/min. The T_g was determined at the middle point of the endothermic transition using the data from the second heating scan.

Membrane density ρ was determined by flotation of the small membrane samples in a density gradient column, which was maintained at 23°C except for the PTMSP. The density of the PTMSP membrane was determined from the membrane weight and volume at 23°C.

The fractional free volume, *FFV*, is given by,

$$FFV = \frac{V_t - 1.3V_W}{V_t} \qquad (2.\ 1)$$

where V_t is the polymer specific volume and V_w is the van der Waals volume which was calculated from the group contribution method of van Krevelen [8].

The cohesive energy density, *CED*, and solubility parameter, δ, of the polymers were estimated using the group contribution method of Fedors [9].

Wide angle X-ray diffraction (WAXD) patterns were taken using a RINT-1200 X-ray diffractometer (Rigaku Corp., Tokyo, Japan) with a scanning speed of 2°/min using Cu Kα radiation at 40 kV and 20 mA in the dispersion angle from 3–50°.

2.3.3. Measurement of permeation properties of pure vapor

The permeation properties of each pure single component (i.e., benzene vapor, water vapor, and nitrogen) in polymer membranes were determined through the constant volume-variable pressure method at 35°C. The permeability coefficient, P (cm^3(STP)cm/($cm^3 \cdot s \cdot cmHg$)), was determined from equation (2. 2).

$$P = \frac{dp}{dt}\frac{273V}{760(273+T)}\frac{1}{A}\frac{1}{p}\ell \qquad (2.\ 2)$$

where dp/dt is the pressure increase in time, t, at steady-state, V (cm^3) is the downstream volume, T (°C) is the temperature, A (cm^2) is the membrane area, p (cmHg) is the upstream pressure, and ℓ (cm) is the thickness of the membrane. The downstream pressure was maintained under vacuum during experiments.

The saturated vapor pressure, p_{sat}, values were 15.4 cmHg for benzene vapor and 4.26 cmHg for water vapor at 35°C [2]. Experiments were performed in the order of increasing relative feed pressure, p/p_{sat}, at an interval. As benzene is a good solvent for PTMSP and PTMSMMA, both membranes were unstable at higher vapor pressure. Therefore, in this study, the p/p_{sat} varied from 0.03 to 0.4 for benzene vapor and 0.2 to 0.5 for water vapor. The nitrogen permeation was obtained at 1 atm. All permeation data were determined for at least three membrane samples to confirm the reproducibility

of the experimental results.

The apparent diffusion coefficient, D (cm^2/s), was determined from time-lag (θ), the period of time for reaching the steady state, and the intercept with the time axis θ of the plot p against t as follows:

$$D = \frac{\ell^2}{6\theta} \tag{2. 3}$$

According to the solution-diffusion mechanism, the apparent solubility coefficient S ($cm^3(STP)/(cm^3 \cdot cmHg)$) may be evaluated by equation (2. 4):

$$S = \frac{P}{D} \tag{2. 4}$$

The ideal permselectivity for benzene vapor/nitrogen and water vapor/nitrogen is described as *P(vapor)/P(nitrogen)*. Factoring permeability into diffusivv city and solubility terms, the selectivity is expressed for vapor/nitrogen separations as follows:

$$\frac{P(vapor)}{P(nitrogen)} = \frac{D(vapor)}{D(nitrogen)} \times \frac{S(vapor)}{S(nitorgen)} \tag{2. 5}$$

the first term is called diffusivity selectivity, while the second is solubility selectivity.

2.4. RESULTS AND DISCUSSION

2.4.1. Polymer characterization

The properties of the silicon-containing polymers and fluorine-containing polymers are summarized in Table 2. 1. The ranking of T_g was 6FDA-TeMPD > 6FDA-TMPD > 6FDA-MPD > 6FDA-mPD > PTMSMMA > PDMS. The value of PTMSP was not determined as reported in the literature [10], and it was higher than 250°C. At the temperature of permeation measurements, PDMS was rubbery, while PTMSMMA, PTMSP, and 6FDA-based polyimides were glassy.

The ranking of ρ was 6FDA-mPD > 6FDA-MPD > 6FDA-TMPD > 6FDA-TeMPD > PTMSMMA > PDMS > PTMSP. The ρ value of PDMS, PTMSMMA, and PTMSP was below 1.0 g/cm^3, while that of 6FDA-based polyimide was above 1.0 g/cm^3.

The *FFV* value of the membranes varied from 0.17 to 0.29. The ranking of the *FFV* was PTMSP > PDMS = 6FDA-TMPD = 6FDA-TeMPD > 6FDA-mPD = 6FDA-MPD = PTMSMMA. The *FFV* of PTMSMMA was lower than the value expected from the order of the density.

The WAXD patterns of the membranes are presented in Figure 2. 2. PDMS, PTMSP, and all 6FDA-based polyimides showed one broad halo, while the PTMSMMA had two broad halos, indicating that all membranes were amorphous structures. The 2θ value of PDMS, PTMSP, and all 6FDA-based polyimides had a distance between their polymer segments. In the case of PTMSMMA, the halo in the small angle appeared at a distance between polymer segments, whereas that in the large angle was attributed to the intermolecular distance between long side chains. In this regard, all membranes had a wide distribution in the distance between polymer segments, which could contribute to gas diffusion in a membrane. In general, the *d*-spacing value is estimated as the distance between polymer segments based on the maximum 2θ intensity value. However, as is evident in Figure 2. 2, it was difficult for these membranes to indicate accurately the maximum 2θ intensity value for the evaluation of diffusivity, solubility, and permeability of vapors. However, relatively, the ranking of the *d*-spacing of the maximum 2θ intensity value was PTMSMMA (between polymer segments) > PTMSP > PDMS > 6FDA-TeMPD > 6FDA-TMPD > 6FDA-MPD >

6FDA-mPD > PTMSMMA (between long side chains). This order was different from the ranking of ρ and *FFV* in that there was a difference in the size and distribution of the space in the membrane.

The ranking of the *CED* and δ was 6FDA-mPD > 6FDA-MPD > 6FDA-TMPD > 6FDA-TeMPD > PTMSMMA > PTMSP > PDMS.

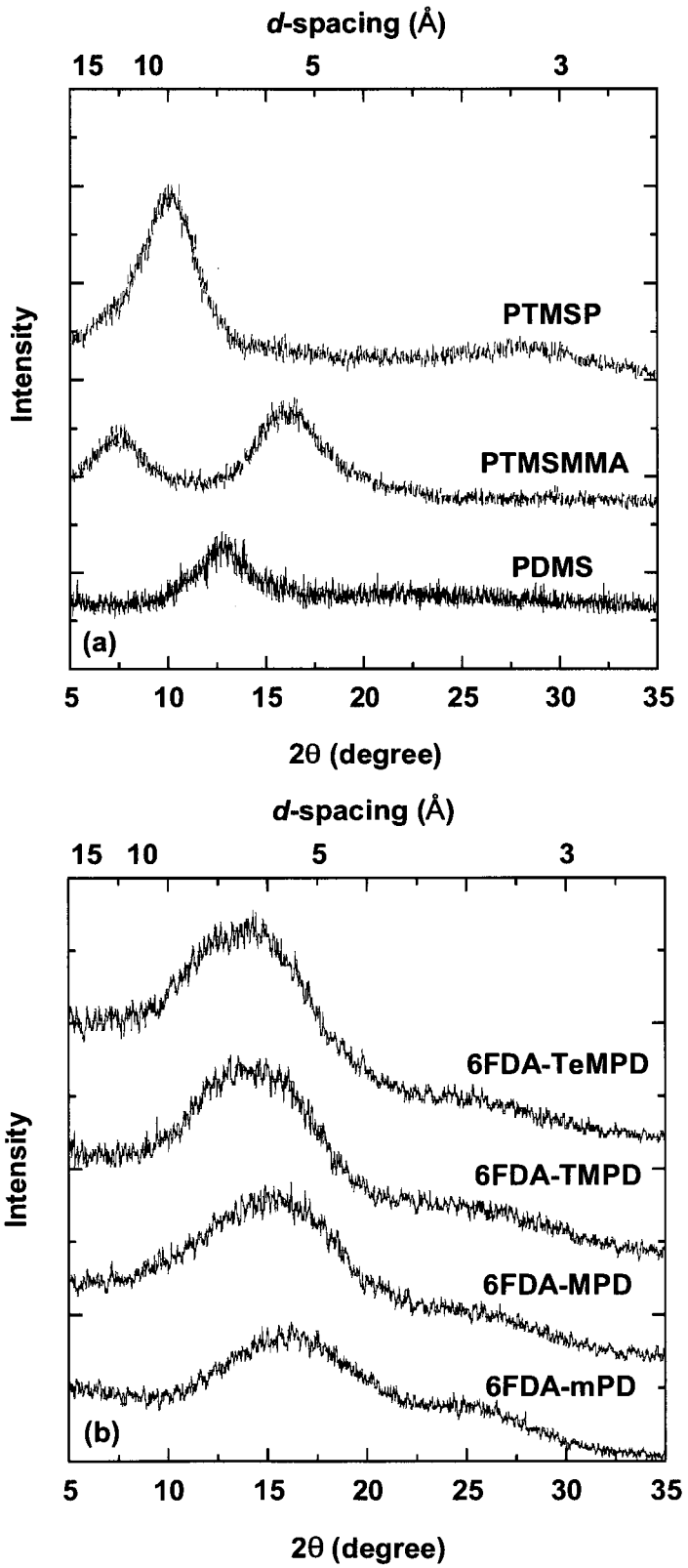

Figure 2. 2 Wide-angle X-ray diffraction patterns of (a) silicon-containing and (b) fluorine-containing polymers.

2.4.2. Diffusivity

During the permeation experiments hysteresis was not observed in the permeation data (i.e., diffusion, solubility, and permeability coefficients) in all membranes.

The diffusion coefficients of silicon- and fluorine-containing polymers for benzene and water vapors at 35°C as a function of the relative feed pressure, p/p_{sat}, across a polymer membrane are presented in Figure 2. 3. The benzene vapor diffusivity of 6FDA-mPD and 6FDA-MPD could not be monitored for 2 days at 1.54 cmHg (p/p_{sat} = 0.1). It was estimated that the benzene vapor diffusion coefficients of 6FDA-mPD and 6FDA-MPD were below the order of 10^{-11} cm^2/s using equation (2. 3).

In the whole range of relative pressures, silicon-containing polymers showed higher diffusivity of benzene and water vapors than fluorine-containing polymers. The diffusion coefficient of benzene vapor was in the order of 10^{-6} cm^2/s for PDMS and PTMSP, 10^{-8} cm^2/s for PTMSMMA, and 10^{-10}–10^{-8} cm^2/s for 6FDA-TMPD and 6FDA-TeMPD, while that of water vapor was in the order of 10^{-5}–10^{-4} cm^2/s for PDMS, 10^{-7}–10^{-6} cm^2/s for PTMSMMA and PTMSP, 10^{-8} cm^2/s for 6FDA-mPD and 6FDA-MPD, and 10^{-7} cm^2/s for 6FDA-TMPD and 6FDA-TeMPD.

Compared with fluorine-containing polymers, the benzene vapor diffusivity of silicon-containing polymers showed less pressure dependency. The benzene vapor diffusivity of 6FDA-TMPD and 6FDA-TeMPD clearly increased as the relative feed pressure increased. The water vapor diffusivity of PTMSP and fluorine-containing polymers showed less pressure dependency. The water vapor diffusivity of PDMS and PTMSMMA clearly decreased as the relative feed pressure increased.

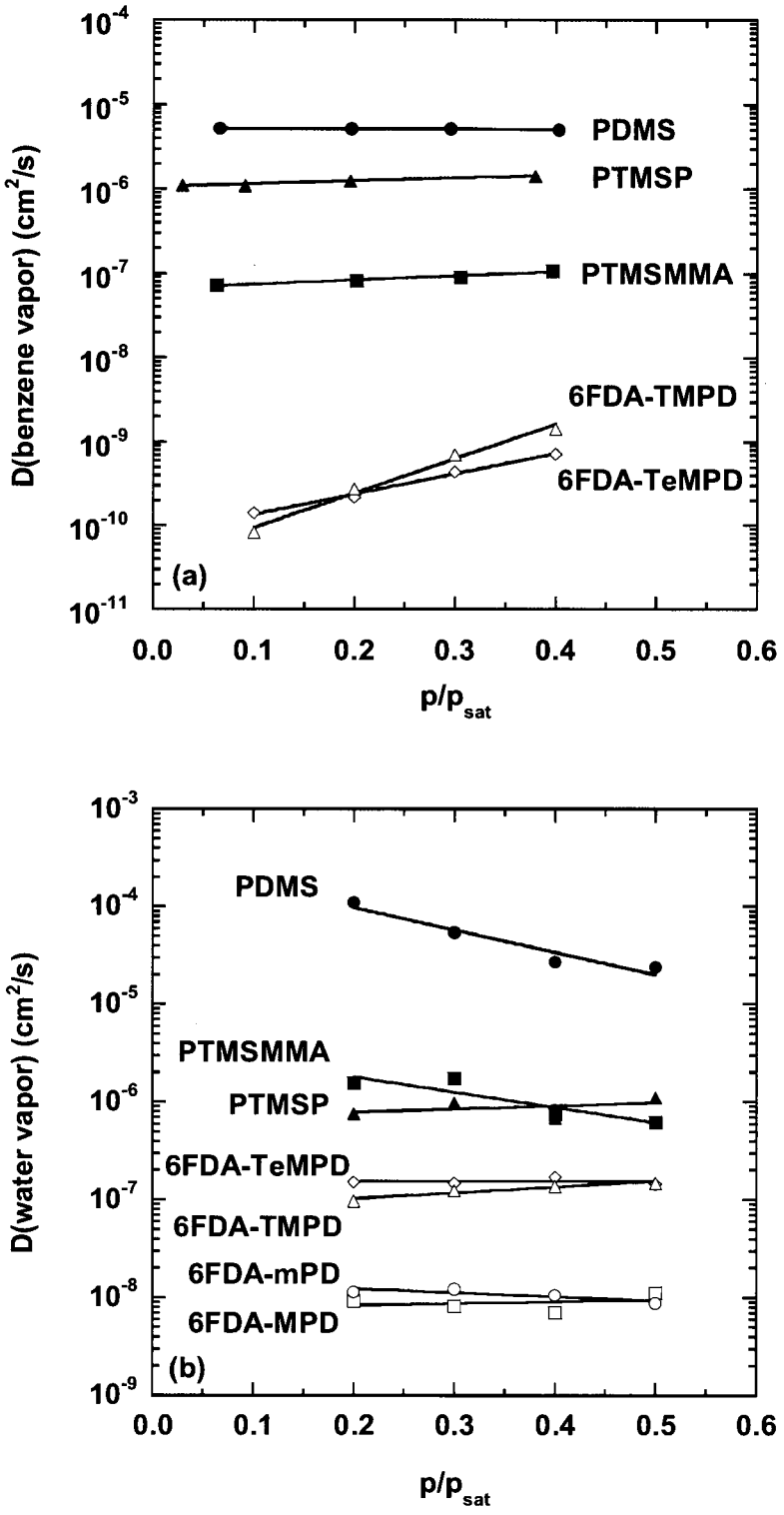

Figure 2. 3 Diffusion coefficients of (a) benzene vapor and (b) water vapor in silicon- or fluorine-containing polymers as a function of the relative feed pressure difference, p/p_{sat}, at 35°C. Polymers: PDMS (●), PTMSMMA (■), PTMSP (▲), 6FDA-mPD (○), 6FDA-MPD (□), 6FDA-TMPD (△), 6FDA-TeMPD (◇).

As shown in Figure 2. 3, there was a linear relationship between vapor diffusivity and relative feed pressure in all membranes, which can be represented as follows [11]:

$$D = D_0 \exp(\beta \frac{p}{p_{sat}}) \qquad (2.\ 6)$$

where D_0 is the infinite-dilution diffusion coefficient at $p/p_{sat} = 0$, and β is a parameter that characterizes the pressure dependence of diffusion coefficients.

Table 2. 2 Infinite-dilution transport parameters of diffusion, D_0, solubility, S_0, and permeability, P_0, coefficients of benzene vapor in silicon- and fluorine-containing polymer membranes at 35°C

Type	Polymer	$D_0\times10^8$ $\left(\frac{cm^2}{s}\right)$	β	$S_0\times10^2$ $\left(\frac{cm^3(STP)}{cm^2\cdot cmHg}\right)$	γ	$P_0\times10^{10}$ $\left(\frac{cm^3(STP)cm}{cm^2\cdot s\cdot cmHg}\right)$	α
Si-containing polymer	PDMS	520	−0.045	270	0.95	140000	0.90
	PTMSMMA	6.6	1.2	110	−3.5	730	−2.3
	PTMSP	110	0.79	3100	−1.0	340000	−0.23
F-containing polymer	6FDA-mPD	< 0.001	ND[a)]	ND[a)]	ND[a)]	< 0.1	ND[a)]
	6FDA-MPD	< 0.001	ND[a)]	ND[a)]	ND[a)]	< 0.1	ND[a)]
	6FDA-TMPD	0.0037	9.5	4300	1.5	16	11
	6FDA-TeMPD	0.0078	5.6	2300	3.8	18	9.4

a) Not determined.

Table 2. 3 Infinite-dilution transport parameters of diffusion, D_0, solubility, S_0, and permeability, P_0, coefficients of water vapor in silicon- and fluorine-containing polymer membranes at 35°C

Type	Polymer	$D_0\times10^8$ $\left(\frac{cm^2}{s}\right)$	β	$S_0\times10^2$ $\left(\frac{cm^3(STP)}{cm^2\cdot cmHg}\right)$	γ	$P_0\times10^{10}$ $\left(\frac{cm^3(STP)cm}{cm^2\cdot s\cdot cmHg}\right)$	α
Si-containing polymer	PDMS	28000	−5.3	0.54	5.7	15000	0.39
	PTMSMMA	370	−3.6	6.5	4.1	2400	0.47
	PTMSP	68	0.74	140	2.3	9200	3.0
F-containig polymer	6FDA-mPD	1.5	−0.93	430	3.5	650	2.6
	6FDA-MPD	0.77	0.42	1700	2.4	1300	2.8
	6FDA-TMPD	7.8	1.4	1500	1.1	12000	2.5
	6FDA-TeMPD	16	−0.081	880	2.5	14000	2.4

Tables 2. 2 and 2. 3 summarize the D_0 and β values of silicon- and fluorine-containing polymers for benzene and water vapors, respectively. The ranking of D_0 was PDMS > PTMSP > PTMSMMA > 6FDA-TeMPD > 6FDA-TMPD for benzene vapor and PDMS > PTMSMMA > PTMSP > 6FDA-TeMPD > 6FDA-TMPD > 6FDA-mPD > 6FDA-MPD for water vapor. The ranking of β was 6FDA-TMPD > 6FDA-TeMPD > PTMSMMA > PTMSP > PDMS for benzene vapor and 6FDA-TMPD > PTMSMMA > 6FDA-MPD > 6FDA-TeMPD > 6FDA-mPD > PTMSMMA > PDMS for water vapor.

The D_0 of silicon- and fluorine-containing polymers for benzene vapor and for water vapor as a function of the β across a polymer membrane are presented in Figure 2. 4. The D_0 of benzene and water vapor decreased as the β increased. The D_0 decreased from the order of 10^{-6} to 10^{-11} cm^2/s for benzene vapor as β increased in the

positive area and decreased from the order of 10^{-4} to 10^{-8} cm^2/s for water vapor as β increased in the positive and negative area. The D_0 was located in a large area, while β was located in a small area for benzene vapor. The positive β value depends on plasticization, while the negative value of β depends on unplasticization. The β value of about zero does not depend on both. This result indicates that benzene vapor caused plasticization in the polymer membrane used in this study, while water vapor caused both plasticization and unplasticization. In each parameter of diffusion, we systematically studied the relationship between the physical properties of polymer membranes and these parameters.

Diffusivity is expected to be correlated to molecular size (e.g., critical volume), chain mobility (e.g., T_g), packing condition (e.g., *CED*), and diffusion space (e.g., *FFV*) in a membrane. The D_0 of silicon- and fluorine-containing polymers for benzene vapor and for water vapor as a function of T_g, which is the standard of polymer mobility and *CED*, which is the standard of polymer cohesiveness across a polymer membrane, are presented in Figure 2. 5. All polymer membranes in this study showed less benzene vapor diffusivity than water vapor diffusivity (Figure 2. 5(a)). This result indicates that the diffusivity of benzene vapor, which showed larger molecular size than water vapor, strongly depended on molecular size.

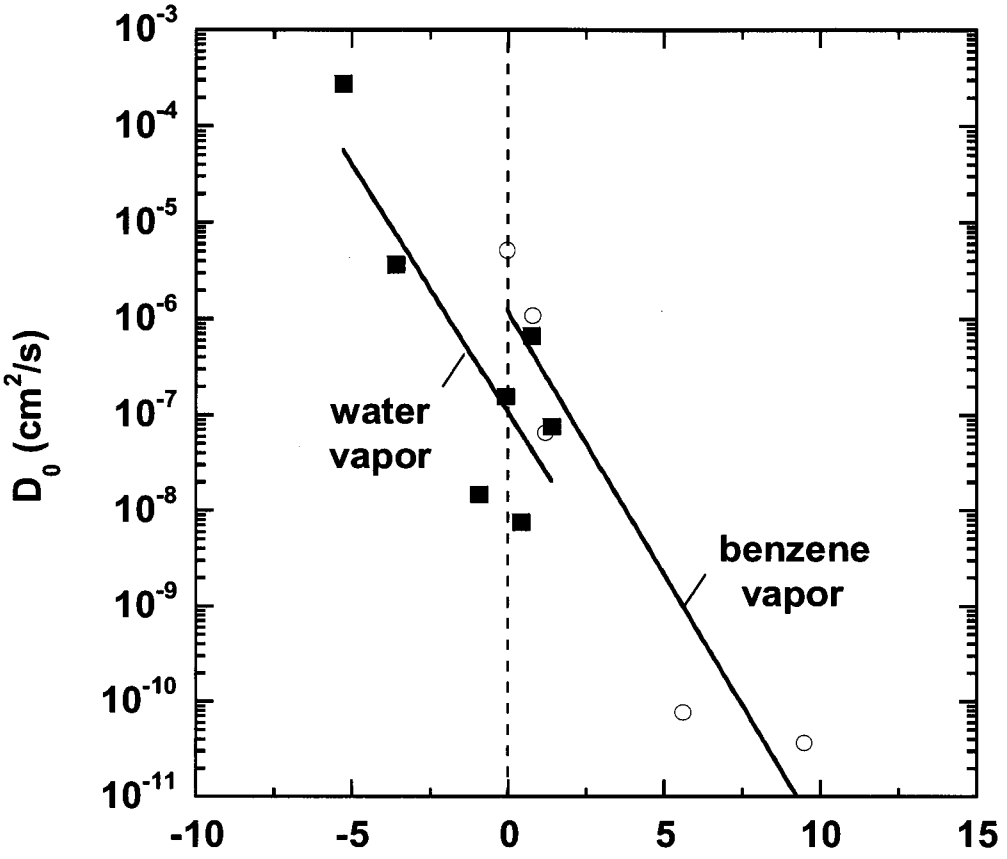

Figure 2. 4 The infinite-dilution diffusion coefficient, D_0, of silicon- and fluorine-containing polymers as a function of the constant characterized by the pressure dependence of diffusivity, β. Penetrants; benzene vapor (○), water vapor (■).

In the polymer membrane where $T_g - 35$ was less than 250°C, the diffusivity decreased from 10^{-6} to 10^{-11} cm^2/s for benzene vapor and from 10^{-4} to 10^{-8} cm^2/s for water vapor as T_g increased. This depends on the decrease in polymer mobility. On the other hand, in the polymer membrane where $T_g - 35$ was more than 250°C, the diffusivity increased from 10^{-11} to 10^{-10} cm^2/s for benzene vapor and from 10^{-8} to 10^{-7} cm^2/s for water vapor as T_g increased. These polymers had higher *FFV* and *d*-spacing than the other polymers, which relatively had less T_g. This is because the glassy polymer that showed high T_g has a bulk polymer segment and integrity polymer chain.

This result indicates that D_0 was dependent on the space between polymer chains more than polymer mobility; thus, there was a tendency for D_0 to show opposite behavior in glassy polymer.

In Figure 2. 5(b), with an increase in *CED*, that is, as polymer cohesiveness increased, the D_0 decreased from 10^{-6} to 10^{-11} cm^2/s for benzene vapor and increased from 10^{-4} to 10^{-8} cm^2/s for water vapor. The reduction ratio of a larger molecule, benzene vapor, was more remarkable than that of a smaller molecule, water vapor.

In general, as *FFV* in a polymer increases, gas diffusion coefficient increases. However, there was a wide distribution of gas diffusion coefficients for the polymers which had the same *FFV* value [12]. For example, the carbon dioxide diffusion coefficient in various types of polymers with an *FFV* values of 0.14 varied from 10^{-7} to 10^{-9} cm^2/s. In Table 2. 1, PTMSMMA, 6FDA-mPD, and 6FDA-MPD had the same *FFV* value of 0.17. PDMS, 6FDA-TMPD, and 6FDA-TeMPD had the same *FFV* value of 0.19. As a result, for these polymers, no relationship between D_0 and *FFV* was calculated using the group contribution method.

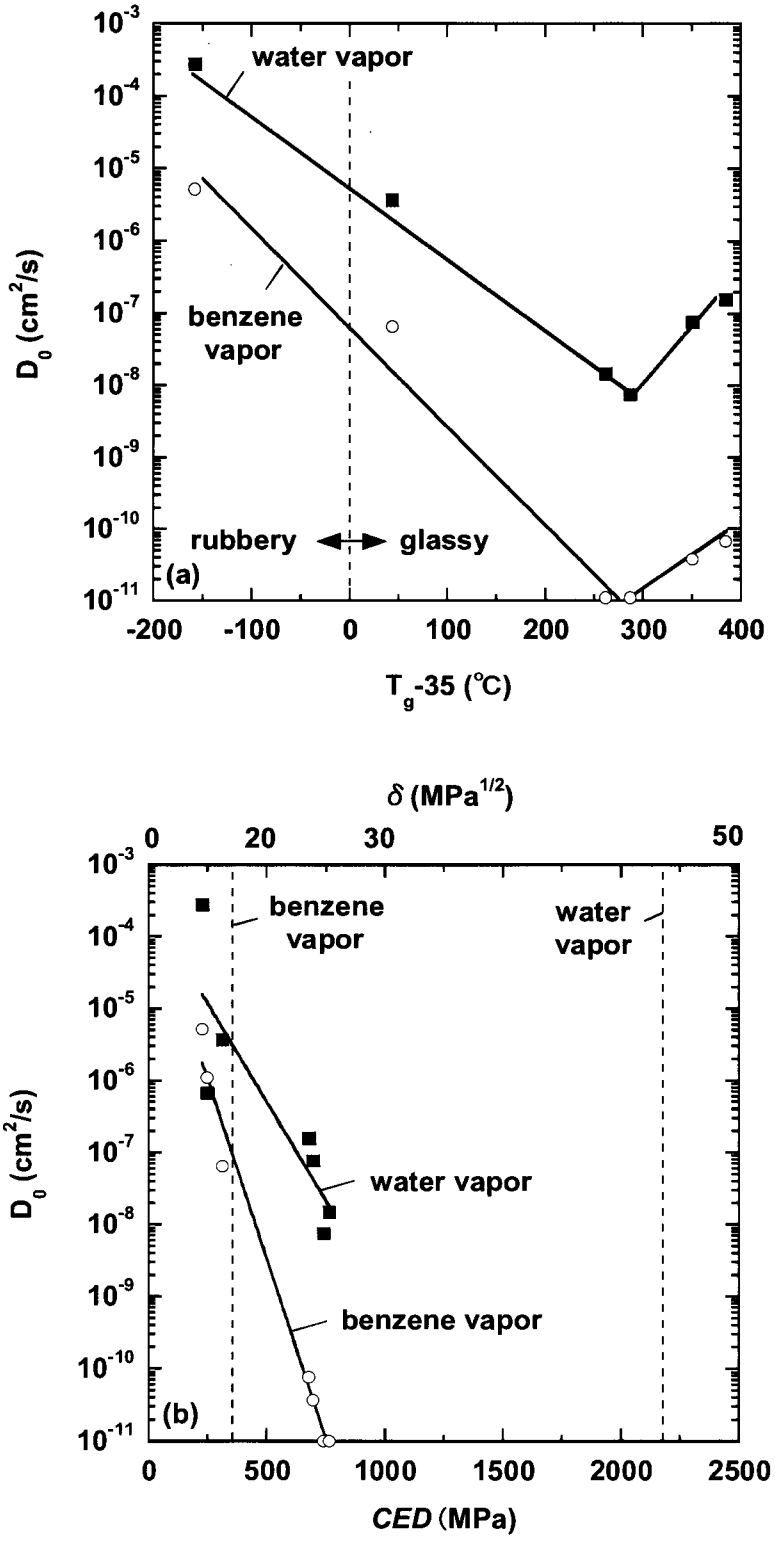

Figure 2. 5 The infinite-dilution diffusion coefficient, D_0, for benzene and water vapors at 35°C in silicon- or fluorine-containing polymers as a function of (a) glass transition temperature, T_g, and (b) polymer cohesive energy density, *CED*. Penetrants; benzene vapor (○), water vapor (■).

The relationship between β and the physical properties of polymer membrane was also studied. The β of silicon- and fluorine-containing polymers for benzene vapor and for water vapor as a function of T_g and *CED* across a polymer membrane are presented in Figure 2. 6. The positive β value indicated plasticization behavior, while the negative one showed unplasticization behavior. All polymer membranes in this study showed less β of water vapor than that of benzene vapor in all T_g (Figure 2. 6(a)). The β increased in the positive area for benzene vapor and from negative to positive area for water vapor as T_g increased. This tendency was different from that of D_0 (Figure 2. 5(a)), and it showed a linear relationship in all T_g. The β increased in the positive area for benzene vapor as *CED* increased and from the negative to the positive area for water vapor as *CED* increased in all polymer membranes (Figure 2. 6(b)).

These results in Figures 2. 5 and 2. 6 indicate that polymer cohesiveness increased as vapor diffusivity in the infinite dilution state decreased, and it strongly depended on plasticization. Moreover, these results indicate that polymer mobility decreased as the influence of plasticization increased, and that the polymers depended on unplasticization in the polymer with less T_g and *CED* (i.e., less polymer mobility and small polymer cohesiveness).

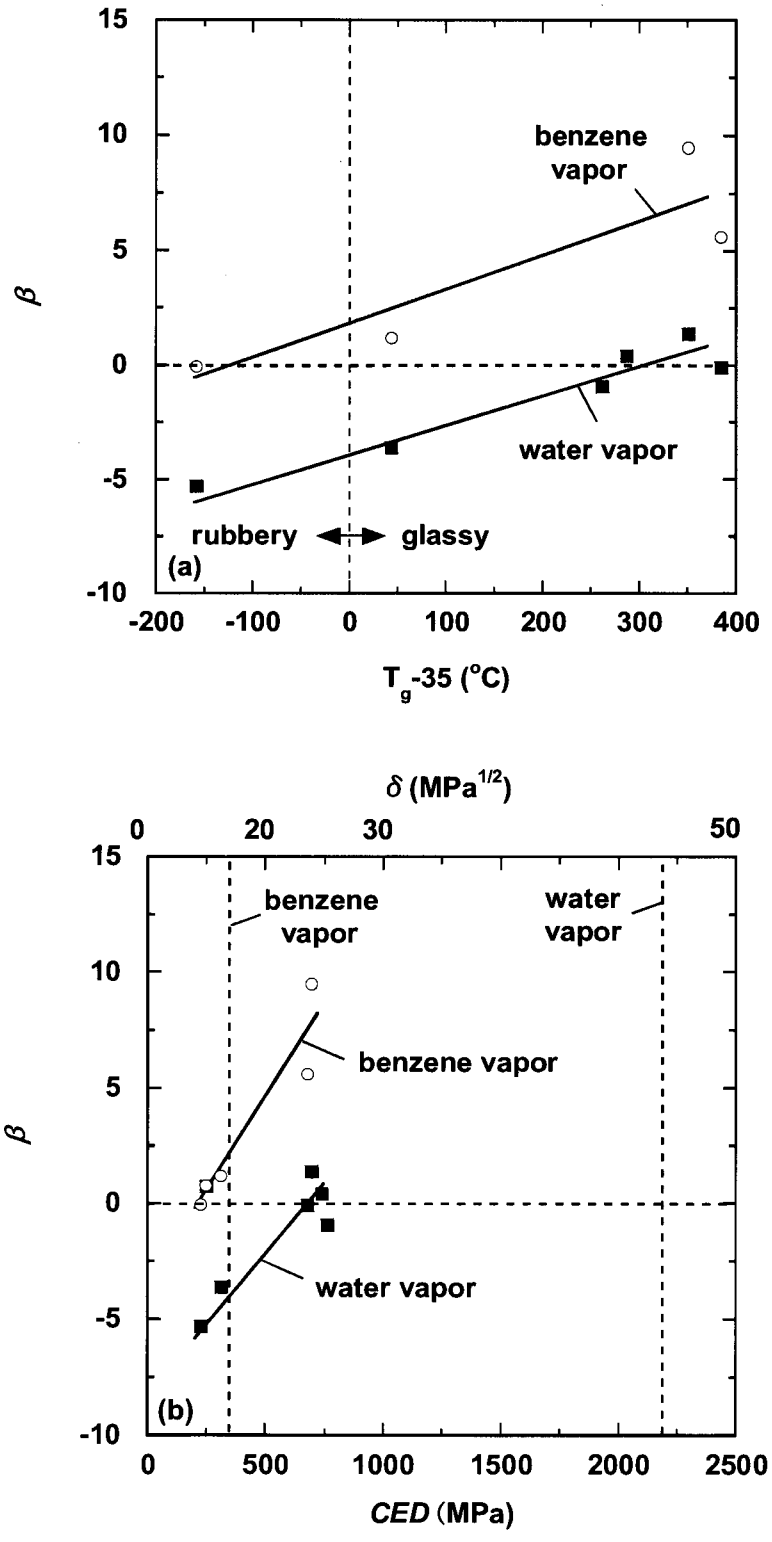

Figure 2. 6 The constant characterized the pressure dependence of diffusivity, β, for benzene and water vapors at 35°C in silicon- or fluorine-containing polymers as a function of (a) glass transition temperature, T_g, and (b) polymer cohesive energy density, *CED*. Penetrants; benzene vapor (○), water vapor (■).

2.4.3. Solubility

The solubility coefficients of silicon- and fluorine-containing polymers for benzene and water vapors at 35°C as a function of p/p_{sat} across a polymer membrane are presented in Figure 2. 7. As the benzene vapor solubility of 6FDA-mPD and 6FDA-MPD could not be monitored for 2 days at 1.54 cmHg (p/p_{sat} = 0.1), it was not determined.

In the whole range of relative pressures, silicon-containing polymers showed smaller solubility of benzene and water vapors than fluorine-containing polymers. The solubility coefficient of benzene vapor was in the order of 1 cm^2 (STP)/(cm^3 cmHg) for PDMS, 10^{-1} cm^2 (STP)/(cm^3 cmHg) for PTMSMMA, 10 cm^2 (STP)/(cm^3 cmHg) for PTMSP, and $10–10^2$ cm^2 (STP)/(cm^3 cmHg) for 6FDA-TMPD and 6FDA-TeMPD, while that of water vapor was in the order of 10^{-2} cm^2 (STP)/(cm^3 cmHg) for PDMS, 10^{-1} cm^2 (STP)/(cm^3 cmHg) for PTMSMMA, 1 cm^2 (STP)/(cm^3 cmHg) for PTMSP, and $10–10^2$ cm^2 (STP)/(cm^3 cmHg) for all 6FDA-based polyimides.

The benzene vapor solubility of PTMSP showed less pressure dependency. As the relative feed pressure increased, the benzene vapor solubility of PTMSMMA decreased, whereas that of PDMS, 6FDA-TMPD, and 6FDA-TeMPD increased. The water vapor solubility of all polymers in this study increased as the relative feed pressure increased.

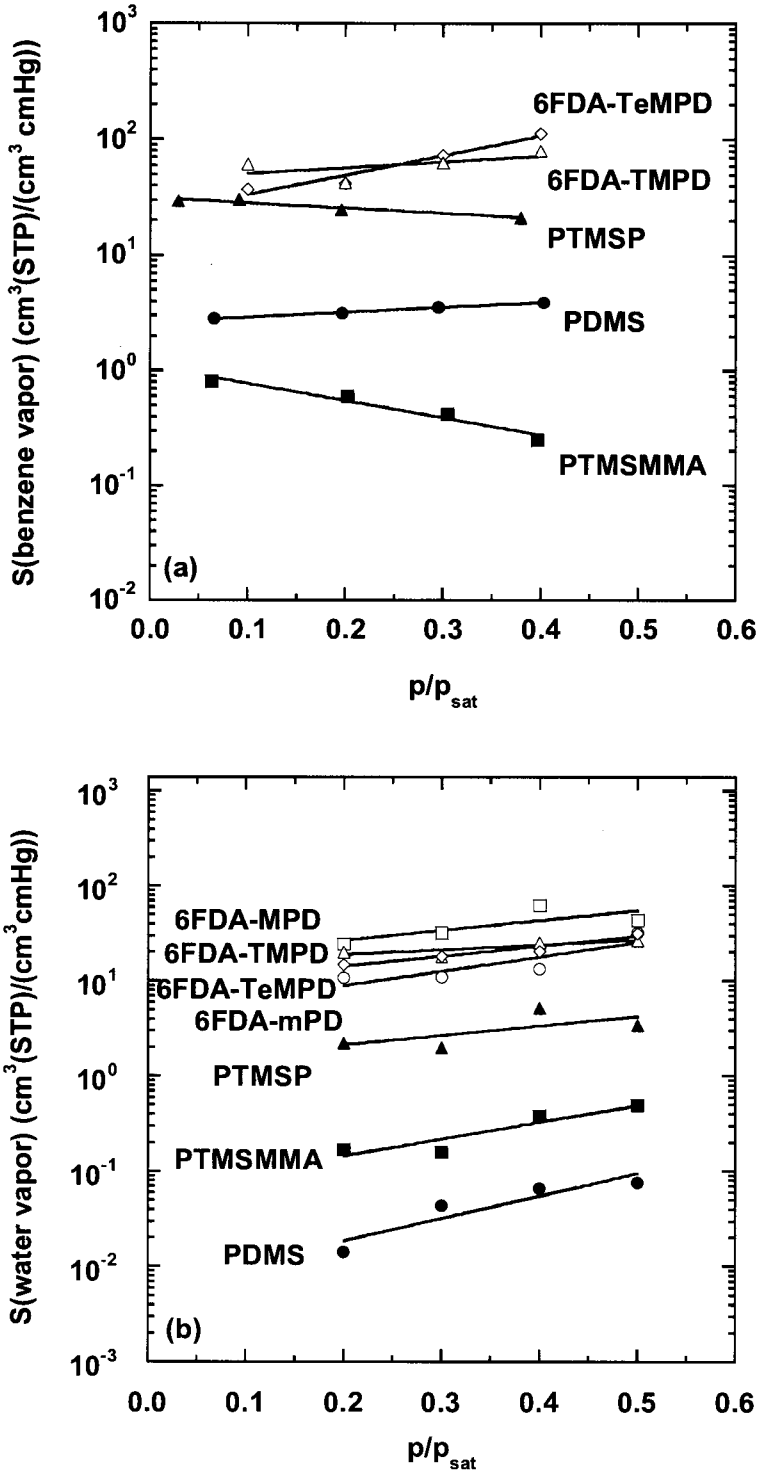

Figure 2. 7 Solubility coefficients of (a) benzene vapor and (b) water vapor in silicon- or fluorine-containing polymers as a function of the relative feed pressure difference, p/p_{sat}, at 35°C. Polymers: PDMS (●), PTMSMMA (■), PTMSP (▲), 6FDA-mPD (○), 6FDA-MPD (□), 6FDA-TMPD (△), 6FDA-TeMPD (◇).

As shown in Figure 2. 7, there was a linear relationship between vapor solubility and relative feed pressure in all membranes. It can be represented as follows:

$$S = S_0 \exp(\gamma \frac{p}{p_{sat}}) \qquad (2.\ 7)$$

where S_0 is the infinite-dilution solubility coefficient at $p/p_{sat} = 0$, and γ is a parameter that characterizes the pressure dependence of solubility coefficients.

Tables 2. 2 and 2. 3 summarize S_0 and γ values of silicon- and fluorine-containing polymers for benzene and water vapors, respectively. The ranking of S_0 was 6FDA-TMPD > PTMSP > 6FDA-TeMPD > PDMS > PTMSMMA for benzene vapor and 6FDA-MPD > 6FDA-TMPD > 6FDA-TeMPD > 6FDA-mPD > PTMSP > PTMSMMA > PDMS for water vapor. The ranking of γ was 6FDA-TeMPD > 6FDA-TMPD > PDMS > PTMSP > PTMSMMA for benzene vapor and PDMS > PTMSMMA > 6FDA-mPD > 6FDA-TeMPD > 6FDA-MPD > PTMSP > 6FDA-TMPD for water vapor.

The S_0 of silicon- and fluorine-containing polymers for benzene vapor and for water vapor as a function of the γ across a polymer membrane are presented in Figure 2. 8. The S_0 of benzene vapor was located from 1 to 10 cm^2 (STP)/(cm^3 cmHg) in the positive and negative area of γ , while the water vapor decreased from 10 to 10^{-3} cm^2 (STP)/(cm^3 cmHg) as the γ increased in the positive area. The solubility for benzene vapor showed both dual-mode sorption mode and plasticization, while the solubility for water vapor showed plasticization.

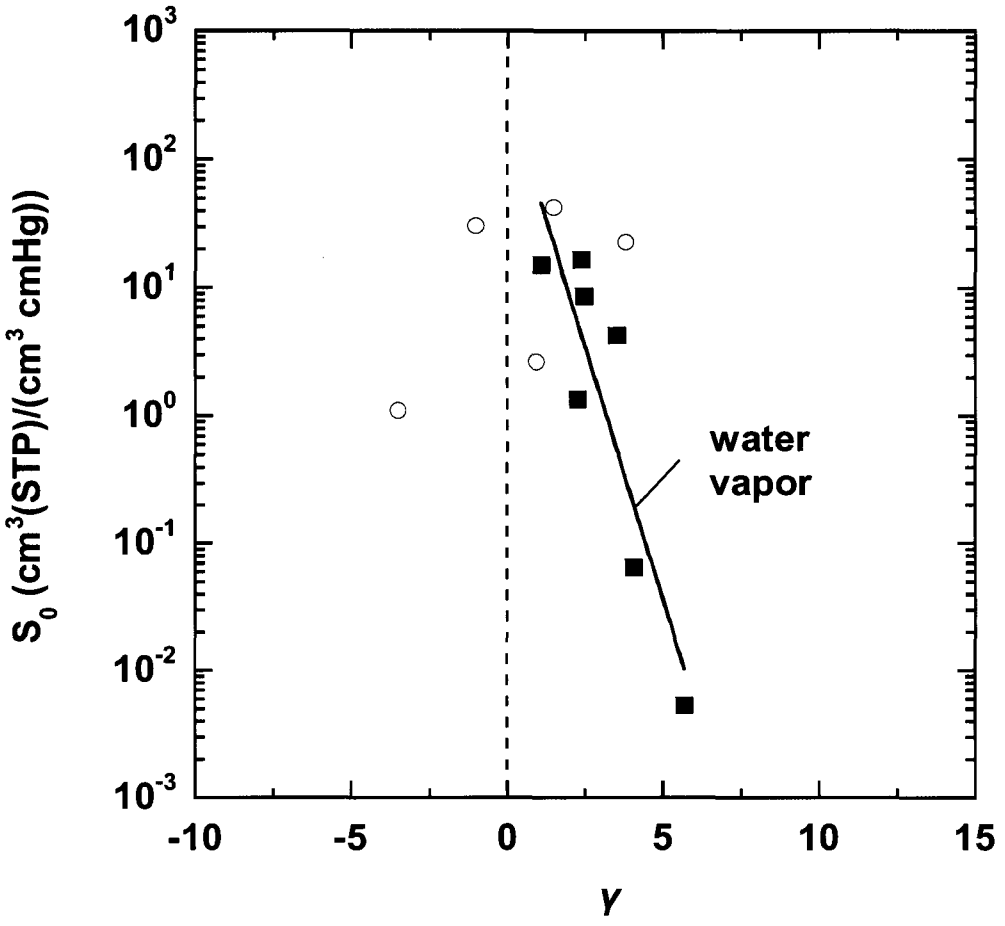

Figure 2. 8 The infinite-dilution solubility coefficient, S_0, of silicon- and fluorine-containing polymers as a function of the constant characterized by the pressure dependence of solubility, γ. Penetrants; benzene vapor (○), water vapor (■).

Solubility is expected to be dependent on chain mobility (e.g., T_g) and molecular polarity (e.g., δ). The S_0 of silicon- and fluorine-containing polymers for benzene vapor and for water vapor as a function of T_g, δ, and *CED* across a polymer membrane are presented in Figure 2. 9. All polymer membranes in this study showed higher benzene vapor solubility than water vapor solubility (Figure 2. 9(a)). The S_0 increased from 1–10 cm^2 (STP)/(cm^3 cmHg) for benzene vapor and 10^{-3} to 10 cm^2 (STP)/(cm^3 cmHg) for water vapor as T_g increased. The solubility settled as T_g increased. This result indicates that S_0 increased as the mobility of polymer decreased.

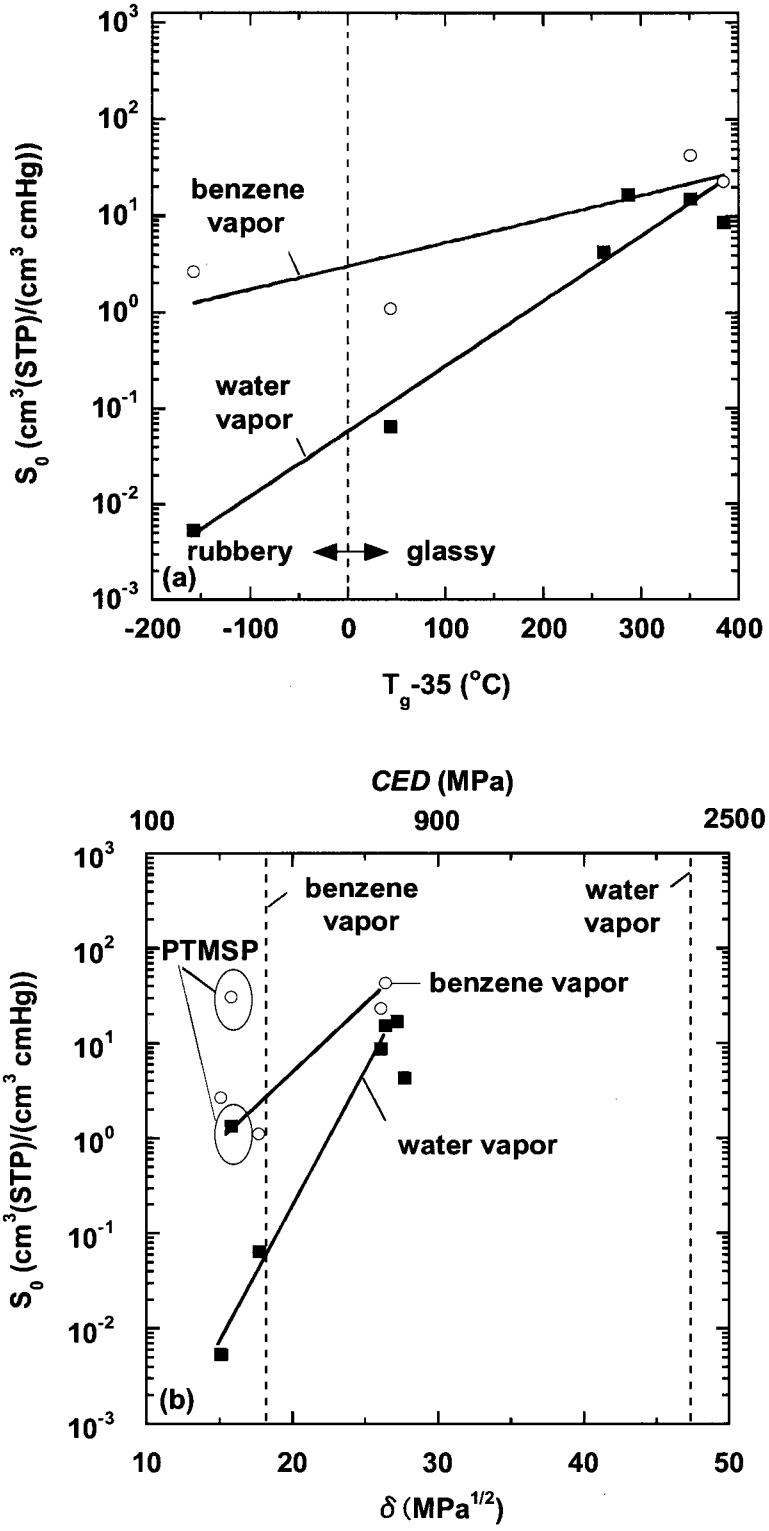

Figure 2. 9 The infinite-dilution solubility coefficient, S_0, for benzene and water vapors at 35°C in silicon- or fluorine-containing polymers as a function of (a) glass transition temperature, T_g, and (b) polymer solubility parameter, δ. Penetrants; benzene vapor (○), water vapor (■).

Generally, glassy polymers show higher vapor solubility than rubbery. Moreover, if the value of δ for vapor is near to that of polymer, the solubility increases. Like general cases, the S_0 located from 1 to 10 cm^2 (STP)/(cm^3 cmHg) for benzene vapor as δ increased, except for PTMSP (Figure 2. 9(b)), and increased from 10^{-3} to 10 cm^2 (STP)/(cm^3 cmHg) as δ neared the value of water vapor, except for that. The reason why PTMSP did not obey the rule was unclear.

The relationship between γ and the physical properties of polymer membrane was also studied. The γ of silicon- and fluorine-containing polymers for benzene vapor and for water vapor as a function of T_g, δ, and *CED* across a polymer membrane are presented in Figure 2. 10. The positive value of γ showed plasticization, while the opposite value showed dual-mode sorption behavior. If γ approaches near zero, it exhibits the Henry-law behavior.

In the case of benzene vapor, there was no tendency for wide distribution from the positive to the negative area at each T_g (Figure 2. 10(a)). On the other hand, the γ decreased in the positive area for water vapor as T_g increased. This result indicates that it was difficult to cause plasticization because the mobility of the polymer chain decreased. There was no relationship between the γ of benzene vapor and water vapor and δ (Figure 2. 10(b)). In other word, there was no dependency between the γ of the water vapor and affinity of polymer and vapor.

These results in Figures 2. 9 and 2. 10 indicate that like common polymer, the high free volume polymers obeyed the solubility rule at infinite dilution. The solubility of the polymers increased as polymer mobility had larger decreased and as affinity of polymer and vapor increased. However, there was no clear rule with plasticization behavior and physical properties of polymers and vapors.

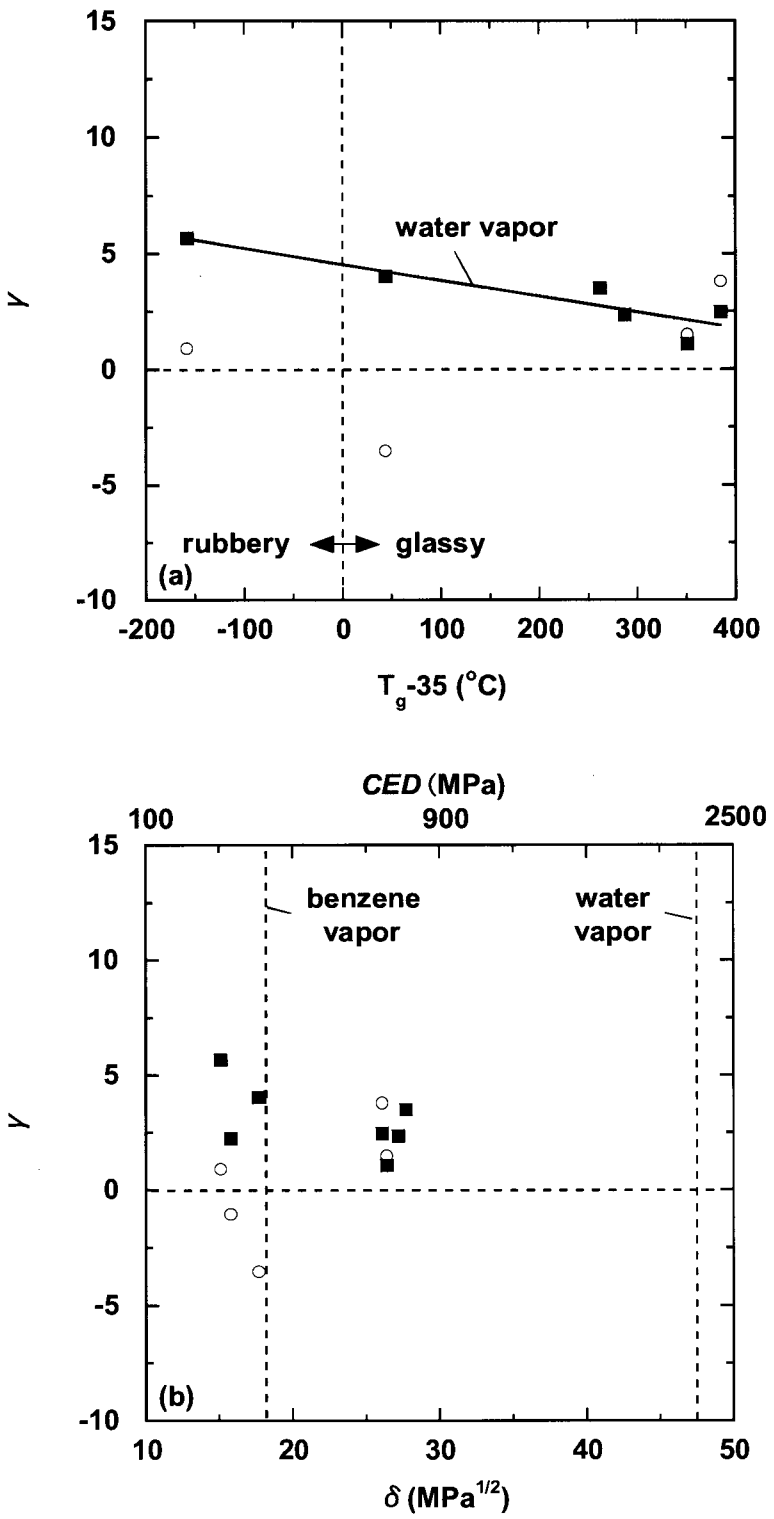

Figure 2. 10 The constant characterized by the pressure dependence of solubility, γ, for benzene and water vapors at 35°C in silicon- or fluorine-containing polymers as a function of (a) glass transition temperature, T_g, and (b) polymer solubility parameter, δ. Penetrants; benzene vapor (○), water vapor (■).

2.4.4. Permeability

The permeability coefficients of silicon- and fluorine-containing polymers for benzene and water vapors at 35°C as a function of p/p_{sat} across a polymer membrane are presented in Figure 2. 11. As the benzene vapor permeability of 6FDA-mPD and 6FDA-MPD could not be monitored for 2 days at 1.54 cmHg (p/p_{sat} = 0.1), it was estimated that the benzene vapor permeability coefficients of 6FDA-mPD and 6FDA-MPD were below the order of 10^{-11} cm^3(STP)cm/(cm^2 s cmHg).

PDMS and PTMSP showed high benzene vapor permeability among the polymers in this study. The permeability coefficient of benzene vapor was in the order of 10^{-5} cm^3(STP)cm/(cm^2 s cmHg) for PDMS and PTMSP, 10^{-8} cm^3(STP)cm/(cm^2 s cmHg) for PTMSMMA, and 10^{-9}–10^{-7} cm^3(STP)cm/(cm^2 s cmHg) for 6FDA-TMPD and 6FDA-TeMPD, while that of water vapor was in the order of 10^{-6} cm^3(STP)cm/(cm^2 s cmHg) for PDMS, PTMSP, 6FDA-TMPD, and 6FDA-TeMPD, and 10^{-7} cm^3(STP)cm/(cm^2 s cmHg) for PTMSMMA, 6FDA-mPD, and 6FDA-MPD.

Compared with other polymers, the benzene vapor permeability of PDMS and PTMSP showed less pressure dependency. As the relative feed pressure increased, the benzene vapor permeability of PTMSMMA decreased, whereas that of 6FDA-TMPD and 6FDA-TeMPD increased. The water vapor permeability of all polymers in this study increased as the relative feed pressure increased.

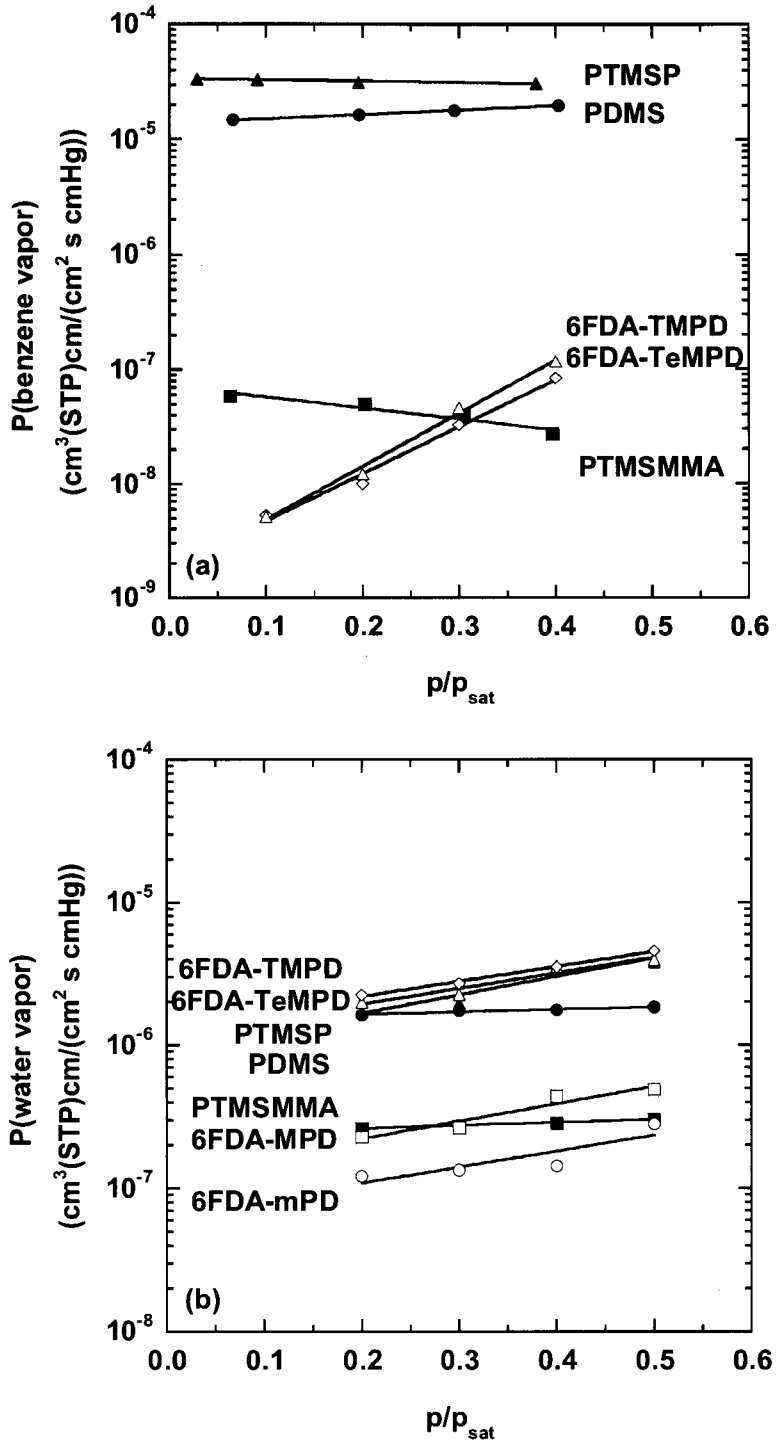

Figure 2. 11 Permeability coefficients of (a) benzene vapor and (b) water vapor in silicon- or fluorine-containing polymers as a function of the relative feed pressure difference, p/p_{sat}, at 35°C. Polymers: PDMS (●), PTMSMMA (■), PTMSP (▲), 6FDA-mPD (○), 6FDA-MPD (□), 6FDA-TMPD (△), 6FDA-TeMPD (◇).

As is evident from Figure 2. 11, there was a linear relationship between vapor permeability and relative feed pressure in all the polymers. In general, glassy polymers show dual-mode transport behavior during gas permeation at a lower relative pressure [3]. Gas-induced plasticization behavior sometimes appears at high relative pressure. It is difficult to explain these phenomena for vapor permeation using the dual-mode transport behavior. Therefore, according to the solution-diffusion mechanism, the lines in this figure are represented as follows:

$$P = D \times S = D_0 \, exp(\beta \frac{p}{p_{sat}}) \cdot S_0 \, exp(\gamma \frac{p}{p_{sat}}) \qquad (2.\ 8)$$

where P_0 is the infinite-dilution permeability coefficient at $p/p_{sat} = 0$ (i.e., $D_0 \cdot S_0$), and the slope, α, characterizes the pressure dependence of permeability (i.e., $\beta+\gamma$).

Tables 2. 2 and 2. 3 summarize the P_0 and α values of silicon- and fluorine-containing polymers for benzene and water vapors, respectively. The ranking of P_0 was PTMSP > PDMS > PTMSMMA > 6FDA-TeMPD > 6FDA-TMPD for benzene vapor and PDMS > 6FDA-TeMPD > 6FDA-TMPD > PTMSP > PTMSMMA > 6FDA-MPD > 6FDA-mPD for water vapor. The ranking of α was 6FDA-TMPD > 6FDA-TeMPD > PDMS > PTMSP > PTMSMMA for benzene vapor and PTMSP > 6FDA-MPD > 6FDA-mPD > 6FDA-TMPD > 6FDA-TeMPD > PDMS > PTMSMMA for water vapor.

The P_0 of silicon- and fluorine-containing polymers for benzene vapor and for water vapor as a function of the α across a polymer membrane are presented in Figure 2. 12. The P_0 decreased from 10^{-5} to 10^{-9} cm^3(STP)cm/(cm^2 s cmHg) for benzene vapor as the α increased from the negative to positive area. On the other hand, that of water vapor was located from 10^{-6} to 10^{-8} cm^3(STP)cm/(cm^2 s cmHg) in the positive area near

zero. When we considered diffusivity and solubility (Figures 2. 4 and 2. 8), benzene vapor permeability showed diffusivity controlled behavior, while water vapor permeability showed diffusivity and solubility controlled behavior. Hence, water vapor permeability settled at a definite value. In each parameter of permeability, we systematically studied the relationship between the physical properties of polymer membranes and these parameters.

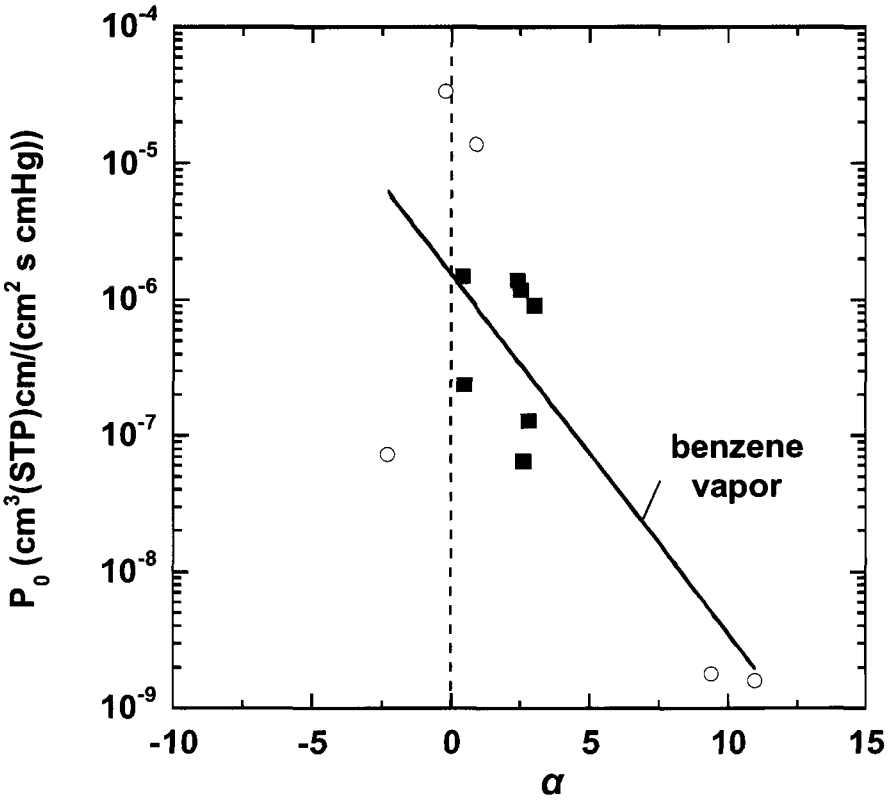

Figure 2. 12 The infinite-dilution permeability coefficient, P_0, of silicon- and fluorine-containing polymers as a function of the constant characterized the pressure dependence of permeability, α. Penetrants; benzene vapor (○), water vapor (■).

Permeability is dependent on either diffusion or solution factor or balance of them. The P_0 of silicon- and fluorine-containing polymers for benzene vapor and for water vapor as a function of T_g, *CED*, and δ across a polymer membrane are presented in Figure 2. 13.

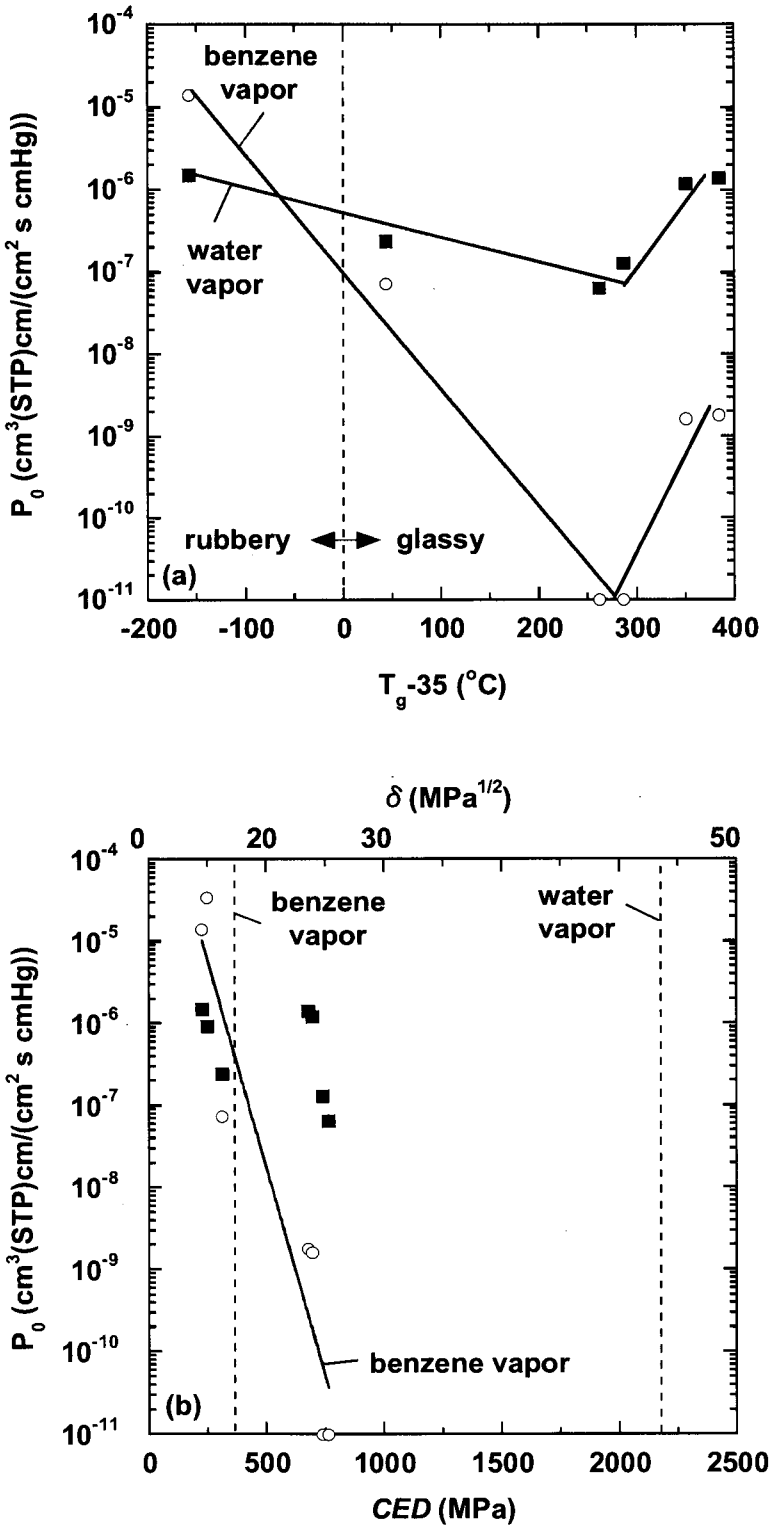

Figure 2. 13 The infinite-dilution permeability coefficient, P_0, for benzene and water vapors at 35°C in silicon- or fluorine-containing polymers as a function of (a) glass transition temperature, T_g, and (b) polymer cohesive energy density, *CED*. Penetrants; benzene vapor (○), water vapor (■).

The order of P_0 in rubbery was benzene vapor > water vapor, while that of glassy was the opposite. In the polymer membrane where $T_g - 35$ was less than 250°C, the permeability decreased from 10^{-5} to 10^{-11} cm^3(STP)cm/(cm^2 s cmHg) for benzene vapor and from 10^{-6} to 10^{-8} cm^3(STP)cm/(cm^2 s cmHg) for water vapor as T_g increased (Figure 2. 13(a)). On the other hand, in the polymer membrane where $T_g - 35$ was more than 250°C, the permeability increased from 10^{-11} to 10^{-9} cm^3(STP)cm/(cm^2 s cmHg) for benzene vapor and from 10^{-8} to 10^{-6} cm^3(STP)cm/(cm^2 s cmHg) for water vapor as T_g increased.

In the polymer membrane where *CED* was less than 300 MPa, the order of P_0 was benzene vapor > water vapor, while that where *CED* was more than 300 MPa showed the opposite behavior. (Figure 2. 13(b)). The P_0 decreased from 10^{-4} to 10^{-11} cm^3(STP)cm/(cm^2 s cmHg) for benzene vapor, and it was located from 10^{-8} to 10^{-6} cm^3(STP)cm/(cm^2 s cmHg) for water vapor as *CED* increased.

These dependences of T_g and *CED* on P_0 were dependent on those on D_0 (Figure 2. 5) as compared to those on S_0 (Figure 2. 9). The P_0 of benzene vapor and water vapor was diffusion controlled and did not depend on either the mobility of the polymer segments, the space between polymer segments, or polymer cohesiveness but was dependent on the balance among them.

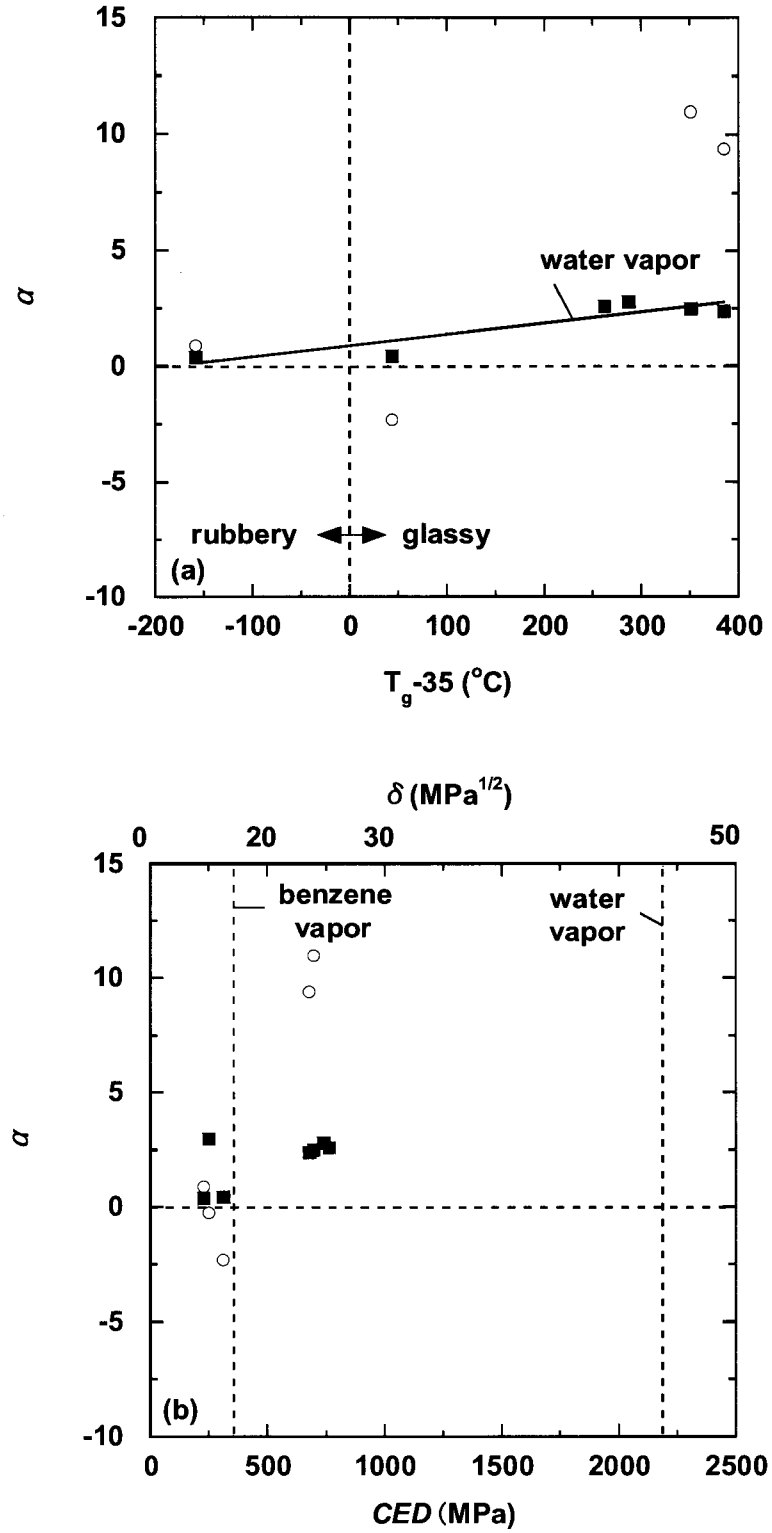

Figure 2. 14 The constant characterized by the pressure dependence of permeability, α, for benzene and water vapors at 35°C in silicon- or fluorine-containing polymers as a function of (a) glass transition temperature, T_g, and (b) polymer cohesive energy density, *CED*. Penetrants; benzene vapor (○), water vapor (■).

The relationship between α and the physical properties of the polymer membrane was also studied. The α of silicon- and fluorine-containing polymers for benzene vapor and for water vapor as a function of T_g, *CED*, and δ across a polymer membrane are presented in Figure 2. 14. The positive α value showed plasticization, while the opposite value showed dual-mode sorption behavior in glassy polymer membrane. If α nears zero, it shows that there is no dependence on both of them.

In the case of benzene vapor, there was no tendency for wide distribution from the positive to the negative area at each T_g (Figure 2. 14(a)). On the other hand, the α increased in the positive area for water vapor as T_g increased. In the entire range of *CED*, the α of benzene vapor dispersed in the positive and negative area, while that of water vapor was located in the positive area at about zero. From β (Figure 2. 6) and γ (Figure 2. 10), the α of benzene vapor and water vapor depended on the tendency of γ more than that of β. This result indicates that the α of benzene vapor was solubility controlled. Therefore, there was no clear rule with plasticization behavior and physical properties of polymers and vapors.

2.4.5. Selectivity

Tables 2. 4 and 2. 5 summarize the ideal diffusivity selectivity, solubility selectivity, and permselectivity for benzene vapor/nitrogen and water vapor/nitrogen in the silicon- and fluorine-containing polymers at 35°C. For vapor separation from air, we used the value of nitrogen at 1 atm.

Table 2. 4 Diffusivity selectivity, solubility selectivity, and permselectivity of benzene vapor over nitrogen in silicon- and fluorine-containing polymer membranes at 35°C

Type	Polymer	$\frac{D_0(benzene\ vapor)}{D_{1atm}(nitrogen)}$	$\frac{S_0(benzene\ vapor)}{S_{1atm}(nitrogen)}$	$\frac{P_0(benzene\ vapor)}{P_{1atm}(nitrogen)}$
Si-containing Polymer	PDMS	0.19	1600	300
	PTMSMMA	0.11	610	73
	PTMSP	0.018	2400	44
F-containig Polymer	6FDA-mPD	< 0.0028	ND[a)]	< 0.18
	6FDA-MPD	< 0.00083	ND[a)]	< 0.05
	6FDA-TMPD	0.00029	3100	0.94
	6FDA-TeMPD	0.00028	1400	0.42

b) Not determined.

Table 2. 5 Diffusivity selectivity, solubility selectivity, and permselectivity of water vapor over nitrogen in silicon- and fluorine-containing polymer membranes at 35°C

Type	Polymer	$\frac{D_0(water\ vapor)}{D_{1atm}(nitrogen)}$	$\frac{S_0(water\ vapor)}{S_{1atm}(nitrogen)}$	$\frac{P_0(water\ vapor)}{P_{1atm}(nitrogen)}$
Si-containing Polymer	PDMS	10	3.2	32
	PTMSMMA	6.4	36	240
	PTMSP	0.011	100	1.2
F-containig Polymer	6FDA-mPD	4.2	270	1100
	6FDA-MPD	0.64	990	650
	6FDA-TMPD	0.60	1100	710
	6FDA-TeMPD	0.57	550	330

All polymer membranes in this study showed less benzene vapor/nitrogen diffusivity selectivity than water vapor/nitrogen diffusivity selectivity. All benzene vapor/nitrogen diffusivity selectivity showed less than 1 (i.e., nitrogen-selective). The water vapor/nitrogen diffusivity selectivity of PTMSP, 6FDA-MPD, 6FDA-TMPD, and 6FDA-TeMPD was also smaller than 1, while PDMS, PTMSMMA, and 6FDA-mPD showed the selectivity of larger than 1 (i.e., vapor-selective). All polymer membranes in this study showed higher benzene vapor/nitrogen solubility selectivity than water

vapor/nitrogen solubility selectivity. The benzene vapor/nitrogen and water vapor/nitrogen solubility selectivity values were more than 1. Both showed vapor solubility selective behavior.

All silicon-containing polymers used in this study showed benzene vapor/nitrogen permselectivity of larger than 1 (i.e., benzene vapor-permselective), while all fluorine-containing polymers had the opposite property (i.e., nitrogen-permselective). All polymers used in this study showed water vapor/nitrogen permselectivity of larger than 1 (i.e., water vapor-permselective). According to equation (2.5), the benzene vapor/nitrogen permselectivity depended on diffusivity selectivity for fluorine-containing polymers and solubility selectivity for silicon-containing polymers. Additionally, the water vapor/nitrogen permselectivity depended on solubility selectivity for PTMSP, 6FDA-MPD, 6FDA-TMPD, and 6FDA-TeMPD, and both selectivity balance for PDMS, PTMSMMA, and 6FDA-mPD.

2.5. CONCLUSIONS

The P_0 of benzene vapor and water vapor through high free volume silicon- or fluorine-containing polymers used in this study was diffusion controlled and did not depend on either the mobility of the polymer segments, the space between polymer segments, or polymer cohesiveness but was dependent on the balance among them. All silicon-containing polymers used in this study showed benzene vapor-permselective behavior while all fluorine-containing polymers had the opposite property (i.e., nitrogen-permselective). All polymers used in this study showed water vapor-permselective behavior. The benzene vapor/nitrogen permselectivity depended on diffusivity selectivity for fluorine-containing polymers and solubility selectivity for

silicon-containing polymers. The water vapor/nitrogen permselectivity depended on solubility selectivity for PTMSP, 6FDA-MPD, 6FDA-TMPD, and 6FDA-TeMPD, and both selectivity balance for PDMS, PTMSMMA, and 6FDA-mPD.

2.6. REFERENCES

[1] New Energy and Industrial Technology Development Organization (NEDO) Report. (2003)

[2] B.E. Poling, *The Properties of Gases and Liquids*, McGraw-Hill, New York, United States. (2001)

[3] R. W. Baker, *Membrane Technology and Applications*, McGraw-Hill, New York, United States. (2000)

[4] S.V. Dixon-Garrett, K. Nagai, B.D. Freeman, Ethylbenzene solubility, diffusivity, and permeability in poly(dimethylsiloxane), *J. Polym. Sci.: Part B: Polym. Phys.* **38** (2000) 1461-1473.

[5] S. Miyata, S. Sato, K. Nagai, T. Nakagawa, K. Kudo, Relationship between gas transport properties and fractional free volume determined from dielectric constant in polyimide films containing the hexafluoroisopropylidene group, *J. Appl. Polym. Sci.* **107** (2008) 3933-3944.

[6] K. Nagai, T. Nakagawa, Effects of aging on the gas permeability and solubility in poly(1-trimethylsilyl-1-propyne)membranes synthesized with various catalysts, *J. Membrane Sci.* **105** (1995) 261-272.

[7] T. Nakagawa, S. Nagashima, A. Higuchi, Synthesis and gas transport properties of new copolymer membranes with trimethylsilyl group, *Desalination.* **90** (1992) 183-192.

[8] D. W. van Krevelen, *Properties of Polymers. Third Ed.*, Elsevier, Amsterdam, Netherlands. (1990)

[9] R. F. Fedors, A method for estimating both the solubility parameters and molar volumes of liquids, *Polym. Eng. Sci.* **14** (1974) 147-154.

[10] K. Nagai, T. Masuda, T. Nakagawa, B.D. Freeman, I. Pinnau, Poly[1-(trimethylsilyl)-1-propyne] and related polymers: synthesis, properties and functions, *Prog. Polym. Sci.* **26** (2001) 721-798.

[11] J. Crank, G.S. Park, *Diffusion in polymers*, Academic Press, London. (1968)

[12] S. Kanehashi, K. Nagai, Analysis of dual-mode model parameters for gas sorption in glassy polymers, *J. Membrane Sci.* **253** (2005) 117-138.

Chapter 3

RELATIONSHIP BETWEEN GAS TRANSPORT PROPERTIES AND REFRACTIVE INDEX IN HIGH FREE VOLUME FLUORINE-CONTAINING POLYIMIDE MEMBRANES

3.1. ABSTRACT

The refractive index and gas transport properties (i.e., permeability, diffusivity, and solubility) in the 4,4-(hexafluoro-isopropylidene) diphthalic anhydride (6FDA) -based polyimides were systematically investigated in terms of their polymer *FFV*s. The permeability and diffusion coefficients of the 6FDA-based polyimide membranes to hydrogen, oxygen, nitrogen, methane, and carbon dioxide were correlated with their *FFV*s estimated using van Krevelen's group contribution method. Linear correlations were also observed between the gas transport properties and refractive index of these polyimides. We discribed *FFV* as a function of the refractive index based on Lorentz-Lorenz equation. Linear correlations were observed between their refractive index-based *FFV* and gas permeability, diffusivity, and solubility coefficients of these 6FDA-based polyimides membranes. However, the FFVs of the 6FDA-based polyimides calculated from refractive index were 1.16–1.37 times larger than their *FFV* values. This *FFV* was dependent on free-volume space and optical factors, such as refractive index and molar refraction, which affected the electronic structure and the interactions between the gas molecules and the polymer segments.

Keywords: fluorine-containing polyimide; refractive index; fractional free volume; gas permeation; gas diffusion

3.2. INTRODUCTION

The optical property of polymer materials is very important property in designing optic devices. Amorphous transparent polymer components are indispensable for such applications because they are used for the manufacture of optical fiber [1], compact discs [2], and display materials [3]. As a factor contributing to transparency, the reflection / absorption / dispersion properties of photon are necessary in designing optics polymer materials, particularly, the development of anti-reflection films that possess surfaces able to prevent optical reflection from the outside. The material characteristic of reflectance is important in next-generation displays. The effect of reflectance on the refractive index of materials may be evaluated by Fresnel's equation [4].

$$R = \left(\frac{n-1}{n+1}\right)^2 \qquad (2.\ 1)$$

where R is the reflectance and n is the refractive index of materials. A low refractive index is necessary for next-generation anti-reflection films. Refractive index is the ratio of the velocity of the photon in the vacuum and material. In material properties, this is the standard of diffusivity of the photon. Refractive index is one of the important parameters for clarifying material structure [5].

The permeability of small molecules is also a very important property for next-generation anti-reflection films in order to prevent material degradation (e.g., oxidation), caused by air exposure during use. The barrier property of carbon dioxide

is necessary for packing materials. In designing anti-reflection films, considering the relationship between its refractive index and gas transport properties (i.e., permeability, diffusivity, and solubility) is crucial. However, there is no physical chemistry-based linkage between mass transport and refractive index.

Among polymer materials, polyimides have higher heat and chemical resistance properties; thus, they are widely used as electronics materials, such as in overcoats of semiconductors and interlayer insulation films. The refractive index of general polyimides is more than 1.6, and Kapton is 1.78 [6-9]. However, the fluorine-containing polyimides are expected to show higher heat resistance, as well as lower dielectric constant and refractive index. Fluorine atom has high electronegativity, whereas C–F combination has high binding energy and low polarizability. Thus, fluorine-containing polyimides have high potential as materials in electronic applications [10,11]. Furthermore, fractional free volume (*FFV*), which is standard of the space between polymers segments, increases upon introduction of substituent that have high volume among atoms, such as fluorine atom.

Polymers with higher *FFV* have greater permeabilities and diffusivities. Based on the free-volume theory, the logarithm of the permeability and diffusion coefficients of small molecules in a polymer is linearly correlated with the reciprocal of its *FFV* [12]. However, even though polymers have the same *FFV*s, their gas permeabilities and diffusivities are not identical. This is one of the reasons *FFV* is calculated using group contribution method. For instance, the carbon dioxide diffusion coefficient in various types of polymers with an *FFV* value of 0.18 varies from 10^{-6} to 10^{-8} cm^2/s [13].

Hence, this study systematically investigates the refractive index and

permeabilities of various gases (i.e., hydrogen, oxygen, nitrogen, and methane, as well as carbon dioxide) in a family of 4,4-(hexafluoro-isopropylidene) diphthalic anhydride (6FDA)-based polyimides in terms of their *FFV*s. Based on Lorentz-Lorenz equation, the *FFV* of the polymer as a function of its refractive index is described. The relationship between the gas transport properties (i.e., permeability, diffusivity, and solubility) and the refractive index-based polymer *FFV* is also investigated.

3.3. EXPERIMENTAL

3.3.1. Membrane preparation

The 6FDA-based polyimides membranes used in this research were the same samples employed in our previous study [14]. The chemical structure of each product, as shown in Figure 3. 1, was confirmed by infrared (IR) and unclear magnetic resonance (NMR) analyses. The 6FDA-based polyimides were 6FDA-1,3-phenylene diamine (mPD), 6FDA-4-methyl-1,3-phenylene diamine (MPD), 6FDA-2,4,6-trimethyl-1,3-phenylene diamine (TMPD), and 6FDA-2,3,5,6-tetramethyl-1,4-phenylene diamine (TeMPD). The thickness of the membranes varied from 30 to 40 μm for permeation tests, with uncertainty of ± 2 μm.

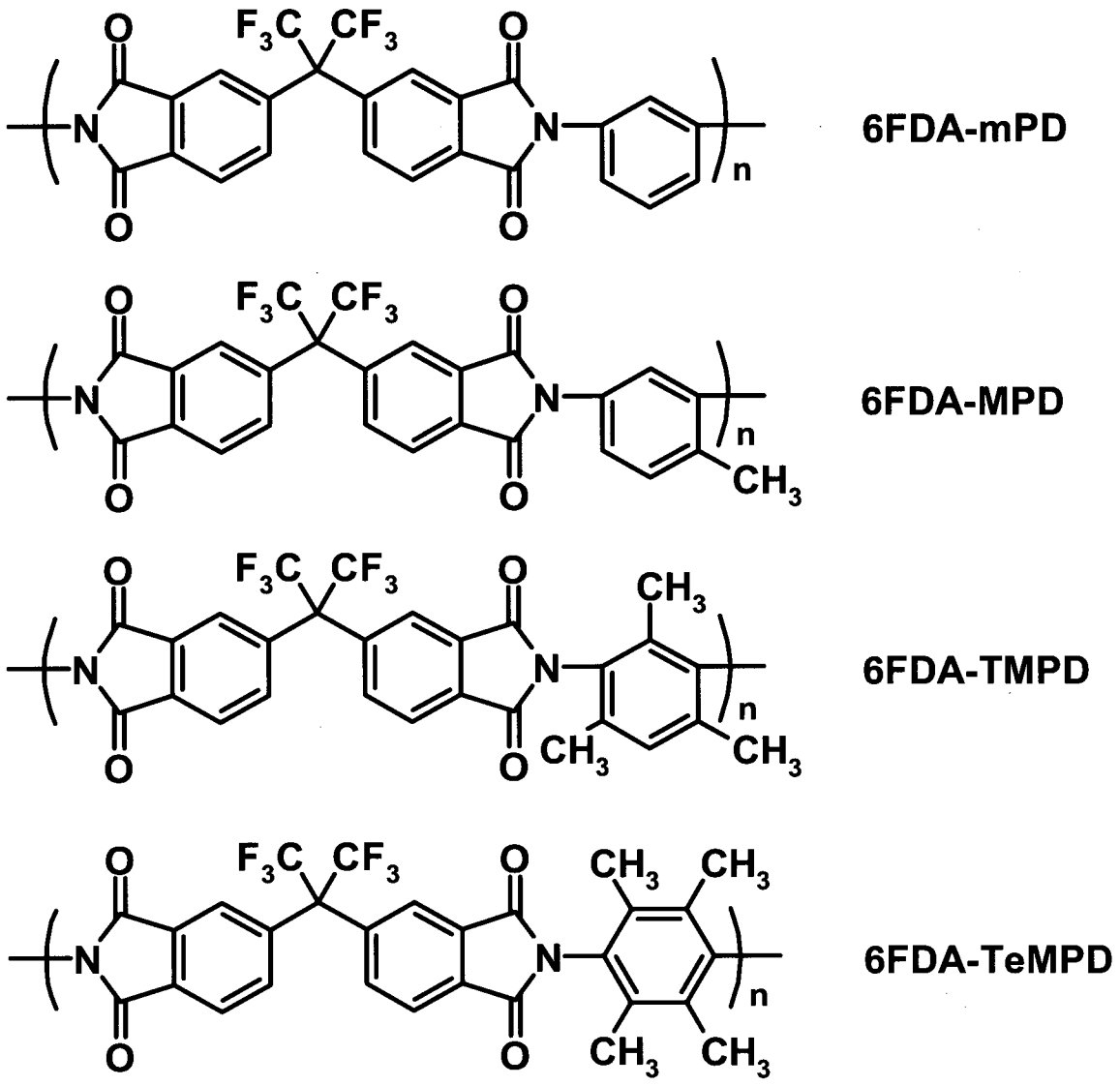

Figure 3. 1 Chemical structures of fluorine-containing polyimides: 6FDA-based polyimides: 4,4-(hexafluoro-isopropylidene) diphthalic anhydride (6FDA), 1,3-phenylene diamine (mPD), 4-methyl-1,3-phenylene diamine (MPD), 2,4,6-trimethyl-1,3-phenylene diamine (TMPD), and 2,3,5,6-tetramethyl-1,4-phenylene diamine (TeMPD).

3.3.2. Membrane characterization

All characterization data were determined in membrane state for at least three samples to confirm the reproducibility of the experimental results. Membrane density was determined by flotation of the small membrane samples in a density gradient

column, which was maintained at 23±1°C. FFV is given by

$$FFV = \frac{V_t - 1.3V_W}{V_t} \quad (3.\ 2)$$

where V_t is the polymer specific volume and V_w is the van der Waals volume, which is calculated from the group contribution method of van Krevelen [4].

The thermal analysis data were measured with a Diamond DSC differential scanning calorimeter (Perkin-Elmer, Inc., Shelton, USA) at a heating rate of 10°C/min. Wide-angle X-ray diffraction (WAXD) measurements were performed on a Rint 1200 X-ray diffractometer (Rigaku, Co. Ltd., Tokyo, Japan) using a Cu-Kα radiation source. The wavelength of the radiation was 1.54 Å and the maximum intensity in a halo peak was 2θ.

3.3.3. Optical property measurement

Refractive index measurements were performed on a UVISEL ellipsometry (Jobin Yvon. S.A.S., Longjumeau, France) at 23±1°C. The Abbe number, v_D, is given by [15]

$$v_D = \frac{n_D - 1}{n_F - n_C} \quad (3.\ 3)$$

where n_D is the refractive index at 589 nm, n_F is the refractive index at 486 nm, and n_C is the refractive index at 656 nm. All optical properties were determined for at least three samples to ensure reproducibility of the experimental results.

3.4. RESULTS AND DISCUSSION

3.4.1. Membrane characterization

The 6FDA-polyimides used in this research were the same samples employed in our previous study [14]. The density, ρ, value of the 6FDA-mPD, 6FDA-MPD, 6FDA-TMPD, and 6FDA-TeMPD polyimides were 1.47, 1.42, 1.36, and 1.34 g/cm^3, respectively. The *FFV* values of the 6FDA-mPD, 6FDA-MPD, 6FDA-TMPD, and 6FDA-TeMPD polyimides determined from equation (3. 2) were 0.162, 0.171, 0.177, and 0.177, respectively. The glass transition temperature, T_g, values of the 6FDA-mPD, 6FDA-MPD, 6FDA-TMPD, and 6FDA-TeMPD polyimides were 298°C, 335°C, 380°C, and 427°C, respectively. The T_g value was much higher than the temperature employed in all the permeation measurements. In the gas permeation conditions, all 6FDA-based polyimides were glassy and completely amorphous.

The wavelength dispersions of the refractive index of 6FDA-based polyimides in this study are shown in Figure 3. 2. As wavelength increased, the refractive index decreased. In the whole range of wavelength, the ranking of refractive index was 6FDA-mPD > 6FDA-MPD > 6FDA-TMPD > 6FDA-TeMPD. The n_F, n_D, n_C, and v_D values of the 6FDA-based polyimides, other polyimides, and general polymers are summarized in Table 3. 1 [6-9,15,16]. As the number of the methyl side chain groups in the diamine moiety increased, the refractive index decreased from 1.616 to 1.543 for n_F, from 1.598 to 1.534 for n_D, and from 1.589 to 1.530 for n_C. Additionally, the v_D value increased from 22.13 to 41.14 as the number of the methyl side chain groups in the diamine moiety increased. The refractive index of non-fluorine polyimides showed from 1.595 to 1.78. Hence, polyimides containing the 6FDA group had lower refractive index properties compared with non-fluorine polyimides.

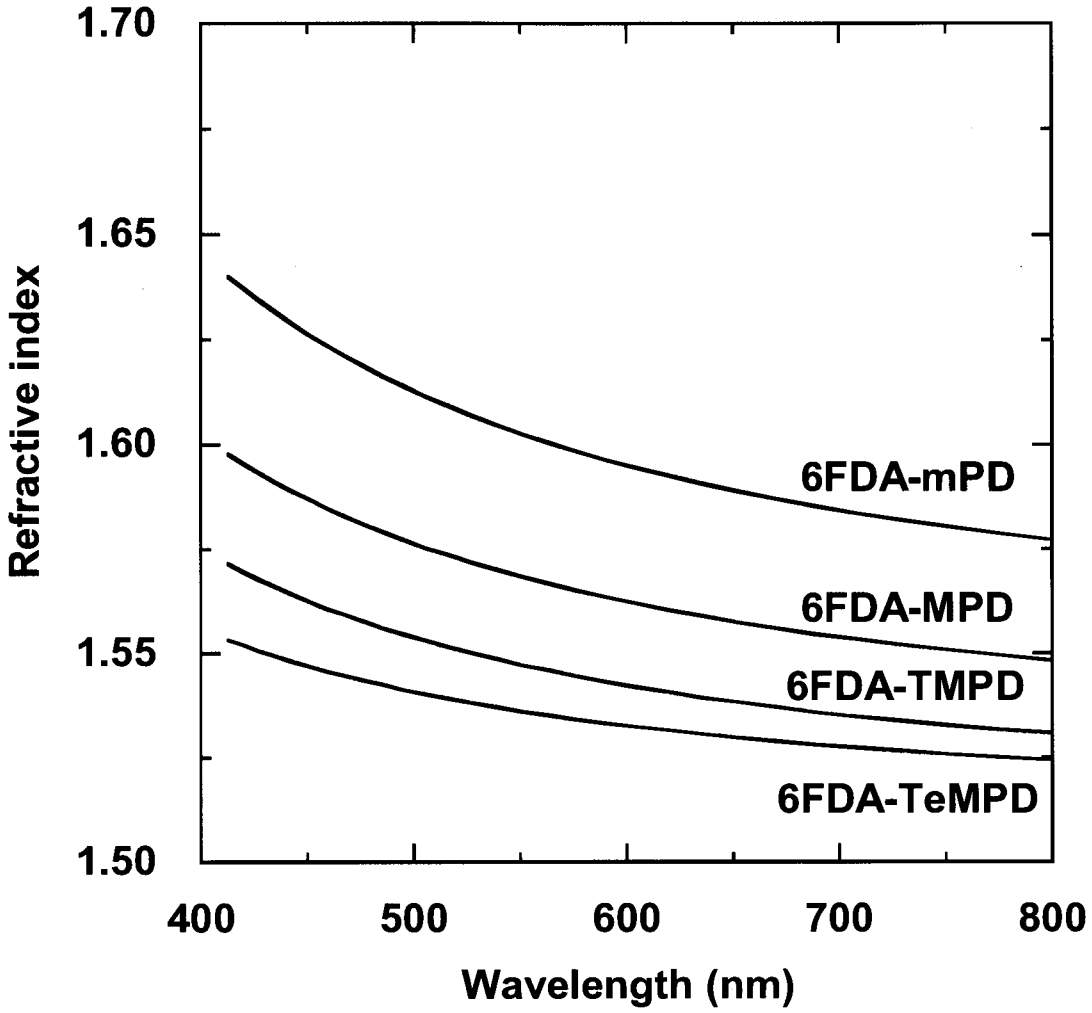

Figure 3. 2 Wavelength dispersion of the refractive index of various polyimides. Polyimides; 6FDA-mPD, 6FDA-MPD, 6FDA-TMPD, 6FDA-TeMPD.

Table 3. 1 Optical properties of the 6FDA-based polyimides, non-fluorine polyimides, and general polymers

Polymer		Refractive index			v_D	Reference
		n_F	n_D	n_C		
Polyimides with F atom	6FDA-mPD	1.616 ± 0.001	1.597 ± 0.001	1.589 ± 0.001	22.13 ± 2.63	This study
	6FDA-MPD	1.579 ± 0.015	1.572 ± 0.010	1.558 ± 0.008	27.24 ± 9.54	This study
	6FDA-TMPD	1.556 ± 0.002	1.544 ± 0.003	1.538 ± 0.003	30.22 ± 1.78	This study
	6FDA-TeMPD	1.543 ± 0.012	1.534 ± 0.013	1.530 ± 0.009	41.14 ± 6.19	This study
Polyimides without F atom	Kapton	–	1.78	–	–	[6]
	Poly(2,2'-bis(methyl)-4,4'-biphenylene pyromellitimide)	–	1.723	–	–	[7]
	Poly(p-phenylene-4,4'-oxydiphthalitimide)	–	1.691	–	–	[7]
	Poly(p-phenylene biphenyltetracarboximide)	–	–	1.771	–	[8]
	Poly(4,4'-biphenylene pyromellitimide)	–	–	1.764	–	[9]
	Poly(p-phenylene pyromellitimide)	–	–	1.743	–	[8]
	Poly(2,2'-bis(fluoro)-4,4'-biphenylene pyromellitimide)	–	–	1.729	–	[9]
	Poly(4,4'-oxydiphenylene pyromellitimide)	–	–	1.700	–	[8]
	Poly(2,2'-bis(methyl)-4,4'-biphenylene pyromellitimide)	–	–	1.695	–	[9]
	Poly(2,2'-bis(methoxy)-4,4'-biphenylene pyromellitimide)	–	–	1.693	–	[9]
	Poly (4,4'-oxydiphenylene benzophenonetetracarboximide)	–	–	1.684	–	[8]
	Poly(2,2-bis(trifluoromethyl)-4,4-biphenylene pyromellitimide)	–	–	1.595	–	[9]
General Polymers	Poly(styrene)	–	1.590	–	30.9	[15]
	Poly(carbonate)	–	1.586	–	29.8	[15]
	Styrene-methyl methacrylate copolymer	–	1.562	–	34.7	[15]
	Epoxy resin	–	1.56	–	36.0	[16]
	Poly(vinyl alcohol)	–	1.55	–	42.0	[16]
	Poly(methyl methacrylate)	–	1.491	–	57.2	[15]
	Poly(4-methyl-1-pentene)	–	1.466	–	56.4	[15]

The Abbe number, v_D, as a function of the refractive index, n_D, of 6FDA-based polyimides and general polymers is presented in Figure 3. 3. The n_D of the 6FDA-based polyimide in this study shows the error of the value determined from at least three samples. Generally, as refractive index increased, the Abbe number decreased. Moreover, the linear correlation between refractive index and Abbe number was also observed [7,16]. As evident from Figure 3. 3, the relationship between refractive index and Abbe number of 6FDA-based polyimides in this study was similar to that of general polymers. This result indicates that the optical data of 6FDA-based polyimides is reliable.

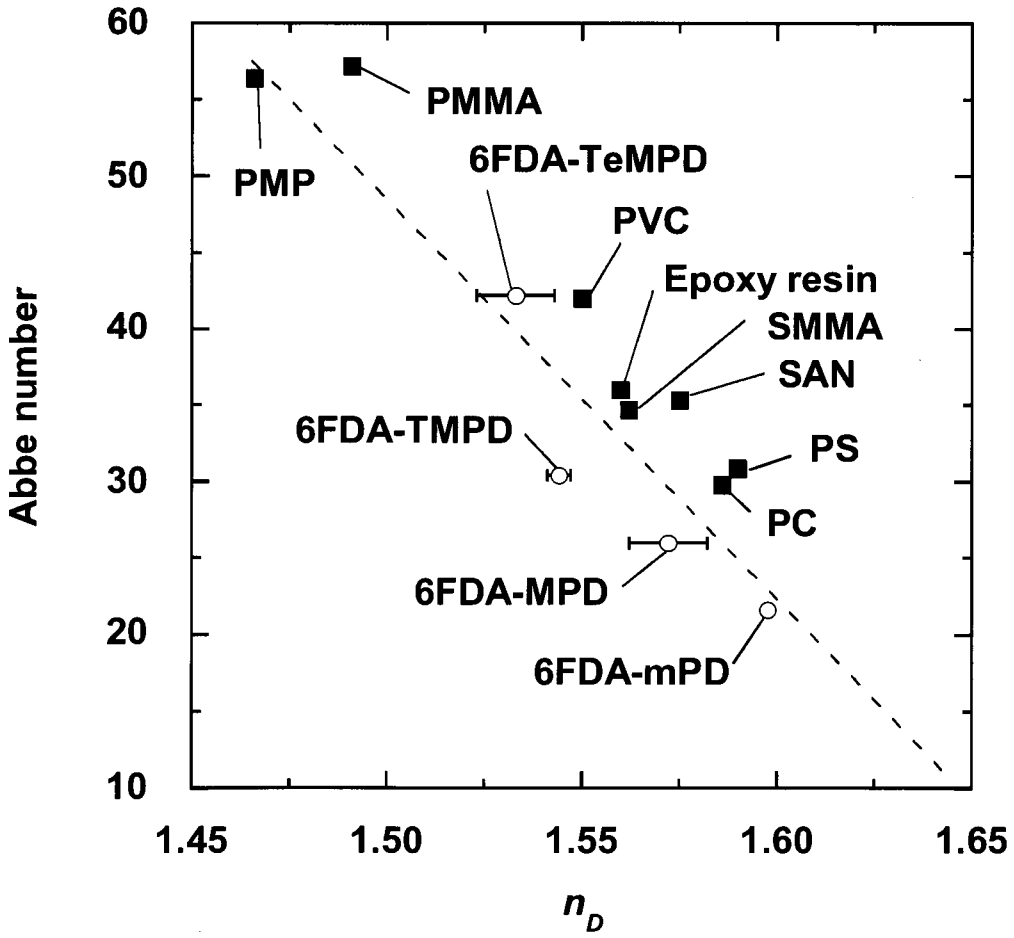

Figure 3. 3 Abbe number as a function of refractive index. Data; 6FDA-based polyimides in this study (○), Ref. [19,20] (■).

The gas permeability, the apparent diffusion, and solubility coefficients at 30°C of the 6FDA-polyimides were similar to the data in the previous study [14]. The free-volume theory provides gas permeability, diffusivity, and solubility as a function of *FFV* [17,18]

$$P = A_P \exp\left(\frac{-B_P}{FFV}\right) \quad (3.\ 4)$$

$$D = A_D \exp\left(\frac{-B_D}{FFV}\right) \quad (3.\ 5)$$

$$S = A_S \exp\left(\frac{-B_S}{FFV}\right) \quad (3.\ 6)$$

where A_P, A_D, A_S, B_P, B_D, and B_S are adjustable constants. The free-volume theory was initially proposed for gas diffusion. Here, A_D and B_D are inherent diffusion parameters that are correlated with the penetrant size and shape. However, these parameters have not been clearly discussed thus far. Other parameters (i.e., A_P, A_S, B_P, and B_S) might be also correlated with the penetrant size and shape. However, similar to A_D and B_D, these parameters have not been discussed in detail. Generally, polymers with larger *FFV* have greater diffusivities. However, even though polymers have the same *FFV*s, their gas diffusivities are not exactly the same. For instance, the carbon dioxide diffusion coefficient in various types of polymers with an *FFV* value of 0.18 varies from 10^{-6} to 10^{-8} cm^2/s [13]. This illustrates the limited usage of the current free-volume theory in 6FDA-TMPD and 6FDA-TeMPD with the same *FFV* value 0.177.

3.4.2. Relationship between gas transport properties and refractive index

Figure 3. 4 presents the gas permeability, diffusion, and solubility coefficients in the 6FDA-based polyimides as a function of the refractive index of D line, which

mainly used general refractive index. For the 6FDA-based polyimides, linear relationships also appeared among the gas permeability, diffusivity, and solubility of hydrogen, oxygen, nitrogen, carbon dioxide, and methane. As the refractive index increased, the gas permeability, diffusion, and solubility coefficients decreased.

Unfortunately, there is no physical chemistry-based linkage between mass transport and photon transport properties. Hence, we described *FFV* as a function of the refractive index based on Lorentz-Lorenz equation, and investigated the relationships between gas transport properties and the refractive index-based polymer *FFV*. Equation (3. 7) is derived from the Lorentz-Lorenz equation, which is used to calculate the refractive index of polymer material [4].

$$\frac{n_D^2 - 1}{n_D^2 + 2} = \frac{R_{LL}}{V} \tag{3. 7}$$

where R_{LL} is the molar refraction (cm^3/mol) and V is the polymer molar volume (cm^3/mol). When polymer samples are isotropic dense homopolymer membranes without any additives, the V in equation (3. 2) is equal to the V in equation (3. 7). Hence, equation (3. 2) can be rewritten in equation (3. 7) as a function of the refractive index, n_D.

$$FFV = 1 - 1.3\frac{V_W}{R_{LL}}\frac{n_D^2 - 1}{n_D^2 + 2} = 1 - \varphi \tag{3. 8}$$

Equations (3. 4–3. 6) can be described with equation (3. 8) as a function of the refractive index-based *FFV*, $1-\varphi$. Hence, equations (3. 4–3. 6) can be rewritten as equations (3. 9–3. 11).

$$P = A'_P \exp\left(\frac{-B'_P}{1-\varphi}\right) \tag{3. 9}$$

$$D = A'_D \exp\left(\frac{-B'_D}{1-\varphi}\right) \tag{3. 10}$$

$$S = A'_S \exp\left(\frac{-B'_S}{1-\varphi}\right) = \frac{A'_P}{A'_D}\exp\left(\frac{-(B'_P - B'_D)}{1-\varphi}\right) \tag{3. 11}$$

$$A'_S = \frac{A'_P}{A'_D} \qquad B'_S = B'_P - B'_D \tag{3. 12}$$

where A'_P, A'_D, A'_S (i.e., A'_P/A'_D), B'_P, B'_D, and B'_S (i.e., $B'_P - B'_D$) are adjustable constants.

Figure 3. 5 presents the gas permeability, diffusion, and solubility coefficients in the 6FDA-based polyimides as functions of the reciprocal of $1-\varphi$. As the $1-\varphi$ value increased, gas permeability and diffusivity values also increased. However, gas solubility showed a slight increase with the increase in $1-\varphi$ value. Linear correlations were also observed between $1-\varphi$ and the gas permeability, diffusivity, and solubility; thus, the gas transport properties can be described as a function of the refractive index.

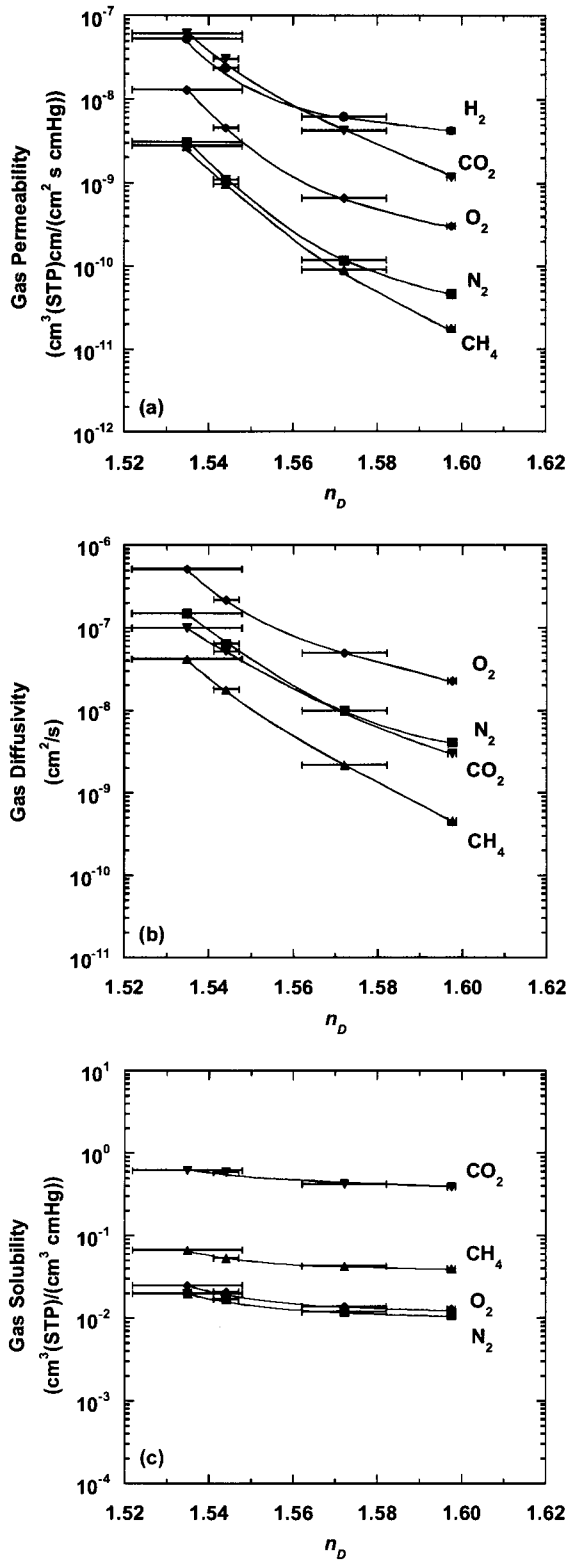

Figure 3. 4 Permeability (a), diffusivity (b), and solubility (c) of various gases at 30°C in the 6FDA-based polyimides as a function of the refractive index. Gases; hydrogen (●), nitrogen (■), oxygen (◆), methane (▲), carbon dioxide (▼).

Based on the least-squares fit analysis in Figure 3. 5, the A'_P, A'_D, A'_S, B'_P, B'_D, and B'_S values for each gas are summarized in Table 3. 2. The r^2 value of solubility parameter of $1-\varphi$ varied from 0.823 to 0.916, and that of diffusivity and permeability varied from 0.872 to 0.974. The free-volume theory provides gas permeability, diffusivity, and solubility as a function of *FFVs* of glassy polymer membranes [17, 18]. Since there is a linear relationship between gas transport properties and *FFV* based on refractive index, this parameter adapts to various types of polymers. Therefore, we systematically studied the A'_P, A'_D, A'_S, B'_P, B'_D, and B'_S values of various gases.

The B'_P value (i.e., slope of the lines of gas permeability) was 3.23 for CO_2, 4.07 for CH_4, 3.37 for N_2, 2.97 for O_2, and 1.98 for H_2. These values were similar for the different gases. The difference in B'_P among these gases was much smaller than that in A'_P (i.e., intercept of the lines of gas permeability). In Table 3. 2, for example, the largest value was 3.64×10^{-2} cm^3(STP)cm/(cm^2 s cmHg) for CH_4, whereas the smallest one was 1.20×10^{-4} cm^3(STP)cm/(cm^2 s cmHg) for H_2. Therefore, differences in the permeability values in the 6FDA-based polyimides resulted from the A'_P values.

The B'_D value (i.e., slope of the lines of gas diffusivity) was 2.84 for CO_2, 3.66 for CH_4, 2.91 for N_2, and 2.46 for O_2. These values were similar for the different gases. The difference in B'_D among these gases was much smaller than that in A'_D (i.e., intercept of the lines of gas diffusivity). In Table 3. 2, for example, the largest value was 1.12×10^{-1} cm^2/s for CH_4, and the smallest one was 9.11×10^{-3} cm^2/s for O_2. Therefore, differences in the diffusivity values in the 6FDA-based polyimides also resulted from the A'_P values.

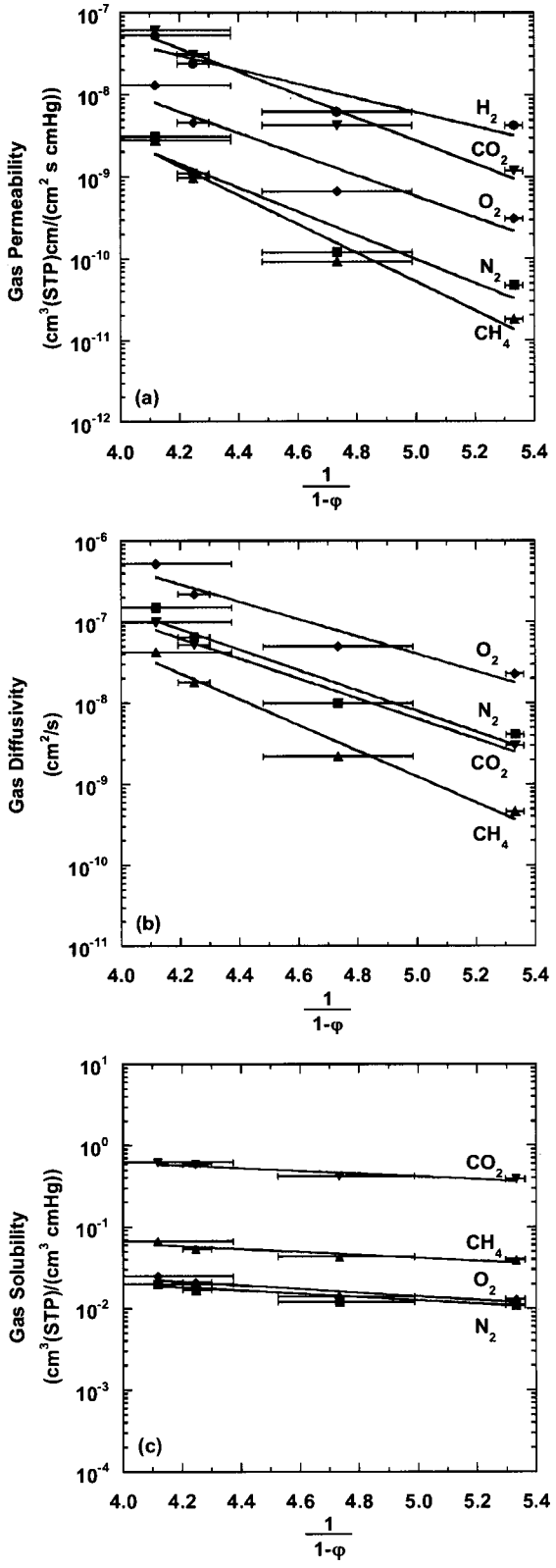

Figure 3. 5 Permeability (a), diffusivity (b), and solubility (c) of various gases at 30°C in the 6FDA-based polyimides as a function of 1−φ. Gases; hydrogen (●), nitrogen (■), oxygen (◆), methane (▲), carbon dioxide (▼).

Table 3. 2 Parameter A' and B' in equation.(3. 9–3. 12) at 30 °C [a]

Gas	A'_P (cm^3(STP)cm/ (cm^2 s cmHg))	B'_P	A'_D (cm^2/s)	B'_D	A'_S (cm^3(STP)/ (cm^3 cmHg))	B'_S
CO_2	2.85×10^{-2}	3.23	9.74×10^{-3}	2.84	2.93	0.39
CH_4	3.64×10^{-2}	4.07	1.12×10^{-1}	3.66	0.325	0.41
N_2	2.08×10^{-3}	3.37	1.65×10^{-2}	2.91	0.126	0.46
O_2	1.65×10^{-3}	2.97	9.11×10^{-3}	2.46	0.181	0.51
H_2	1.20×10^{-4}	1.98	–	–	–	–

[a] There values were determined from the least-squares fit analyses in Figure 3. 5.

The B'_S value (i.e., slope of the lines of gas solubility) was 0.39 for CO_2, 0.41 for CH_4, 0.46 for N_2, and 0.51 for O_2. These values were similar for the different gases. The difference in B'_S among these gases was much smaller than that in A'_S (i.e., intercept of the lines of gas solubility). In Table 3. 2, for example, the largest value was 2.93 cm^3(STP)/(cm^3 cmHg) for CO_2, while the smallest one was 0.126 cm^3(STP)/(cm^3 cmHg) for N_2. Therefore, differences in the solubility values in the 6FDA-based polyimides also resulted from the A'_S values, similar to gas permeability and diffusivity.

Based on the results in Table 3. 2, the parameters A'_P, A'_D, A'_S, B'_P, B'_D, and B'_S seem dependent on penetrant size, shape, and condensability. The order of these parameters was correlated with that of critical volume, V_c, which is standard of penetrant size, and that of critical temperature, T_c, which is standard of penetrant condensability [19]. The parameters A'_P, A'_D, and A'_S are plotted as functions of V_c in Figure 3. 6 and T_c in Figure 3. 7. The parameters B'_P, B'_D, and B'_S are not presented in the figure, because, as previously explained, these values were similar to each other, indicating that they were independent on any penetrant properties. The linear correlation between parameter of permeation, A'_P, and V_c (Figure 3. 6) and T_c (Figure 3.

7). The parameter increased, as V_c and T_c increased. The gas permeability did not depend on either the penetrant size or condensability; rather, it was dependent on the balance between them. Additionally, when the gas diffusion and solution parameters were analyzed based on solution-diffusion mechanism, the parameter A'_D increased as V_c increased (Figure 3. 6). There was no relationship between A'_D and T_c (Figure 3. 7). However, the parameter A'_S showed opposite properties. There was no relationship between A'_D and V_c (Figure 3. 6). The parameter A'_S increased as T_c increased (Figure 3. 7).

The results in Figures 3. 6 and 3. 7 indicate that the A'_D depends on penetrant size, and the A'_S depends on penetrant condensability. Therefore, A'_P (i.e., $A'_D \times A'_S$) is dependent on penetrant size or condensability factor or the balance between them. Based on the free-volume theory based on refractive index, the gas diffusivity depends on penetrant size, and gas solubility depends on penetrant condensability. Gas permeability depends on the balance between them.

Table 3. 3 summarizes the group contribution-based *FFV* in equation (3. 2) and the refractive index-based *FFV*, $1-\varphi$ in equation (3. 8) in the 6FDA-based polyimides. The $1-\varphi$ values of the 6FDA-based polyimides were 1.16–1.37 times larger than their *FFV* values. As expected from equation (3. 2), the *FFV* was mainly dependent on free-volume space in a membrane. In contrast, the $1-\varphi$ (i.e., *FFV* determined from equation (3. 8)) was dependent on free-volume space and optical factors, such as refractive index and molar refraction, which affected the electronic structure and the interactions between the gas molecules and the polymer segments. This factor would provide a more precise adjustment for gas transport in a free volume of a polymer membrane among a family of polymers.

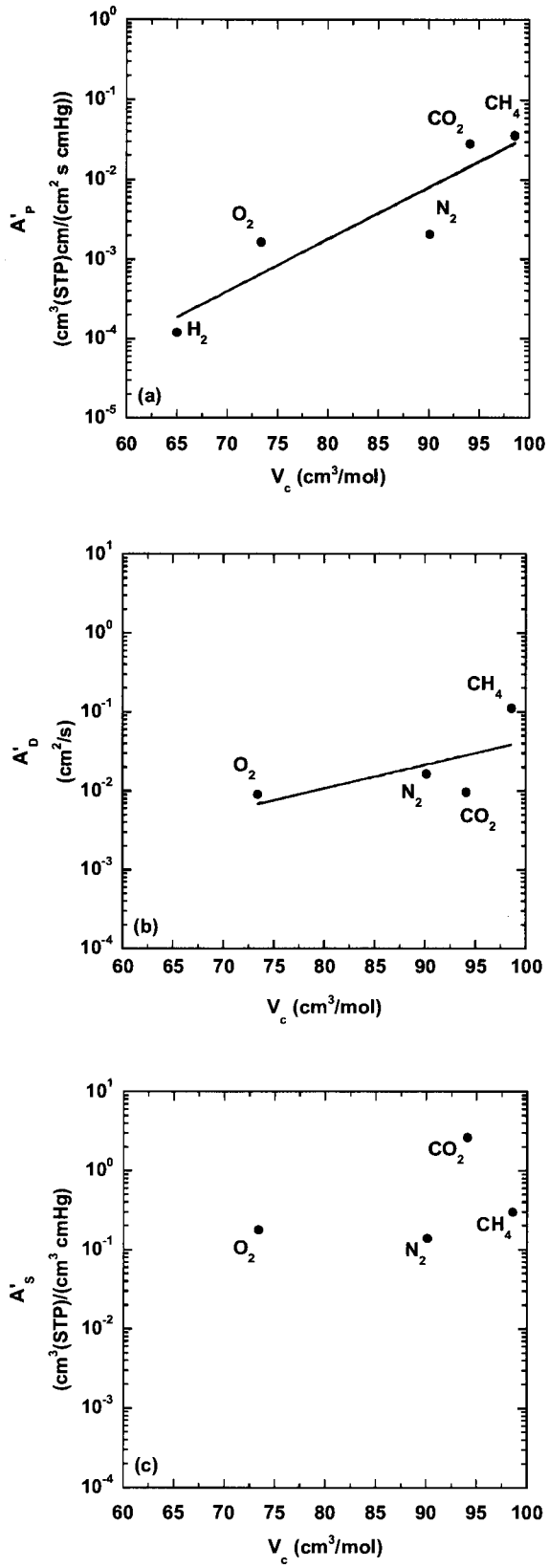

Figure 3. 6 Parameter A'_P (a), A'_D (b), and A'_S (c) at 30°C in the 6FDA-based polyimides as a function of critical volume, V_c of gases [19].

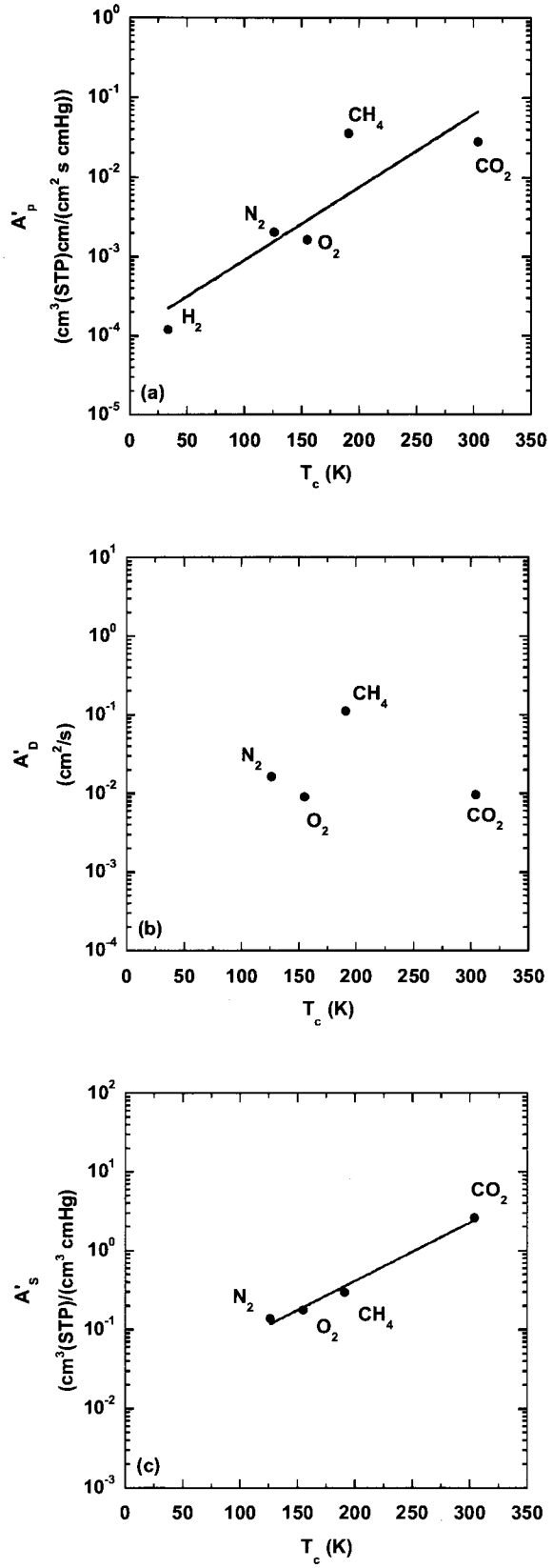

Figure 3. 7 Parameter A'_P (a), A'_D (b), and A'_S (c) at 30°C in the 6FDA-based polyimides as a function of critical temperature, T_c of gases [19].

Table 3. 3 Fractional free volume, *FFV*, values determined from the group contribution method and the refractive index of the 6FDA-based polyimides

Polyimide	*FFV* from equation (3. 2)	1− φ from equation (3. 8)	$\frac{1-\varphi}{FFV}$
6FDA-mPD	0.162 ± 0.01	0.188 ± 0.001	1.16
6FDA-MPD	0.171 ± 0.01	0.211 ± 0.011	1.24
6FDA-TMPD	0.177 ± 0.01	0.236 ± 0.003	1.33
6FDA-TeMPD	0.177 ± 0.01	0.243 ± 0.015	1.37

The photon has two properties: waviness and elementary particle. The photon elementary particle size is not clarified in this study; however, it has been classified as one of the elementary particles and the size is about 1.0×10^{-5} Å which is about 10,000 times smaller than a molecule or an atom. This result indicates the photon can analyze in detail the polymer segment structure as a high-performance probe. Tanio et al. reported the effect of thermal treatment on polymer density based on the difference of the refractive index [20]. This free-volume model considers the electronic structures and the interactions between the gas molecules and polymer segments based on refractive index.

The relationship between the observed and calculated density based on optical properties, such as refractive index and molar refraction of 6FDA-based polyimides, has also been studied. The density can be calculated by refractive index based on the Lorentz-Lorenz equation (3. 13).

$$\rho_{cal} = \frac{M}{R_{LL}} \frac{n_D^2 - 1}{n_D^2 + 2} \qquad (3.\ 13)$$

The ρ_{Cal} value calculated from refractive index was 1.54 for 6FDA-mPD, 1.46 for 6FDA-MPD, 1.36 for 6FDA-TMPD, and 1.33 for 6FDA-TeMPD. The ρ_{Cal} value calculated from refractive index as a function of observed density is presented in Figure 3. 8. As observed density increased, the ρ_{Cal} value increased. The difference in

density between the observed value and the value calculated from refractive index increased as the density of polyimide increased. This result indicates that the dense polyimide affects the influence of the electronic structures and the interactions between the gas molecules and polymer segments. The reason of the difference of density value was also dependent on the electronic structures, which are affected by refractive index. This result indicates that this free-volume model takes into consideration the electronic structures.

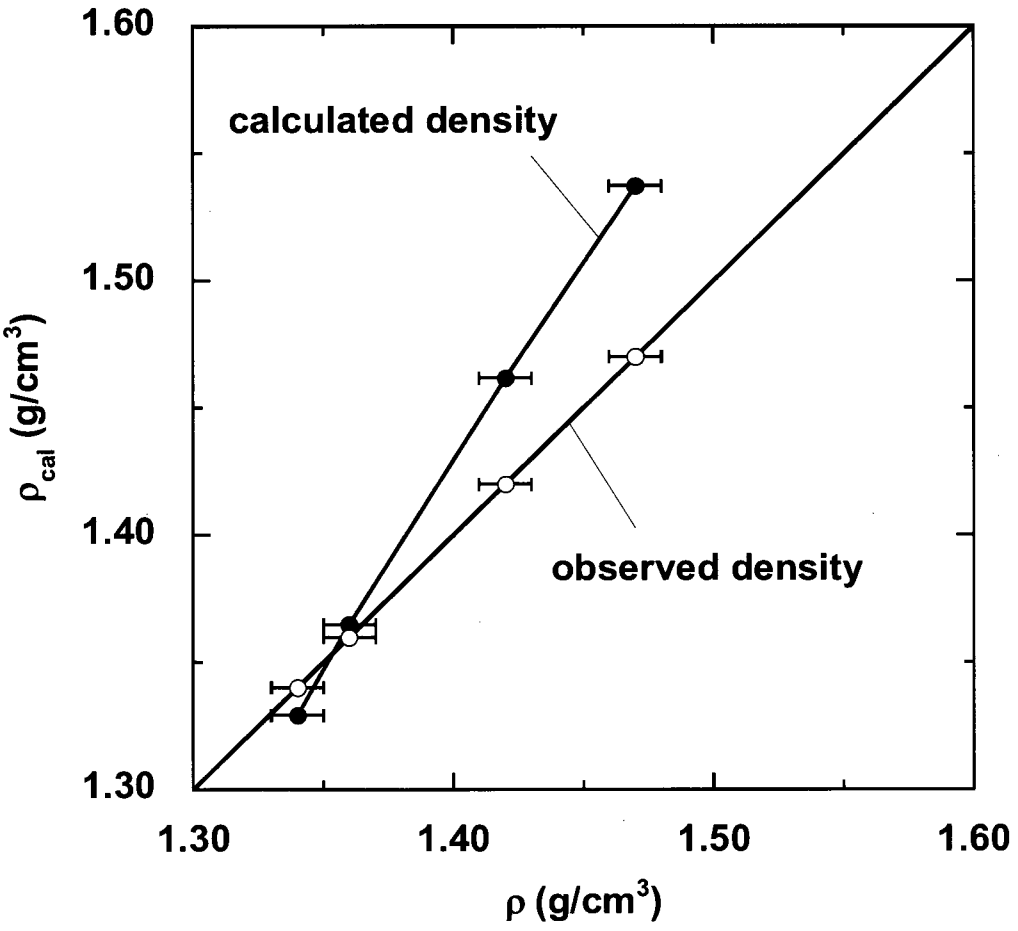

Figure 3. 8 Calculated density as a function of observed density of the 6FDA-based polyimides. Density; observed density (○), calculated density (●)

3.5. CONCLUSIONS

The refractive index and gas transport properties (i.e., permeability, diffusivity, and solubility) in the 4,4-(hexafluoro-isopropylidene) diphthalic anhydride (6FDA)-based polyimides were systematically investigated in terms of their polymer *FFV*s at 30°C. As refractive index decreased, gas permeability increased. Based on the Lorentz-Lorenz equation, the permeability, diffusivity, and solubility as a function of the *FFV* determined from optical constants, such as refractive index and molar refraction, were described. From this model, gas permeability and diffusion coefficients of the 6FDA-based polyimide membranes were found to increase as their refractive index-based *FFV* increased. Gas permeability did not depend on either molecular size or cohesiveness, but was dependent on the balance between them. This is because gas diffusivity is dependent on penetrant size, whereas gas solubility is dependent on the interactions between gas molecules and polymer segments. The *FFV*s of the 6FDA-based polyimides calculated from refractive index were 1.16–1.37 times larger than their *FFV* values. This result indicates polyimide density affects the influence of the electronic structures and the interactions between the gas molecules and polymer segments. This finding leads to the conclusion that electronic structure of the polyimide changes depending on polymer chemical structure.

3.6. REFERENCES

[1] T. Kaino, M. Fujiki, K. Jinguji, Preparation of plastic optical fibers, *Rev. Electr. Commun. Lab.* **32** (1984) 478-488.

[2] D. J. Birkett, The chemistry of optical discs, *Chem. Educ.* **79** (2002) 1081-1087.

[3] S. Nishimura, H. Mazaki, Development of liquid crystalline polymer film "Nisseki LC Film" for viewing angle compensation of various LCD modes, *Mol. Cryst. Liq. Cryst.* **458** (2006) 35-43.

[4] D. W. van Krevelen, *Properties of Polymers. Fourth ed.*, Elsevier B. V., Oxford. (2009)

[5] J. H. Kim, W. J. Koros, D. R. Paul, Physical aging of thin 6FDA-based polyimide membranes containing carboxyl acid groups. Part II. Optical properties, *Polymer.* **47** (2006) 3104-3111.

[6] S. H. Goodman, *Handbook of Thermoset Plastics*, Noyes Publications, Park Ridge, N. J. (1986)

[7] S. Ando, Calculation of refractive indices of polyimides and their molecular packing, *Kobunshi Ronbunshu.* **51** (1994) 251-257.

[8] M. Ree, C. W. Chu, M. J. Goldberg, Influences of chain rigidity, in-plane orientation, and thickness on residual stress of polymer films, *J. Appl. Phys.* **75** (1994) 1410-1419.

[9] S. M. Pyo, S. I. Kim, T. J. Shin, Y. H. Park, M. J. Ree, Synthesis and characterization of fully rodlike poly(4,4'-biphenylene pyromellitimide)s with various short side groups, *Polym. Sci., Part A: Polym. Chem.* **37** (1999) 937-957.

[10] D. Creed, C. E. Hoyle, P. Subramanian, R. Nagarajan, C. Pandey, E. T. Anzures, K. M. Cane, P. E. Cassidy, Photodegradation of polyimides. 6. Effect of donor-acceptor groups on the photooxidative stability of polyimides and model compounds, *Macromolecules*. **27** (1994) 832-837.

[11] C. E. Hoyle, E. T. Anzures, P. Subramanian, R. Nagarajan, D. Creed, Photodegradation of polyimides. 5. An explanation of the rapid photolytic decomposition of a selected polyimide via anhydride formation, *Macromolecules*. **25** (1992) 6651-6657.

[12] D. R. Paul, Y. P. Yampolskii, *Gas Separtion Membranes*, CRC Press, Boca Raton. (1994)

[13] S. Kanehashi, K. Nagai, Analysis of dual-mode model parameters for gas sorption in glassy polymers, *J. Membr. Sci.* **253** (2005) 117-138.

[14] S. Miyata, S. Sato, K. Nagai, T. Nakagawa, K. Kudo, Relationship between gas transport properties and fractional free volume determined from dielectric constant in polyimide films containing the hexafluoroisopropylidene group, *J. Appl. Polym. Sci.* **107** (2008) 3933-3944.

[15] H. Elias, *Macromolecules*, Wiley-VCH, Weinheim. (2009)

[16] H. Dislich, Plastics as optical-materials, *Angew. Chem. Int. Ed. Engl.* **18** (1979) 49-59.

[17] W. M. Lee, Selection of barrier materials from molecular structure, *Polym. Eng. Sci.* **20** (1980) 65-69.

[18] H. Fujita, Diffusion in polymer-diluent systems, *Fortschr. Hochpolymer. Forsch.* **3** (1961) 1-47.

[19] B. E. Poling, *The Properties of Gases and Liquids*, McGraw-Hill, New York.

(2001)

[20] N. Tanio, T. Nakanishi, Physical aging and refractive index of poly(methyl methacrylate) glass, *Polym. J.* **38** (2006) 814-818.

Chapter 4

SUBSTITUTE EFFECT OF FLUORINE-CONTAINING POLYIMIDES WITH HEXAFLUOROISOPROPYLIDENE GROUP ON PHOTO ALIGNMENT OF LIQUID CRYSTAL MOLECULE

4.1. ABSTRACT

The substituent effect of fluorine-containing polyimides with 4,4-(hexafluoro-isopropylidene) diphthalic anhydride (6FDA) group on the photo alignment of the liquid crystal (LC) molecule and the effect of 254 nm linearly polarized ultraviolet (LPUV) irradiation on the chemical structure were systematically investigated. 6FDA-2,3,5,6-tetramethyl-1,4-phenylene diamine (TeMPD) showed the photo alignment characteristic of the LC molecule. Based on the infrared and ultraviolet absorption spectra, the photo-scission reaction of LPUV irradiation was not observed, and photoreaction between polymer segments was observed. The photo alignment characteristic of LPUV-irradiated 6FDA-TeMPD strongly depended on the photoreaction between the C=O group of the imide ring and the CH3 group for phenyl-group π–π^* transitions. The chemical structure changed with the excitation of C=O double bonds and C–H bonds and the formation of hydroperoxide O–H between the intermolecular polymer segment through the LPUV irradiation mechanism. The electron-donating benzene ring and the electron-accepting imide ring then formed charge transfer complexes (CTCs) between the two sides of polymer chains; the combination with the alternation sequence to both cross sides was clearly formed. In

one direction of the photoreaction in the CTC structure, 6FDA-TeMPD showed the photo alignment of the LC molecule.

Keywords: fluorine-containing polyimide, optical property, photo alignment, molecular orbital calculation, liquid crystal

4.2. INTRODUCTION

Recently, in the alignment technology of liquid crystal (LC) molecules, mechanically rubbed films have been extensively used in the industrial field of liquid crystal display (LCD). However, mechanical rubbing causes problems such as electrostatic charge and dust accumulation [1]. To solve the problems caused by the mechanical rubbing alignment method, the development of non-rubbing processes is essential. Therefore, the photo alignment an LC molecule film has received considerable attention because it does not depend on mechanical process with free electrostatic charge and dust. The photo alignment method, in which polyimide films are radiated with linearly polarized ultraviolet (LPUV), is one of the most effective non-rubbing processes [2-4]. K. Ha *et al.* and H. Shitomi *et al.* reported that the photo alignment characteristic of polyimide films clearly depends on the wavelength of the exposure photon, suggesting that the effect of LPUV irradiation on polyimide films should also be investigated [5-7]. However, the mechanism of the LC molecule photo alignment on polyimide films has not yet been reported.

Among polymer materials, polyimides have higher heat and chemical resistance properties; thus, they are widely used as electronic materials, such as in overcoats of semiconductors, interlayer insulation films, and photo alignment of LC

molecule films. 1,2,3,4-Cyclopentanetetracarbo-xylic dianhydride-2,2-bis (4-aminophenoxyphenyl) propane (CBDA-BAPP) is used in the photo alignment of LC molecule films. However, CBDA-BAPP has low optical transparency, with dark brown or yellowish-brown color. The reason is that the photon with about 500 nm (i.e., 2.5 eV) is absorbed in this polyimide [5]. Conversely, 4,4-(hexafluoroisopropylidene) diphthalic anhydri- de (6FDA)-containing polyimides are expected to show higher heat resistance, a lower dielectric constant, and a low refractive index. The fluorine atom has high electronegativity, whereas the C–F combination has high binding energy and low polarizability. Thus, fluorine-containing poly- imides have high potential as a material for use in the LCD industry. Most importantly, the 6FDA is commercially available as a tetracarboxylic dianhydride component, which has led to its widespread use. In general, polyimides containing 6FDA have excellent solubility in polar solvents and high optical transparency together with a low refractive index. However, there is no physical chemistry-based linkage of the LC molecule photo alignment on 6FDA-based polyimides and the chemical structure.

4.3. EXPERIMENTAL

4.3.1. Sample preparation

The chemical structure of each product, as shown in Figure 4. 1 was confirmed by FTIR and nuclear magnetic resonance analyses. The 6FDA-based polyimides were 6FDA-1,3-phenylene diamine (mPD), 6FDA-4-methyl-1,3-phenylene diamine (MPD), 6FDA-2,4,6-trimethyl-1,3-phenylene diamine (TMPD), and 6FDA-2,3,5,6-tetramethyl-1,4-phenylene diamine (TeMPD).

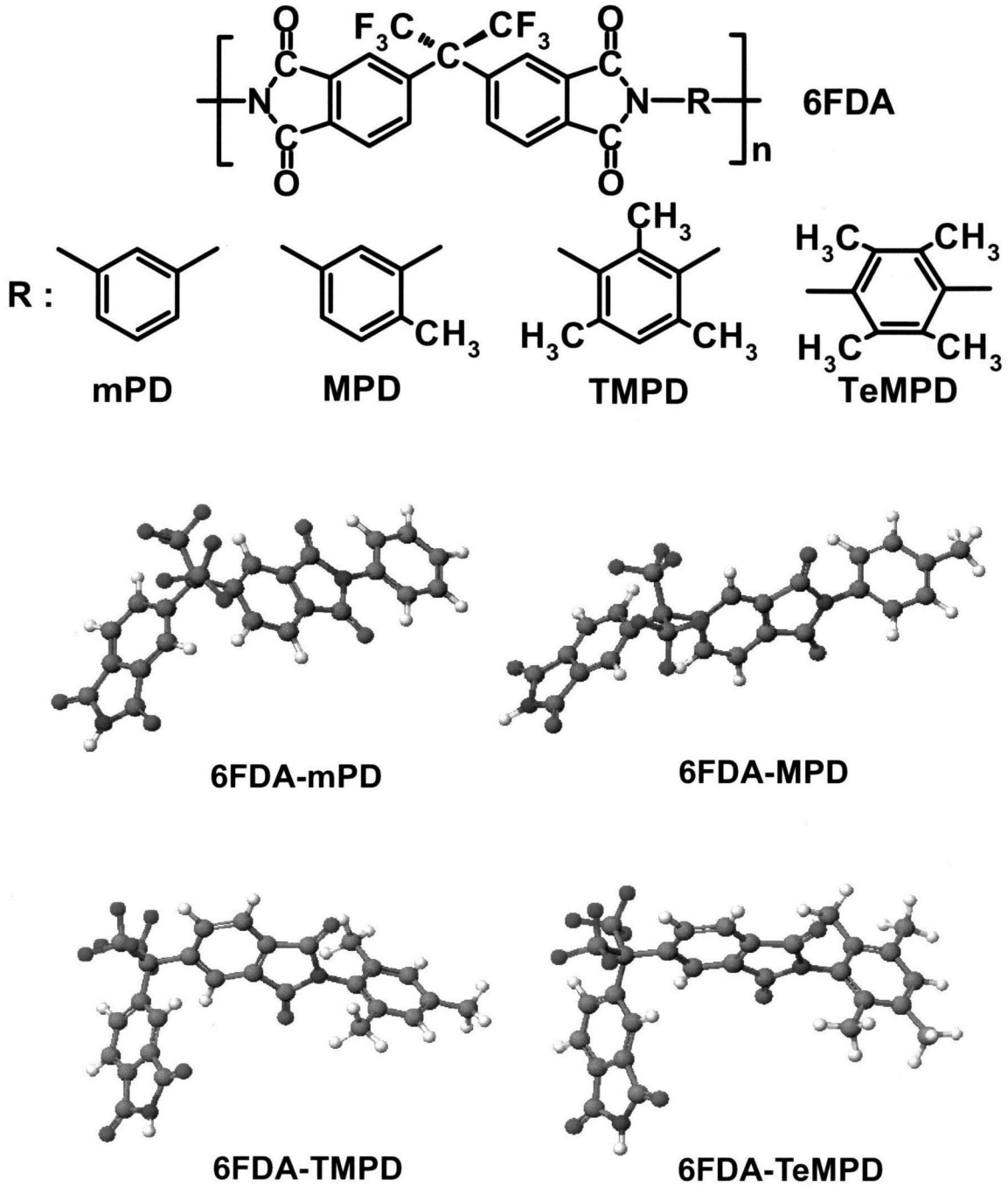

Figure 4. 1 Chemical structures and calculated models of fluorine-containing polyimides: 6FDA-based polyimides: 6FDA-mPD, 6FDA-MPD, 6FDA-TMPD, and 6FDA-TeMPD.

The 6FDA-based polyimides used in the current research were the same samples which we used in a previous study [8-10]. We fabricated isotropic, dense, and

nonporous polyimides films through the spin coating method, casting *N,N*-dimethyl-acetoamide (Junsei Chemistry Co. Ltd., Tokyo, Japan) solution on the substrates typically at 3500 rpm for 30 s. These 6FDA-based polyimides were baked for 40 min at 180°C to remove the solvents. The substrates were allowed to cool to room temperature. LPUV irradiation was performed with a 200 W Hg-Xe lamp light source. The measured polarization degree of the light at 254 nm was 99%. Irradiation intensity was about 700 $\mu W/cm^2$.

4.3.2. Optical measurements

4.3.2.1. Infrared (IR) absorption spectra

All IR spectra were determined in the film state on the CaF_2 substrate in at least three samples to confirm the reproducibility of the experimental results. IR spectra were obtained on an FTIR-8300 spectrometer (Shimadzu Co., Kyoto, Japan) from 1000–4000 cm^{-1} at room temperature.

4.3.2.2. UV absorption spectra

All UV absorption spectra were determined in the film state on the quartz substrate in at least three samples to confirm the reproducibility of the experimental results. UV absorption spectra were obtained on an UV-3100 spectrometer (Shimadzu Co., Kyoto, Japan) from 1.0–6.5 eV at room temperature.

4.3.3. MO calculations

The structure of the 6FDA-based polyimides was optimized by MOPAC (parameters as PM3) or mechanics, as shown in Figure 4. 1. The structure was

calculated by one polymer segment unit with hydrogen termination. These optimized structures and theoretical UV absorption spectra were calculated using the Molecular Mechanics Simulator, CAChe version 6.01 (Fujitsu Co. Ltd., Tokyo, Japan).

4.3.4. Fabrication of LC cells

LC cells were fabricated by assembling two substrates in a way that the polarization of exposed LPUV light was parallel to each other according to the literature [5, 6, 11]. The cell gap was about 25 μm. The guest-host LC was mixed with 100 parts nematic ZLI-2293 LC (Merck Co. Inc., New York, USA) and one part dichroic dye G-256 Lot.07-1 (Hayashibara Biochemical Lab. Inc., Okayama, Japan), heated to 80°C, and then finally injected into the cells in an isotropic phase. The uniformity of the LC alignment was evaluated by orthoscopic observations using a polarization microscope (POM) (Olympus Inc., Tokyo, Japan) under cross Nicol.

4.4. RESULTS AND DISCUSSION

4.4.1. Effect of LPUV irradiation on 6FDA-based polyimides

4.4.1.1. IR absorption spectra

The glass-transition temperature values of the isotropic, dense, and non-porous 6FDA-mPD, 6FDA-MPD, 6FDA-TMPD, and 6FDA-TeMPD polyimide films were 298, 335, 380, and 427°C, respectively [8-10]. The glass-transition temperature value was much higher than the temperature used in all the optical measurements. Under optical measurement conditions, all the 6FDA-based polyimides were glassy and completely amorphous. As the number of methyl groups in the diamine moiety increased, the glass-transition temperature value also increased. The addition of four methyl groups

provided an increase of 129°C. Thus, the methyl groups seemingly restricted the mobility of the polymer segments.

The IR spectra of the LPUV-irradiated 6FDA-based polyimides for 2 J and unirradiated 6FDA-based polyimides are shown in Figure 4. 2. 6FDA-mPD: 1786 cm^{-1} and 1726 cm^{-1} (C=O stretching), 1360 cm^{-1} (C–N stretching), 1346 cm^{-1} (C–H bending). 6FDA-MPD: 1786 cm^{-1} and 1729 cm^{-1} (C=O stretching), 1360 cm^{-1} (C–N stretching), 1345 cm^{-1} (C–H bending). 6FDA-TMPD: 1786 cm^{-1} and 1728 cm^{-1} (C=O stretching), 1358 cm^{-1} (C–N stretching), 1345 cm^{-1} (C–H bending). 6FDA-TeMPD: 1786 cm^{-1} and 1726 cm^{-1} (C=O stretching), 1354 cm^{-1} (C–N stretching), 1342 cm^{-1} (C–H bending). In Figure 4. 2(a), the IR spectra of 6FDA-mPD, 6FDA-MPD, and 6FDA-TMPD did not change through LPUV irradiation. However, for 6FDA-TeMPD, the O–H bond peak intensity near 3500 cm^{-1} slightly increased, the C=O bond peak intensity near 1730 cm^{-1} decreased, and the peak intensity near 1360 cm^{-1} decreased through LPUV irradiation. The C–N and C–H bond peaks were observed in the range of 1300–1400 cm^{-1}. The IR spectra in this range are shown Figure 4. 2(b). The peak, whose intensity decreased through LPUV irradiation, showed the C–H bending of the methyl group in the diamine moiety.

The result indicates that only the 6FDA-TeMPD chemical structure changes with the excitation of the C=O double bond and C–H bond. Additionally, the hydroperoxide O–H bond was newly formed. However, photo-scission reaction of the LPUV irradiation was not observed because the other peak intensities did not change. Therefore, in the current study, the LPUV reaction was systematically studied through its UV absorption and MO calculation.

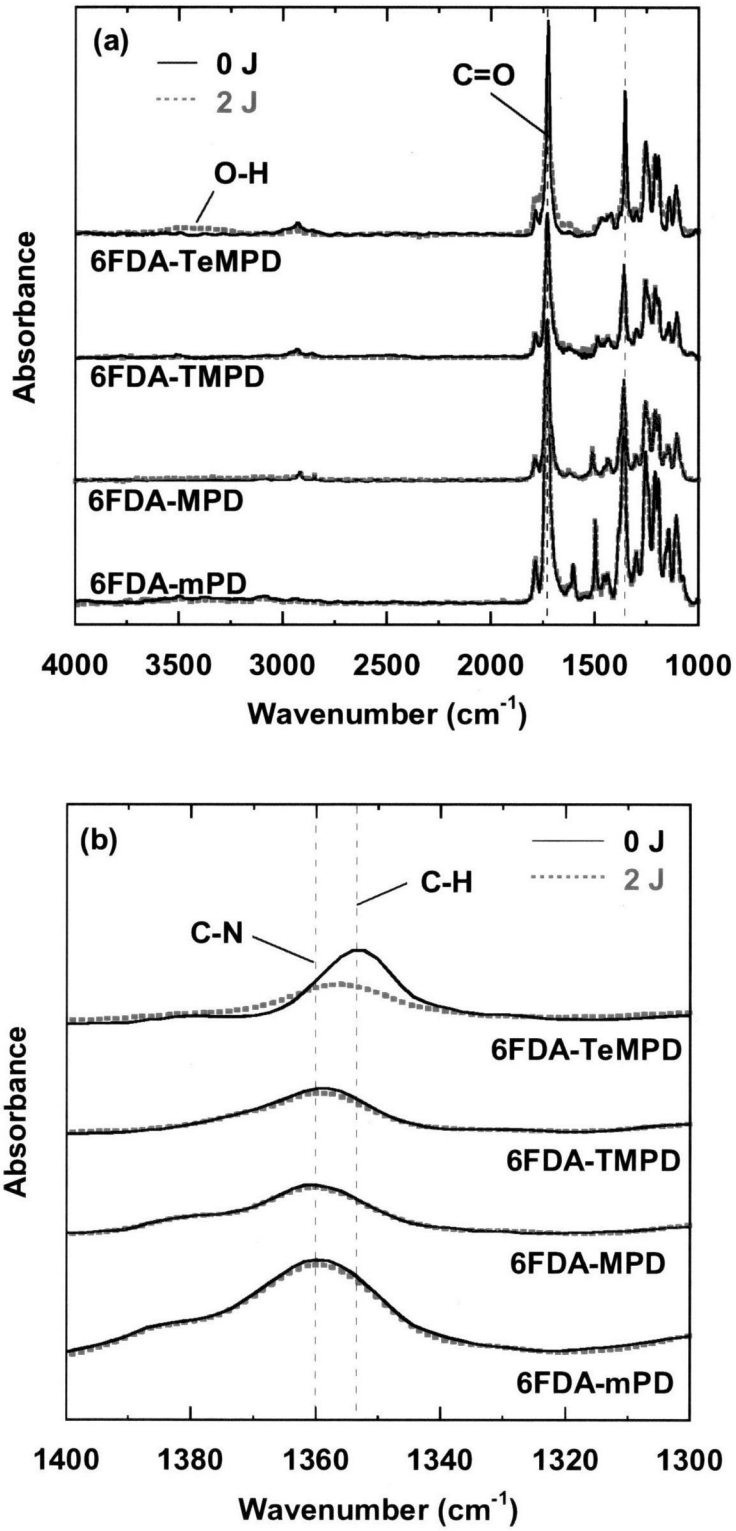

Figure 4. 2 FT-IR spectra of LPUV-irradiated 6FDA-based polyimide membranes from 0 to 2 J: FT-IR spectra range: (a) 1000–4000 cm^{-1}, (b) 1300–1400 cm^{-1}.

4.4.1.2. UV absorption spectra

The UV spectra from 3.5–6.5 eV of these LPUV irradiated and unirradiated 6FDA-based polyimides are shown in Figure 4. 3. Two significant peaks were observed from 5.5–5.7 eV (No. 1) and from 6.2–6.4 eV (No. 2) in 6FDA-based polyimides. The No. 1 peak position shifted to lower energy as the number of methyl groups in the diamine moiety increased. The No. 1 peak positions were 5.68 eV for 6FDA-mPD, 5.62 eV for 6FDA-MPD, 5.53 eV for 6FDA-TMPD, and 5.52 eV for 6FDA-TeMPD. Conversely, the No. 2 peak position did not change. The No. 2 peak positions were about 6.5 eV for 6FDA-mPD and 6FDA-MPD, 6.21 eV for 6FDA-TMPD, and 6.21 eV for 6FDA-TeMPD. The peak position was constant without depending on the number of methyl groups in the diamine moiety.

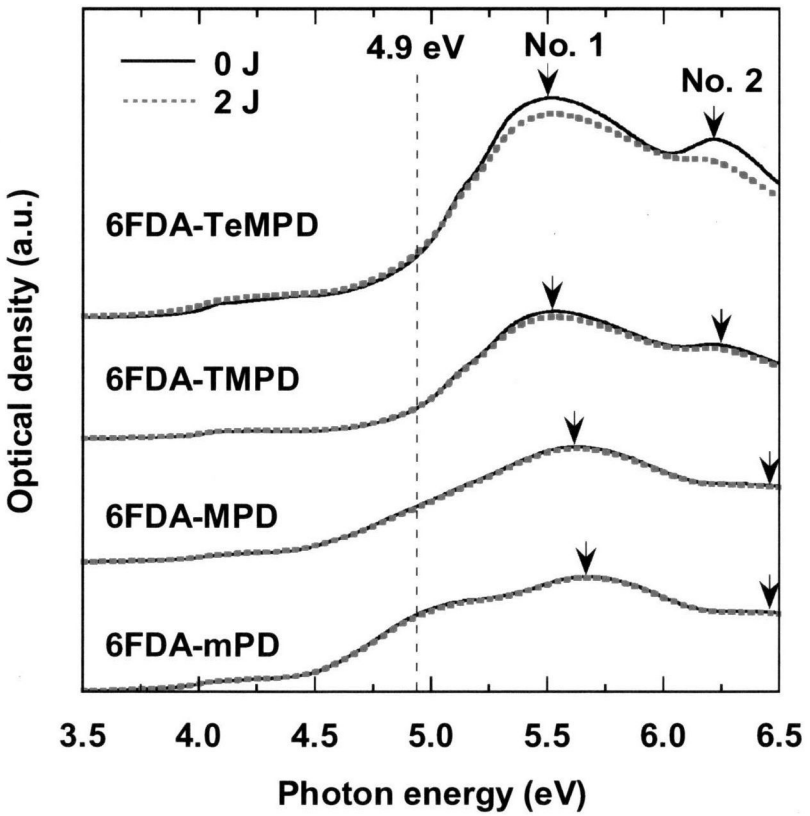

Figure 4. 3 Measured absorption spectra of LPUV-irradiated 6FDA-based polyimide membranes from 0 to 2 J.

The photon energy with 254 nm was 4.9 eV. This photon energy was absorbed in all 6FDA-based polyimides in the current study. The change in peak intensity was not observed in this photon energy range. However, the Nos. 1 and 2 peak intensities of 6FDA-TeMPD clearly decreased through LPUV irradiation. This tendency is in good agreement with that in the IR spectra in Figure 4. 2. This result indicates that the chemical structure of 6FDA-TeMPD was changed by LPUV irradiation. Photo-scission reaction of LPUV irradiation was also not observed because the peak intensity at 4.9 eV did not decrease. Thus, these UV absorption spectra would be investigated later on with the result of the MO calculations.

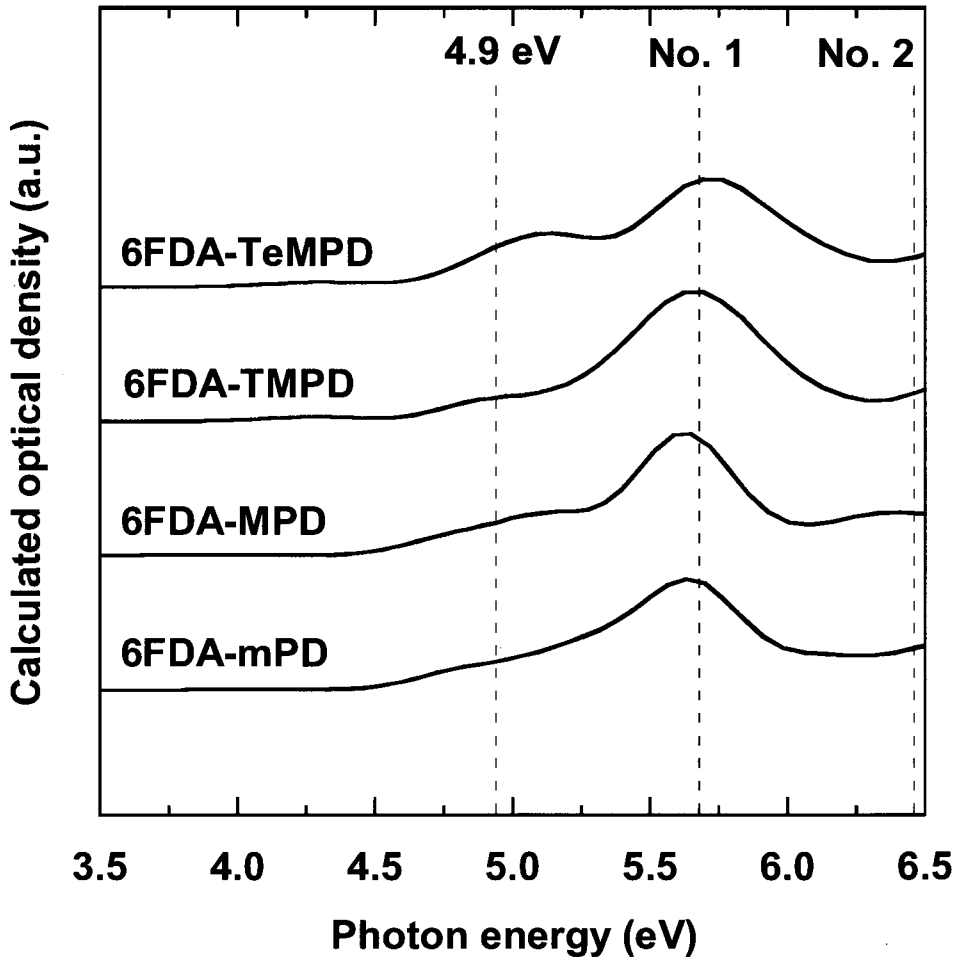

Figure 4. 4 Calculated absorption spectra of 6FDA-based polyimides.

The calculated UV absorptions of 6FDA-based polyimides optimized in Figure 4. 1 are shown in Figure 4. 4. The peak position difference between the observed and calculated absorption spectra was observed because the calculated absorption spectra were one unit of their polymers. However, the tendency of two peak observations in the calculated absorption was in good agreement with that in the observed absorption in the current study. Two significant peaks were observed from 5.6–5.8 eV (No. 1) and 6.5 eV (No. 2) in calculated 6FDA-based polyimides; the peak with 4.9 eV was absorbed. The No. 1 peak positions were 5.69 eV for 6FDA-mPD, 5.66 eV for 6FDA-MPD, 5.67 eV for 6FDA-TMPD, and 5.70 eV for 6FDA-TeMPD. These peak positions were almost constant. However, the calculated peak position was higher than the observed position. Conversely, No. 2 peak position did not change. The calculated peak position was higher than the observed position, similar to the No. 1 peak. Therefore, in 6FDA-TeMPD, these two peaks (i.e., Nos. 1 and 2) changed by LPUV irradiation were assigned based on the result of the MO calculation.

The comparison between the calculated and observed UV absorptions of 6FDA-TeMPD polyimide is shown in Figure 4. 5. The spectrum has two distinct peaks around 5.7 (No.1) and 6.5 eV (No. 2). Although the two peaks are broad and appear not to have fine electronic structures, the spectrum can be deconvoluted with various components considering the possible electronic transitions. The electronic absorption corresponds to the transition from the ground to the first excited state. It is mainly described by one electron excitation from the highest occupied molecular orbital (HOMO) to the lowest occupied molecular orbital (LUMO). Consequently, the HOMO $\rightarrow$ LUMO transition implies electron density transfer. The 6FDA-TeMPD orbital compositions of the frontier molecular orbital are shown in Figure 4. 6. Note

that the charge at HOMO and LUMO is localized on the TeMPD and 6FDA site residues, respectively. This finding indicates that the charge transfer (CT) can take place through the HOMO, HOMO–1 → LUMO, and LUMO+1 transition as well as through the general polyimide. That is, photo absorption depends on the CT transitions from the TeMPD site to 6FDA site because of the phenyl group π–π^* transitions. The components can be provisionally assigned based on the electronic transition of a simple aromatic or imide compound. The band lower than 5.7 eV (No.1) is assignable to the π–π^* transition of the phenyl group and the bands at 5.7 eV (No.1) and 6.5 eV (No. 2) to the π–π^* transition of the phenyl group and n–π^* transition of the carbonyl groups (i.e., HOMO–5 → LUMO or LUMO+1), respectively. As evident in Figure 4. 3, the reduction of the only n–π^* transition of the carbonyl groups depended on the reduction of the photo absorption of Nos. 1 and 2 peaks and not on that lower than 5.7 eV (No.1). This result indicates that the photo-scission reaction of LPUV irradiation did not occur, which is in good agreement with the IR spectra.

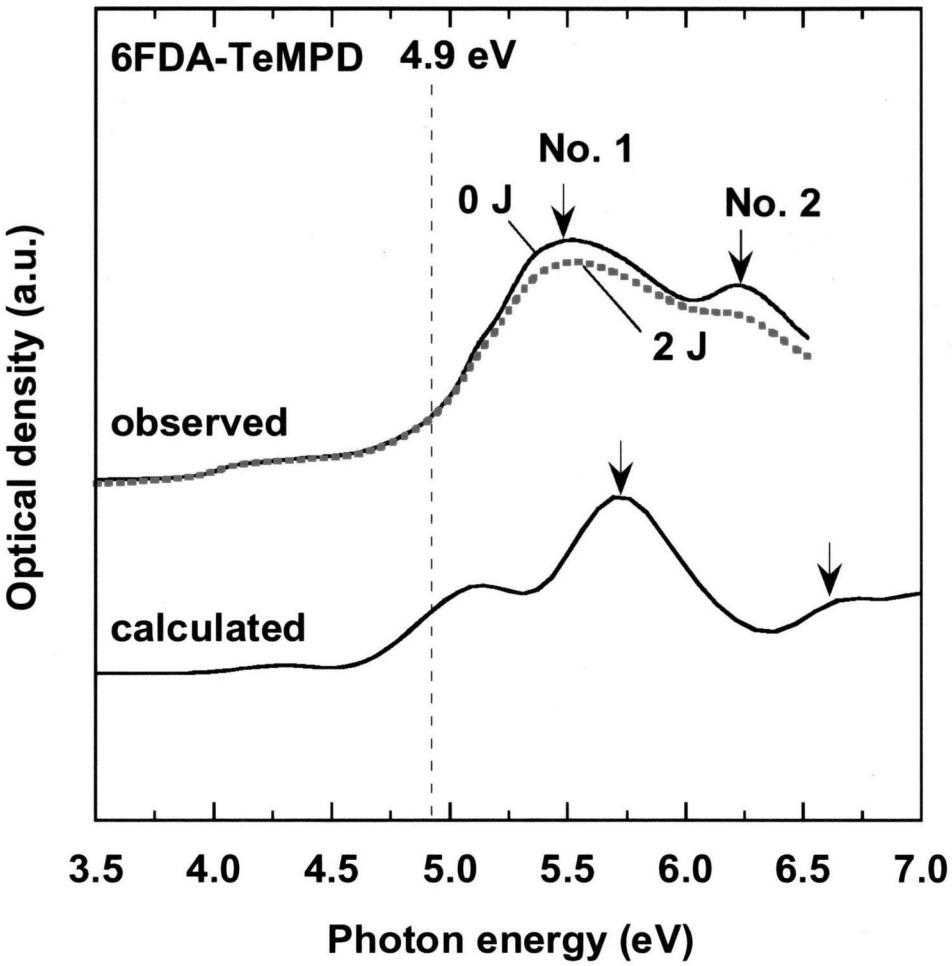

Figure 4. 5 Measured and calculated absorption spectra of 6FDA-TeMPD.

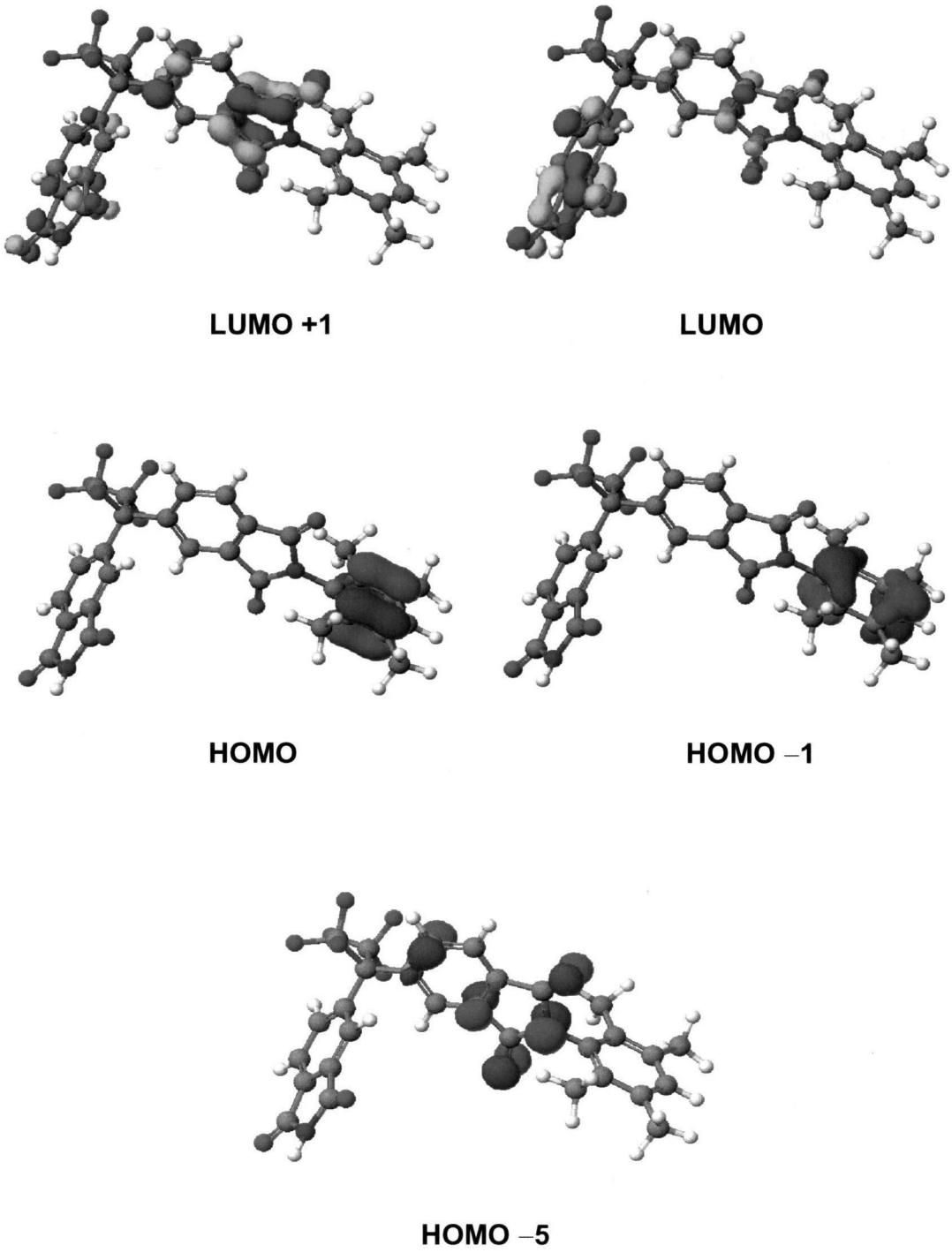

Figure 4. 6 Aromatic orbital HOMO and LUMO compositions of the frontier molecular orbital for 6FDA-TeMPD.

Generally, the behavior is known as the formation of charge transfer complexes (CTCs) or CT interaction in polyimide. This interaction is attributed to the presence of π electrons between the ring structures in polyimides. One of the CTC structures is mixed-layer packing (MLP), which is similar to a sandwich structure between imides and the neighboring benzene rings in the diamine moiety shown in Figure 4. 7(a). MLP can explain 6FDA-TeMPD polyimide films [12]. A large number of aromatic polyimides showing various properties have been systematically synthesized using various chemical structures. The difference in polyimide molecular ordering seems to be closely related to their heat resistance property (i.e., glass transition temperature=427°C). Phenyl-group π–π^* transitions between polymer segments are expected to occur easily. Therefore, in Figure 4. 5, the observed Nos. 1 and 2 peak positions shifted to lower energy compared with the calculated position. The CT interaction between polymer segments strongly depended on the photoreaction by LPUV irradiation.

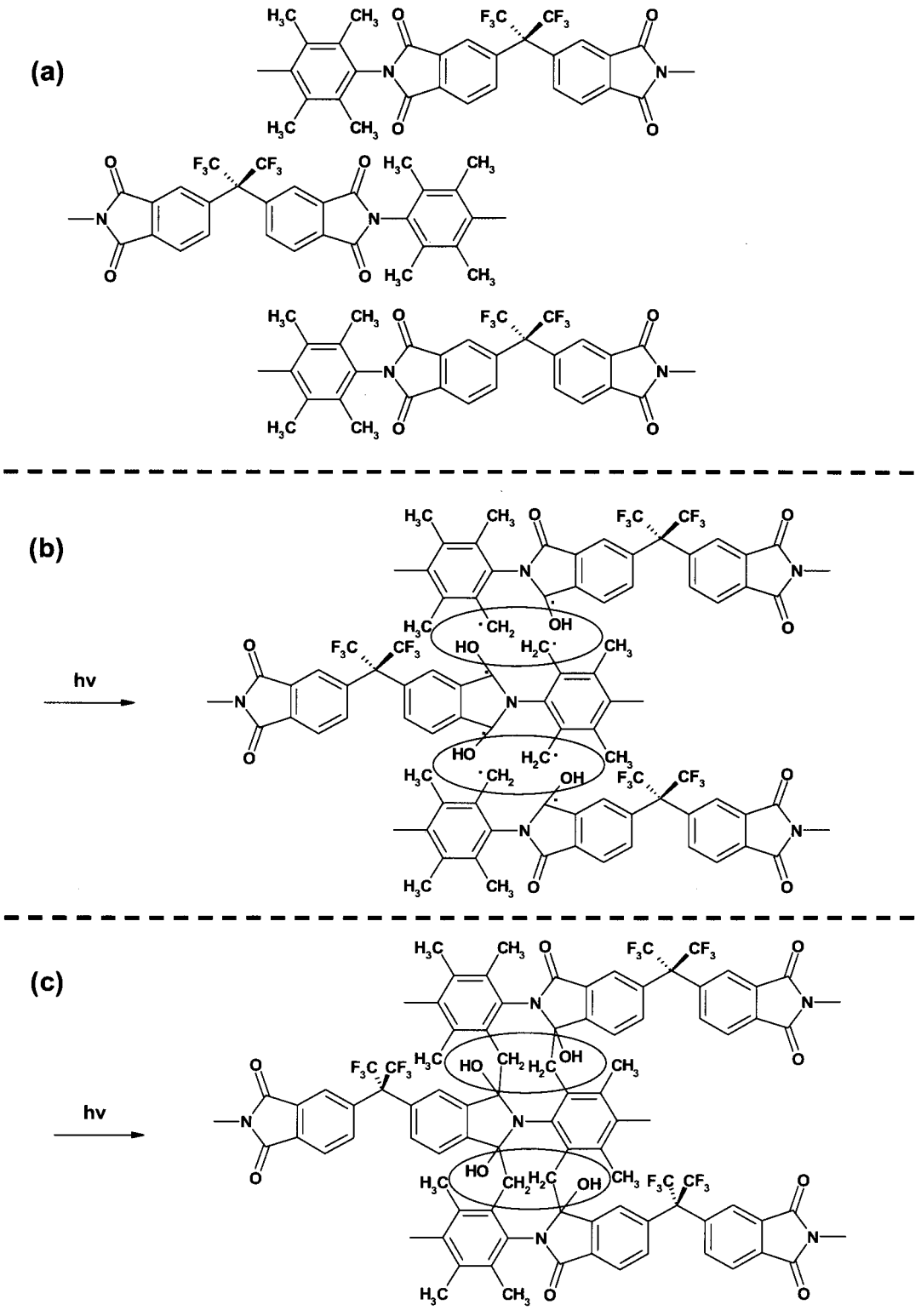

Figure 4. 7 Mechanism for photo-oxidation of 6FDA-TeMPD.

This result indicates that the chemical structure changes with the excitation of the C=O double bonds and C–H bonds and the formation of hydroperoxide O–H between the intermolecular polymer segments through the LPUV irradiation mechanism of 6FDA-TeMPD, as schematically shown in Figure 4. 7. The CTC structure of 6FDA-TeMPD was MLP, which is similar to the sandwich structure presented in a previous study [12]. The electron-donating benzene ring and the electron-accepting imide ring formed CTCs between both sides of the polymer chains in this MLP structure (Figure 4. 7(a)). Therefore, the photoreaction between the C=O group of the imide ring and a CH_3 group through LPUV irradiation occurred in one direction (Figure 4. 7(b)); hydroperoxide O–H was newly formed on the side chain. In the case of the polymer with a symmetric structure, such as 6FDA-TeMPD, the combinations with alternation sequences to both cross sides clearly formed (Figure 4. 7(c)). This result is in good agreement with that of the IR and UV spectra in Figures 4. 2 and 4. 3, respectively.

4.4.2. Photo alignment of the LC molecule in 6FDA-based polyimides

The photo alignment of the LC molecule in 6FDA-TMPD and 6FDA-TeMPD through LPUV irradiation was investigated in our previous study [11]. However, the other 6FDA-based polyimides were not investigated. The POM images in all 6FDA-based polyimides in the current study are presented in Figure 4. 8. The photo alignment characteristic of all LPUV unirradiated 6FDA-based polyimides was not observed. The photo alignment characteristic of LPUV irradiated for 10 J was also not observed in 6FDA-mPD, 6FDA-MPD, and 6FDA-TMPD, as well as in the LPUV unirradiated 6FDA-based polyimide. However, in the case of 6FDA-TeMPD, the

photo alignment characteristic of LPUV irradiated polyimides was observed. The photo alignment characteristic of LPUV irradiated 6FDA-TeMPD was estimated to depend strongly on the photoreaction between the C=O group of the imide ring and a CH_3 group for phenyl-group π–π^* transitions based on Figure 4. 7. The CTCs easily formed in polymers with a large substituent, alternation sequence, and polarizability, such as 6FDA-TeMPD. In one direction of the photoreaction in the CTC structure, only the 6FDA-TeMPD showed photo alignment of the LC molecule. However, 6FDA-mPD, 6FDA-MPD, and 6FDA-TMPD, which were hard to form CTC structures, did not show photo alignment of the LC molecule. The chemical and physical structures of polymer and the polymer cohesiveness strongly affected the photo alignment of the LC molecule.

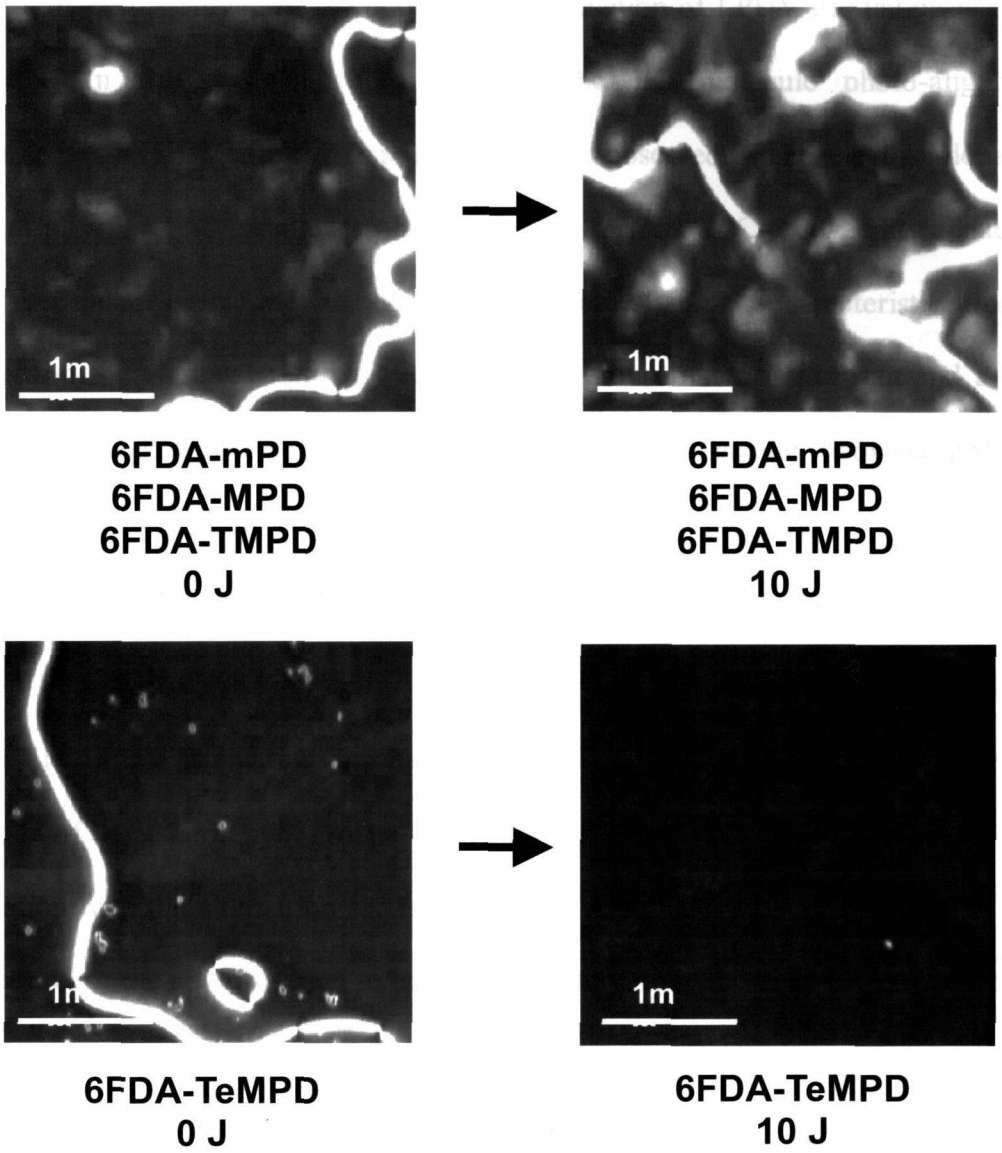

Figure 4. 8 Polarization microscopic images of LPUV-irradiated 6FDA-based polyimide membranes from 0 to 10 J.

4.5. CONCLUSIONS

The substituent effect of fluorine-containing polyimides with 6FDA group on the photo alignment of the LC molecule and the effect of 254 nm LPUV irradiation on the chemical structures through these optical properties and MO calculation were systematically investigated. The chemical structure of 6FDA-TeMPD was changed by

LPUV irradiation. However, the photo-scission reaction of LPUV irradiation was not observed. In the case of 6FDA-TeMPD, the LC molecule photo-alignment characteristic of LPUV irradiated polyimides was observed. The electron-donating benzene ring and the electron-accepting imide ring formed CTCs between two sides of the polymer chains in this MLP structure. The photo alignment characteristic strongly depended on the photoreaction between the C=O group of the imide ring and a CH_3 group for phenyl-group π–π^* transitions. The CT interaction between polymer segments strongly depends on the photoreaction by LPUV irradiation. The chemical structure changed with as the excitation of the C=O double bonds and C–H bonds and the formation of hydroperoxide O–H between the intermolecular polymer segments through the LPUV irradiation mechanism of 6FDA-TeMPD. Therefore, the n–π^* transition of the carbonyl groups decreased through LPUV irradiation. The combination with the alternation sequence to both cross sides was clearly formed. In one direction of the photoreaction in the CTC structure, only the 6FDA-TeMPD showed the photo alignment of the LC molecule.

4.6. REFERENCES

[1] J. Cognard, Alignment of nematic liquid crystals and their mixtures, *Mol. Cryst. Liq. Cryst., Suppl. Ser.* **1** (1982) 1-77.

[2] M. Schadt, K. Schmitt, V. Kozinkov, V. Chigrinov, Surface-induced parallel alignment of liquid crystals by linearly polymerized photopolymers, *Jpn. J. Appl. Phys., Part 1.* **31** (1992) 2155-2164.

[3] T. Tominaga, H. Sugita, Y. Oota, M. Kimura, S. Kimura, H. Nambe, Analysis of surface and inter face of polymer filme by NEXAFS, *JSR TECHNICAL REVIEW.* **112** (2005).

[4] Y. Wang, T. Natsui, Y. Makita, A. Kumano, Y. Takeuchi, Pulsed Laser-induced liquid crystal alignment parallel to the exposure polarization, *JSR TECHNICAL REVIEW.* **108** (2001).

[5] H. Shitomi, T. Ibuki, S. Matsumoto, H. Onuki, Optically controlled alignment of liquid crystal on polyimide films exposed to undulator radiation, *Jpn. J. Appl. Phys., Part 1.* **38** (1999) 176-179.

[6] M. Nishikawa, J. L. West, Order parameter of liquid crystal on polyimide with polarized ultraviolet-light exposure, *Jpn. J. Appl. Phys., Part 2.* **38** (1999) L331-L333.

[7] K. Ha, J. L. West, Studies on the photodegradation of polarized UV-exposed PMDA-ODA polyimide films, *J. Appl. Polym. Sci.* **86** (2002) 3072-3077.

[8] S. Sato, M. Suzuki, S. Kanehashi, K. Nagai, Permeability, diffusivity, and solubility of benzene vapor and water vapor in high free volume silicon- or fluorine-containing polymer membranes, *J. Membr. Sci.* **360** (2010) 352-362.

[9] S. Miyata, S. Sato, K. Nagai, T. Nakagawa, K. Kudo, Relationship between gas

transport properties and fractional free volume determined from dielectric constant in polyimide films containing the hexafluoroisopropylidene group, *J. Appl. Polym. Sci.* **107** (2008) 3933-3944.

[10] S. Sato, T. Ose, S. Miyata, S. Kanehashi, H. Ito, S. Matsumoto, Y. Iwai, H. Matsumoto, K. Nagai, Relationship between the gas transport properties and the refractive index in high-free-volume fluorine-containing polyimide membranes, *J. Appl. Polym. Sci.* **121** (2011) 2794-2803.

[11] H. Ito, T. Mizunuma, S. Sato, K. Nagai, S. Matsumoto, Photo alignment characteristics of fluorine-containing polyimides as an alignment layer, *Proc. of 16th Int. Display Workshops.* **16** (2009) 1667-1670.

[12] S. Kanehashi, S. Sato, K. Nagai, Membrane color and gas permeability of 6FDA-TeMPD polyimide membranes prepared with various membrane preparation protocols, *Polym. Eng. Sci.* in press (2011).

Chapter 5

CONCLUDING REMARKS

This research focuses mainly on the high free volume silicon- or fluorine-containing polymer membranes. The use of high free volume silicon- or fluorine-containing polymers for gas and vapor separation and optical properties is investigated to prepared novel functions. A fundamental investigation of high free volume polymer membranes is carried out for development of novel polymer membranes with high separation, low refractive index, and high photo alignment characteristic including high durability and heat resistance.

Chapter 1 provides general introduction of this dissertation, including some background and perspective of this dissertation.

In Chapter 2, the P_0 of benzene vapor and water vapor through high free volume silicon- or fluorine-containing polymers used in this study was diffusion controlled and did not depend on either the mobility of the polymer segments, the space between polymer segments, or polymer cohesiveness but was dependent on the balance among them. All silicon-containing polymers used in this study showed benzene vapor-permselective behavior while all fluorine-containing polymers had the opposite property (i.e., nitrogen-permselective). All polymers used in this study showed water vapor-permselective behavior. The benzene vapor/nitrogen permselectivity depended on diffusivity selectivity for fluorine-containing polymers and solubility selectivity for silicon-containing polymers. The water vapor/nitrogen permselectivity depended on

solubility selectivity for PTMSP, 6FDA-MPD, 6FDA-TMPD, and 6FDA-TeMPD, and both selectivity balance for PDMS, PTMSMMA, and 6FDA-mPD.

In Chapter 3, the refractive index and gas transport properties (i.e., permeability, diffusivity, and solubility) in the 2,2'-bis (3,4-dicarboxyphenyl) hexafluoropropane dianhydride (6FDA)-based polyimides were systematically investigated in terms of their polymer *FFV*s at 30°C. As refractive index decreased, gas permeability increased. Based on the Lorentz-Lorenz equation, the permeability, diffusivity, and solubility as a function of the *FFV* determined from optical constants, such as refractive index and molar refraction, were described. From this model, gas permeability and diffusion coefficients of the 6FDA-based polyimide membranes were found to increase as their refractive index-based *FFV* increased. Gas permeability did not depend on either molecular size or cohesiveness, but was dependent on the balance between them. This is because gas diffusivity is dependent on penetrant size, whereas gas solubility is dependent on the interactions between gas molecules and polymer segments. The *FFV*s of the 6FDA-based polyimides calculated from refractive index were 1.16–1.37 times larger than their *FFV* values. This result indicates polyimide density affects the influence of the electronic structures and the interactions between the gas molecules and polymer segments. This finding leads to the conclusion that electronic structure of the polyimide changes depending on polymer chemical structure.

Chapter 4 focuses the substituent effect of fluorine-containing polyimides with 6FDA group on the photo alignment of the LC molecule and the effect of 254 nm LPUV irradiation on the chemical structures through these optical properties and MO calculation were systematically investigated. The chemical structure of 6FDA-TeMPD was changed by LPUV irradiation. However, the photo-scission reaction of LPUV

irradiation was not observed. In the case of 6FDA-TeMPD, the LC molecule photo-alignment characteristic of LPUV irradiated polyimides was observed. The electron-donating benzene ring and the electron-accepting imide ring formed CTCs between two sides of the polymer chains in this MLP structure. The photo alignment characteristic strongly depended on the photoreaction between the C=O group of the imide ring and a CH_3 group for phenyl-group π–π^* transitions. The CT interaction between polymer segments strongly depends on the photoreaction by LPUV irradiation. The chemical structure changed with as the excitation of the C=O double bonds and C–H bonds and the formation of hydroperoxide O–H between the intermolecular polymer segments through the LPUV irradiation mechanism of 6FDA-TeMPD. Therefore, the n–π^* transition of the carbonyl groups decreased through LPUV irradiation. The combination with the alternation sequence to both cross sides was clearly formed. In one direction of the photoreaction in the CTC structure, only the 6FDA-TeMPD showed the photo alignment of the LC molecule.

Finally, Chapter 5 concludes this dissertation. These high free volume polymer membranes have interesting function for gas and vapor separation and optical devices. Generally, both gas separation and optical studies was independently, respectively. In this study, new approach was proposed by cross linking both studies. In the future, the study introducing the way of thinking of such a different viewpoint can be developed.